An experimental study on the effect of niobium on the transformation behaviour of a Nb microalloyed High Strength Low Alloy steel

P.G.W. Remijn

Master thesis

March 1997

Supervisors: drs T.A. Kop
dr ir J. Sietsma
prof. dr ir S. van der Zwaag

Delft University of Technology
Department of Materials Science
Heat Treatment Science and Technology Group
Rotterdamseweg 137, 2628 AL Delft

Summary

Phase transformations have always played an important role in metallurgy as they determine the properties of the final product. In order to fully optimise the production of metals and in particular steel, it is important to understand the various processes influencing the transformation behaviour.

A group of construction steels popular for the combination of a low amount of alloying elements and a high strength are the High Strength Low Alloy (HSLA) steels. HSLA steels are a group of low carbon steels to which small amounts of the microalloying elements niobium, titanium and/or vanadium are added. In this work only Nb is considered.

Nb is added to delay the austenite recrystallisation and to slow down the austenite grain growth. During the hot rolling of the steel, the deformation structure from the last finishing stand in the hot rolling mill is therefore retained. This results in a smaller austenite grain size at the start of the transformation leading to a smaller ferrite grain size, thus increasing the strength of the steel. The Nb however, also has a retarding effect on the transformation rate. The mechanism of this effect has however not yet been investigated. This investigation is part of a larger project aimed at improving the process conditions in the hot rolling of HSLA steels. In this work the mechanism in which the microalloying element niobium influences the transformation behaviour is investigated for an undeformed Nb microallyed HSLA steel using Differential Thermal Analysis.

The results found using DTA are compared to a transformation model developed at Cambridge and to results found using Dilatometry. It is found that, without deformation, the austenite grain size increases considerably with increasing austenitising temperatures. Due to the smaller number of grain boundary nucleation sites for increasing austenite grain sizes, the start of the transformation shifts to lower temperatures. It is shown that that the presence of solute Nb at the grain boundary causes a further delay of the ferrite nucleation resulting in even lower transformation temperatures than caused by only an increase of the austenite grain size. As a result of the lowered transformation temperatures and thus larger undercoolings, Widmannstätten ferrite and bainite is formed in addition to the allotriomorphic ferrite and pearlite found for small undercoolings. The times at the austenitising temperature are found to have little influence on the transformation behaviour.
Finally, a new measuring procedure is presented giving guidelines to improve DTA measurements.

Contents

1. Introduction

Phase transformations have always played an important role in metallurgy. Although not understanding why, the Romans already knew that "quenching" their swords increased the strength and hardness of the steel considerably. Whereas the method of controlling the phase transformation has changed from those days (from running a red hot sword through the body of a (preferably strong) slave to the controlled cooling on the run-out table in a hot-rolling mill), the goal has always been to improve the properties of the steel. Although the often used "trial and error" method will certainly result in improvements, in order to fully optimise the properties of a steel, knowledge about the processes taking place during the production of the steel is crucial.

In this work, the effect of niobium on the transformation behaviour of an undeformed High Strength Low Alloy steel (HSLA steel) has been examined. This work is part of a larger project aimed at improving the process conditions in the hot rolling of HSLA steels. The HSLA steels are a group of low-carbon steels to which small amounts of microalloying elements are added. These microalloying elements (Nb, Ti, and V) have a strong affinity to carbon and nitrogen and are therefore capable of forming stable and fine precipitates. These precipitates are able to delay recrystallisation and slow down the austenite grain growth. In the hot-rolling mill, this results in a much finer austenite grain size at the start of the transformation on the run-out table. The refined ferrite grain size formed at the transformation leads to the high strength of the HSLA steels. The steel examined in this work is a commercial steel manufactured at Hoogovens N.V. containing Nb as the only microalloying element.

In chapter 2 the transformation theory for FeC steels and that for the precipitation of microalloying elements are discussed. In this investigation, the transformation behaviour was studied using a Differential Thermal Analyser (DTA). The DTA, which is discussed in chapter 3 measures thermal effects in a sample during cooling at a constant cooling rate by comparing the temperature of a cup holding the sample, to that of an identical cup without a sample. By varying austenitising temperatures and times in the DTA experiments (which are described in chapter 4), the solute fraction of Nb is varied, and as a result, the fraction of precipitated Nb present in the austenite is varied. The decreasing fraction of Nb precipitates with increasing austenitising temperatures also results in an increase of the austenite grain size. To be able to compare the results of these experiments which are presented in chapter 5, the output of the DTA experiments is converted into c_p curves using sapphire as a reference material. The austenite grain sizes and the microstructures of the DTA samples are determined using light microscopy. In chapter 6, the effect of Nb on the transformation is discussed for the varying austenitising conditions and resulting austenite grain sizes. Also the measured transformation behaviour for six different austenitising temperatures is compared to that predicted by a transformation model developed at Cambridge University and to dilatometric results.

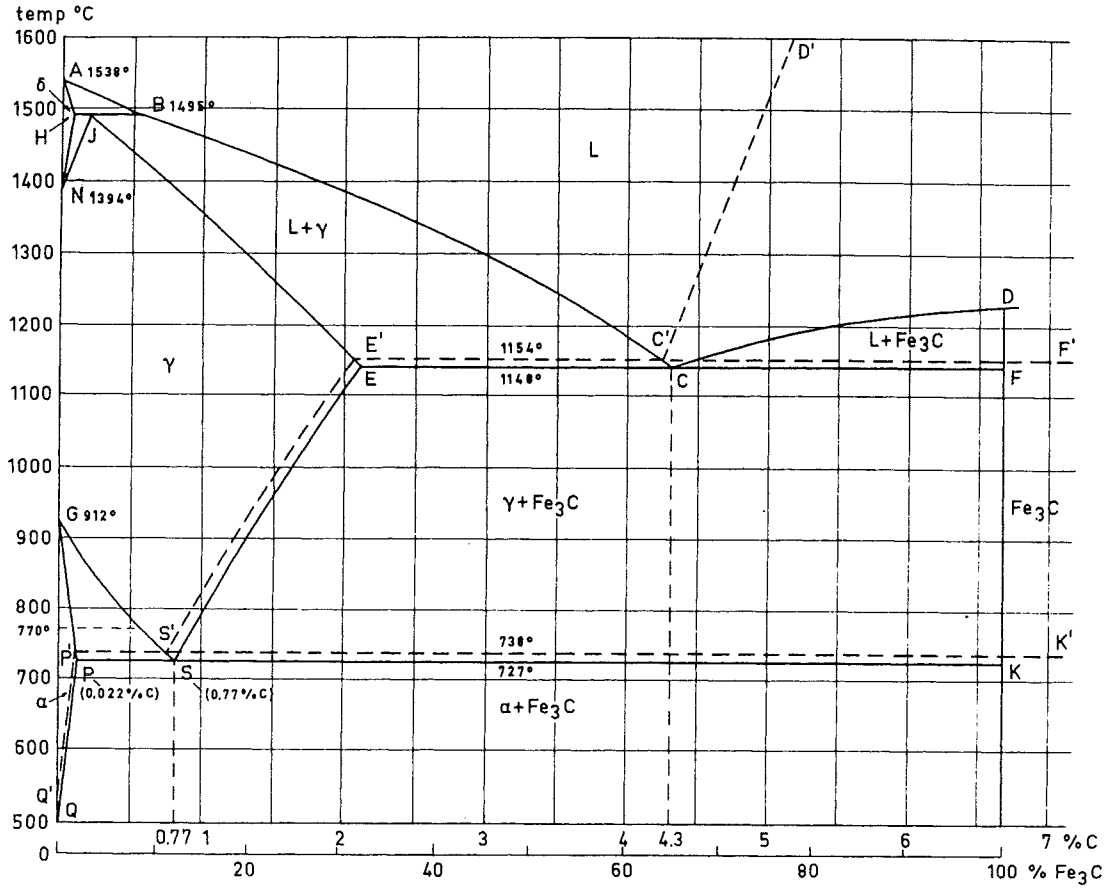

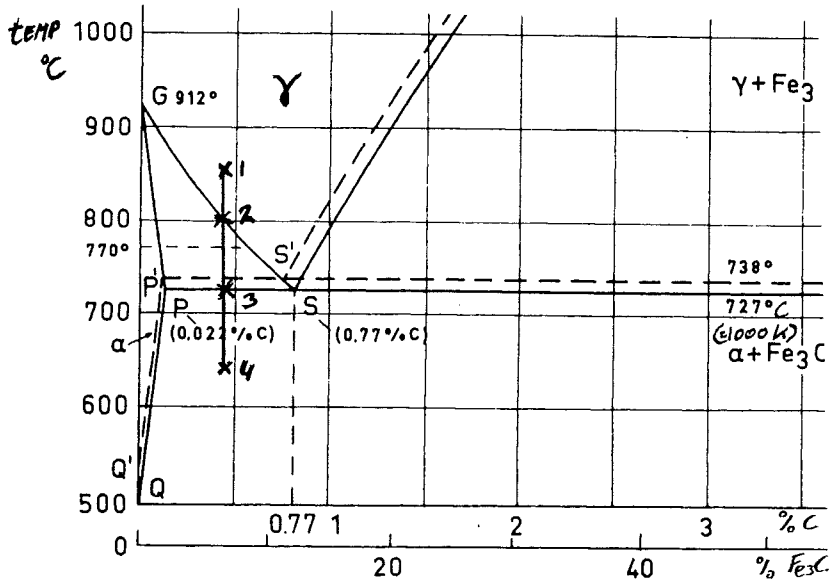

Fig.2.1: The FeC-diagram and a close-up of the γ/α region.

2. Theoretical background

§2.1. Transformation kinetics of an FeC steel

FeC alloys have four different solid equilibrium phases. These phases are α-ferrite, (γ) austenite, δ-ferrite and cementite (Fe_3C). The α-ferrite can be divided into two different morphologies, allotriomorphic ferrite and Widmannstätten ferrite. The first, which is also called primary ferrite, forms at relatively low undercoolings and has equiaxed grains. The Widmannstätten ferrite, also known as sideplate ferrite, forms at high undercoolings and has plate-shaped grains (which, under a microscope, look like needles). Pearlite is a layered structure consisting of alternating layers of ferrite and cementite.
Both α and δ ferrite have the body centred cubic (bcc) crystal structure whereas γ has a face centred cubic (fcc) structure. The γ–α transformation therefore requires a reordering of the atoms from the fcc crystal structure to the bcc structure.
The phases (in equilibrium) as a function of temperature (T) and carbon content can be deduced from the FeC-diagram (see fig.2.1). As can be seen in this diagram, at 1000 K, ferrite can contain 0.022 wt.% C, whereas austenite can contain 0.77 wt.% C at that temperature. The formation of ferrite in alloys and steels containing more than 0.022 wt.% C, therefore requires the diffusion of carbon into the remaining austenite to lower the carbon content of the ferrite forming.
The relevant phase transformation for a low carbon steel is the austenite to ferrite transformation (from point 1 to point 4 (fig.2.1)). Cooling down from point 1 to 4 covers six major processes: the nucleation of ferrite, the growth of ferrite, the enrichment of austenite, the para-magnetic/ferro-magnetic transition, the nucleation of pearlite and finally the growth of pearlite. At large undercoolings bainite and martensite might also form.

§2.1.1. The nucleation of ferrite

The nucleation theory was originally proposed by Gibbs [1] and has since then been extensively developed [2]. Nucleation is the process through which the smallest stable grain of a more stable phase develops from the matrix phase. The process is considered to begin with single atoms joining to produce atom clusters of the new phase. By adding atoms through single atom additions, small clusters of atoms are formed. Clusters that are just large enough so that addition of the next atom yields a decrease in the total free energy change, ΔG_T, are known as "critical nuclei" (see fig.2.2).
The driving force for nucleation is the volume free energy change attending the transformation, ΔG_V. Barriers to nucleation are the volume strain energy, ΔG_ε arising from the size and/or shape misfit between the cluster and the matrix, and the interfacial free energy of the cluster, the matrix interface ΔG_S. ΔG_S is proportional to the surface area of the cluster

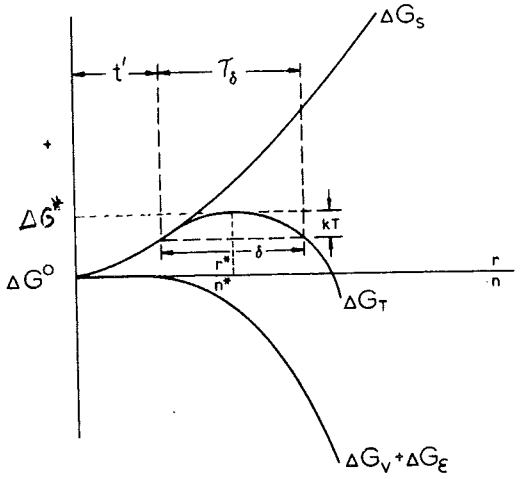

Fig.2.2: The activation energy for the nucleation of a nucleus with radius, r.

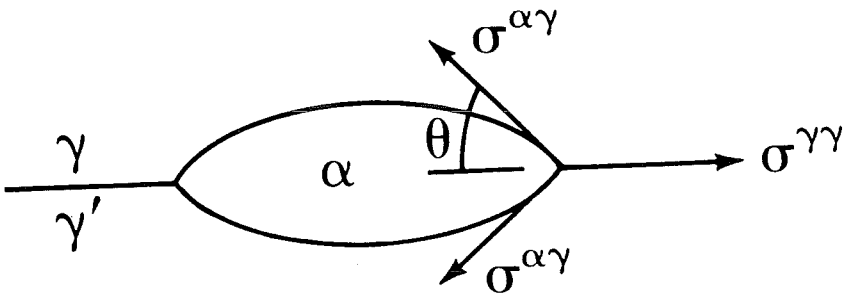

Fig.2.3: θ for the nucleation of a allotriomorphic nucleus on an austenite grain boundary.

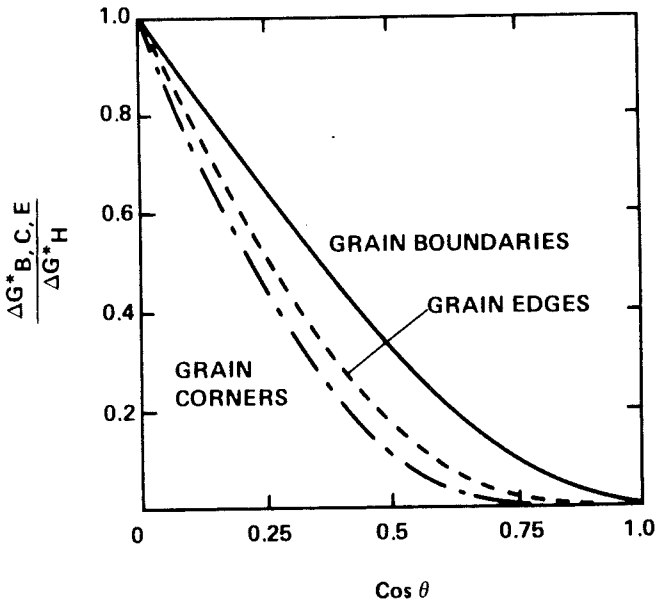

Fig.2.4: The activation energy for nucleation at grain boundaries, grain faces and grain corners as a factor of the activation energy for homogeneus nucleation [4].

(so if the cluster is assumed to be spherical with a radius r, ΔG_S is proportional to r^2), whereas ΔG_V and ΔG_ε are both proportional to the volume of the cluster. Therefore, in the case of a spherical cluster, $(\Delta G_V + \Delta G_\varepsilon)$ is proportional to r^3. In order for the new phase to be able to form, the new phase must be more stable than the existing phase. $\Delta G_V + \Delta G_\varepsilon$ must therefore be negative to enable the new phase to form.

The total free energy change for the nucleation of an embryo, ΔG_T, therefore has three components: ΔG_S, ΔG_V and ΔG_ε. For nucleation to occur ΔG_S is positive and $(\Delta G_V + \Delta G_\varepsilon)$ is negative . ΔG_T is sketched in fig.2.2. For a small radius ΔG_T is positive but for a larger radius ΔG_T will decrease and will become negative. As soon as $\partial \Delta G_T / \partial r < 0$, it is energetically favourable for the nucleus to grow rather than to diminish. The radius at which this occurs is called the critical radius r*. The corresponding ΔG is called ΔG^*, the free energy change for nucleation of the critical nucleus also called the activation energy.

In general, two distinct types of nucleation are possible, i.e. homogeneous and heterogeneous. During homogeneous nucleation, the nucleus forms within a grain and is independent of boundaries, dislocations, etcetera. During heterogeneous nucleation, the nucleus forms at a high-energy site where the available boundary free energy can be used to lower the critical activation energy for the nucleation process.These sites are mainly grain boundaries, grain edges and grain corners. Although the number of sites for homogeneous nucleation is much larger, heterogeneous nucleation dominates most phase transformations because of the much lower activation energy for heterogeneous nucleation. The activation energy ΔG^* for homogeneous nucleation ΔG_h is given by Russel [3] as:

$$\Delta G_H^* = \frac{16\pi\left(\sigma^{\alpha\gamma}\right)^3}{3\left(\Delta G_V^{\gamma\rightarrow\alpha}\right)^2} \qquad (2.1)$$

For heterogeneous nucleation, a dihedral angle is defined by the condition that the surface tensions at the interface between the nucleus and the austenite grain boundary ($\sigma^{\alpha\gamma}$) are in balance. This is illustrated in fig.2.3 where θ is defined for a grain boundary allotriomorph. In fig.2.4, the activation energies for nucleation at grain boundaries (ΔG^*_B), edges (ΔG^*_E) and corners (ΔG^*_C) for varying values of cos θ as presented by Cahn [4] as a fraction of the activation energy for homogeneous nucleation defined by equation 2.1. For the case of nucleation at the grain boundary, cosθ is given by:

$$\sigma^{\gamma\gamma} = 2\,\sigma^{\alpha\gamma}\cos\theta\,. \qquad (2.2)$$

If the surface tension at the $\gamma\gamma$ interface is equal to that to the surface tension at the $\gamma\alpha$ interface ($\sigma^{\gamma\gamma} = \sigma^{\alpha\gamma}$), the activation energy for the heterogeneous nucleation (on a grain boundary) is then approximately 30 % of that for homogeneous nucleation.

The nucleation mechanism of allotriomorphic ferrite and Widmannstätten ferrite is thought to be identical [5] and can be described by the general nucleation theory presented in this paragraph.

Diffusion control: $\Delta x_I \rightarrow 0$
Interface control: $\Delta x_D \rightarrow 0$

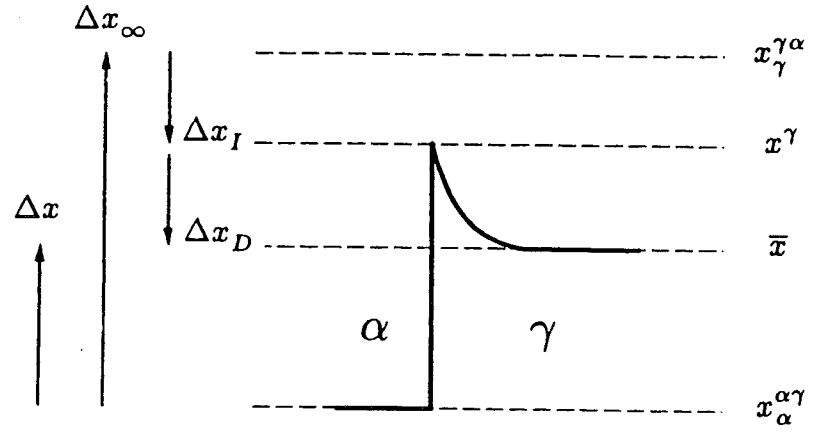

Fig.2.5: The carbon concentrations at the austenite/ferrite interface.

§2.1.2. The growth of ferrite

Growth of allotriomorphic ferrite

Allotriomorphic ferrite is the form of ferrite that forms at relatively small undercoolings below the Ae3 temperature (see fig.2.1). The allotriomorphic ferrite nucleates mainly at austenite grain boundaries. As, due to grain boundary diffusion, these ferrite nuclei tend to grow faster along γ grain boundaries than into the grain [6] [7], the shape of the allotriomorphic ferrite is strongly influenced by the presence of the boundary. Because of these different growth rates, the grain boundaries will be covered by ferrite relatively early in the transformation.

The rate at which the austenite/ferrite interface moves and therefore, the rate at which the ferrite grain grows, depends upon its intrinsic interface mobility (the rate at which the structure can change from fcc to bcc) and on the rate at which during the transformation the diffusing components are partitioned ahead of the moving interface (since the solubility of carbon in ferrite is much less than in austenite this will mostly be C). These two processes are assumed to take place in series, so the slowest process determines the transformation rate. If the diffusion of carbon ahead of the moving interface is the rate determining process the transformation is said to be "diffusion controlled". If the interface mobility is the rate-determining step the transformation is said to be "interface controlled".

Recently, a new model combining these two modes was developed, called the mixed mode model [8]. At low undercoolings, the mode of growth is predicted to be essentially controlled by carbon volume diffusion. By increasing the undercooling the effects of the intrinsic interface mobility become more important and for deep undercoolings the growth kinetics are essentially interface controlled. Interaction between the intrinsic γ/α interface mobility and carbon diffusion in the remaining austenite results in an apparent parabolic growth during more advanced stages of transformation. As the driving force for migration of the interface is no longer one of the two control mechanisms the driving force is now described by thermodynamic properties (difference in chemical potential at the interfaces $\Delta\mu$ or by the difference in free energy at the interfaces ΔG).

When considering the formation of allotriomorphic ferrite from austenite, assuming a two dimensional γ/α interface, the transformation is described based on the carbon concentrations near and at the interface (see fig.2.5). The driving force for the diffusion of the excess carbon ahead of the interface (i.e. the amount of carbon above the solubility in ferrite: Δx) is the concentration gradient resulting from the carbon concentration difference between the ferrite and the austenite (both at the interface and in the bulk). By examining the concentration profile around the interface it can be seen whether the transformation is diffusion controlled, interface controlled or mixed mode controlled.

If the carbon concentration at the interface is much higher than far from the interface ($\Delta x_I << \Delta x_D$), in order for the interface to move, the carbon has to move away from the

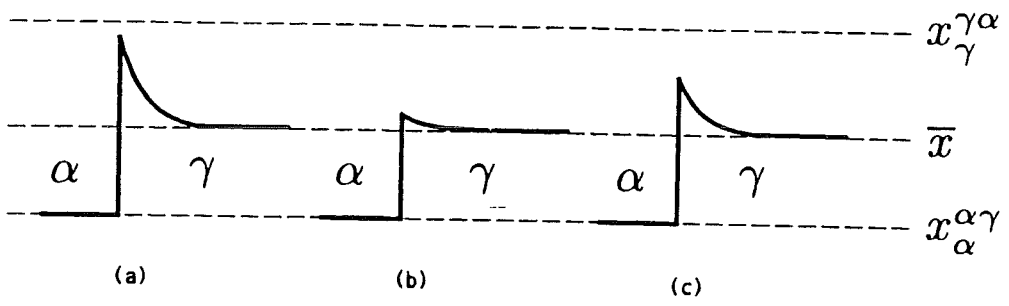

Fig.2.6: The carbon concentration profiles at the austenite/ferrite interface for:
a) diffusion control b) interface control c) mixed mode control

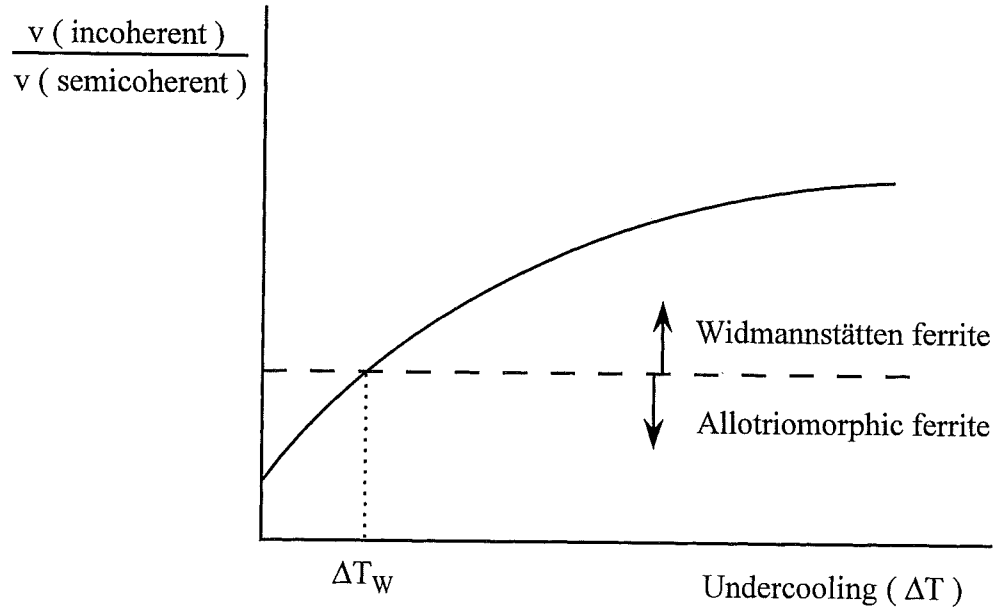

Fig.2.7: The influence of undercooling on the velocity of incoherent and semicoherent interfaces. For undercoolings higher as ΔT_W Widmannstätten ferrite is formed, and for lower undercoolings allotriomorphic ferrite.

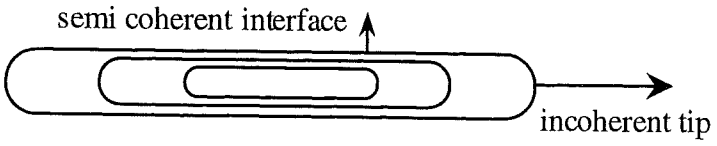

Fig.2.8: The effect of the interface coherency on the shape of the resulting grain. With increasing undercooling the mobility of the incoherent interfaces increases compared to that of the semicoherent interfaces resulting in lengthening in the direction of the incoherent tip.

interface first. So the moving rate of the interface is now determined by the diffusion rate of the carbon and therefore the transformation is diffusion controlled (fig.6a). For high diffusion rates of carbon in austenite, the concentration difference between the carbon concentration at the austenite/ferrite interface and the austenite bulk is very small ($\Delta x_D << \Delta x_I$), the diffusion of carbon into the remaining austenite is very swift and the transformation rate is determined by the interface mobility. The transformation will therefore be interface controlled (fig.6b). In the case of mixed control the concentration difference of carbon between interface and austenite bulk and between interface and equilibrium carbon content in the austenite are of comparable magnitude (fig.6c).

Growth of Widmannstätten ferrite

At higher undercoolings, Widmannstätten ferrite is formed instead of allotriomorphic ferrite. Like for the growth of allotriomorphic ferrite, the growth mechanism of Widmannstätten ferrite might be diffusion controlled [9] or interface controlled [10]. It is, however, still not exactly known which of these two controls the growth mechanism of Widmannstätten ferrite. Both theories will therefore be presented.

When assuming the growth mechanism of Widmannstätten ferrite to be diffusion controlled, it is assumed that because of the lower temperatures and increased carbon content in the remaining austenite (due to enrichment), the diffusion of carbon from the α/γ interface becomes increasingly difficult. As a result of this, Widmannstätten ferrite is formed instead of allotriomorphic ferrite. Like allotriomorphic ferrite, Widmannstätten ferrite nucleates preferably on grain boundaries. Instead of allotriomorphic ferrite which grows in all three directions, however, the Widmannstätten ferrite grows in only one direction, that of the highest carbon diffusion rate, resulting in needle shaped grains. Because of the needle geometry, transport of carbon at the tip can occur in more directions than for flat transformation fronts. This results in a faster transport of the surplus carbon from the transformation front (i.e. the tip of the Widmannstätten needle). In the remaining austenite, the carbon contents in the austenite is somewhat raised making further diffusion of carbon more difficult.

The interface controlled growth of Widmannstätten ferrite is explained by the rate at which the semicoherent and incoherent interfaces can migrate. As presented in fig.2.7 [11], if the ration of the mobility of the incoherent interfaces compared to that of the semicoherent interface exceeds the ratio found for the undercooling ΔT_W, Widmannstätten ferrite is formed instead of allotriomorphic ferrite. For small undercoolings it is suggested that the mobility of semicoherent and incoherent interfaces is comparable. At high undercoolings, the mobility of incoherent interfaces relative to that of semicoherent interfaces increases. As can be seen in fig.2.8, this causes the grain to grow in the direction of the incoherent grain tip.

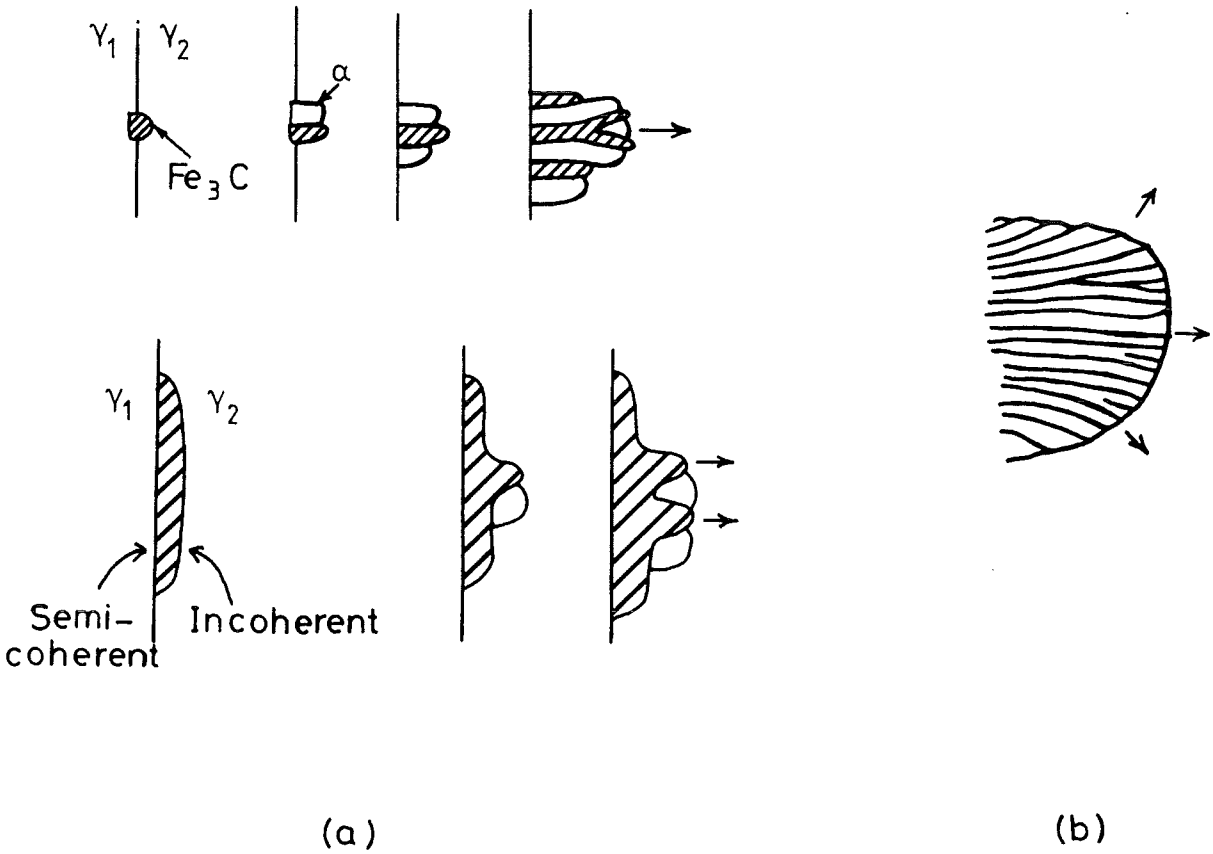

Fig.2.9: a) The nucleation of pearlite either on a clean austenite grain boundary or on a phase (either ferrite or cementite) already covering the austenite grain boundary. The formation of either phase changes the carbon contents in the austenite, making it easier for the other phase to nucleate. The result is a colony of ferrite and cementite layers. b) A pearlite colony at a later stage of growth.

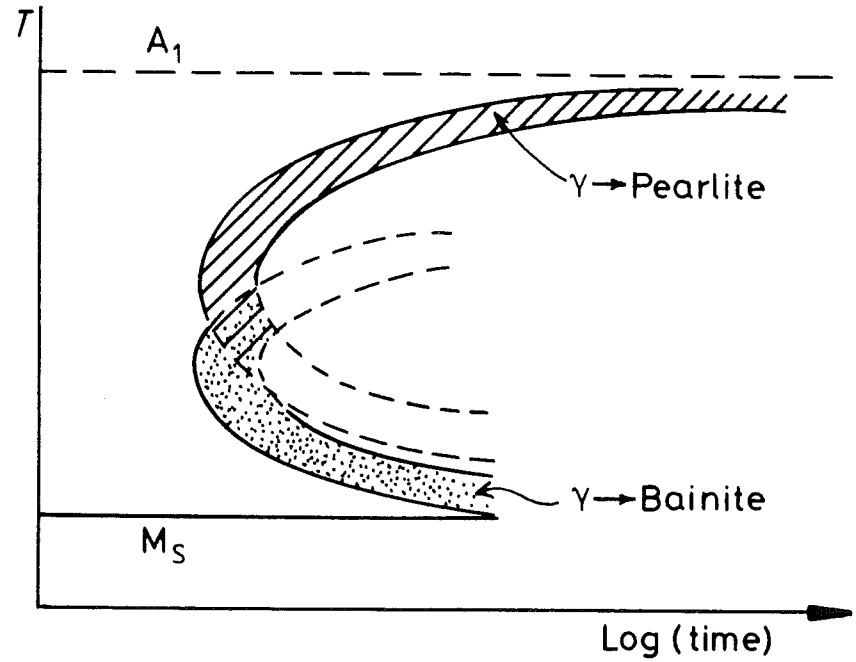

Fig.2.10: The relative positions of the pearlite and bainite transformation curves.

§2.1.3. The nucleation and growth of pearlite

As can be seen in the FeC phase diagram (fig.2.1) at 1000 K both the ferrite and the austenite become supersaturated with carbon (0.022 wt. % C and 0.77 wt. % C respectively). When cooling below this temperature a eutectoid reaction will occur where the austenite is transformed into ferrite and cementite. The two phases form pearlite, which consists of alternating layers of ferrite/cementite. For the nucleation of pearlite in a undereutectoid steel (carbon percentage below 0.77 wt. %) the austenite grains will normally already be covered with allotriomorphic ferrite. When the austenite grain boundaries are already covered with either ferrite or cementite (this will normally be ferrite) the other phase will nucleate on the interface with the remaining austenite (illustrated in fig.2.9a). As the cementite contains more carbon than that present in the enriched austenite, next to the growing cementite plate the carbon concentration is lowered causing ferrite to nucleate and grow along that cementite layer. The pearlite colony grows by the lengthening of these layers of ferrite and pearlite (fig.2.9b).

§2.1.4. The nucleation and growth of bainite

If the transformation is not completed at temperatures around 770 K, both bainite and pearlite are formed. A schematic diagram is given in fig.2.10 indicating the relative positions of the two transformation curves. The bainite formed at this temperature is called upper bainite. The upper bainite differs from pearlite as it consists of cementite precipitates rather than the cementite plates in the pearlite. The ferrite is needle shaped with a growth rate similar to that of Widmannstätten ferrite.

§2.2. Simulation of the transformation behaviour of HO4

At the Department of Materials Science and Metallurgy at the University of Cambridge the transformation behaviour for HO4 was predicted using a transformation model [12] [13]. The input of the model consists of the composition of the steel, the cooling rate and the austenite grain size. The output consists of the fractions of allotriomorphic ferrite, Widmannstätten ferrite and pearlite as a function of temperature. The model calculates the progress of the transformation based on the free energy of the different phases. If the difference of the free energy between one of the phases with austenite increases beyond a for that phase specific value, that phase is allowed to form. The allotriomorphic ferrite is assumed to nucleate at the austenite grain boundaries. The grains are assumed to be disc shaped and are assumed to be growing with a parabolic growth rate. The growth mechanism of the Widmannstätten ferrite is assumed to be diffusion controlled. The start of the formation of Widmannstätten ferrite is determined using the nucleation theory as described in § 2.1.1. but with a required free energy difference between ferrite and austenite of -50 J/mol. The pearlite is not allowed to form at temperatures above the Ae1 temperature and not until

the carbon contents in the remaining austenite reaches the concentration needed for the formation of pearlite. The model does not include the effect of precipitation.

§2.3. The influence of precipitation on the transformation

The main difference between HSLA-steels and C-Mn steel grades is the addition of microalloying elements. The influence of these microalloying elements on the final microstructure is the result of their ability to form stable precipitates with carbon and nitrogen. The main effect of these precipitates is that they keep the austenite grain size small by delaying the recrystallisation of austenite and retardation of the austenite grain growth. Also, the precipitates are believed to have an effect on the austenite to ferrite transformation kinetics. In this section the precipitation and its influence on the transformation are discussed.

All microalloyed steels contain small amounts of one or more of the microalloying elements with a strong chemical affinity to carbon and nitrogen (niobium, titanium and vanadium). In the low alloy steels, these elements form a fine dispersion of carbides and nitrides, from which an excellent combination of strength and ductility can be obtained. These fine precipitates are believed to have three main effects:
- 1) they delay the recrystallization of austenite during controlled rolling. This results in a smaller austenite grain size.
- 2) the precipitates influence the austenite/ferrite transformation affecting ferrite nucleation and growth.
- 3) the strengthening effect of the fine carbides/nitrides dispersion formed during and following the phase transformation.

The first effect leads to a smaller final ferrite grain size and therefore improves the strength of the steel, The second effect could slow down the transformation to lower temperatures leading to larger undercoolings. The third effect has a direct positive effect on the material by way of precipitation hardening.
First the precipitation in the austenite is discussed followed by that in the ferrite. Finally the effects of precipitation on the austenite microstructure and on the austenite to ferrite transformation are discussed.

§2.3.1. Precipitation of microalloyed carbonitrides in austenite

The solubility of the precipitates in austenite controls the volume fraction of the precipitates at a certain temperature. The solubility also influences the particle size through the coarsening of precipitates. Also the grain refining effect of precipitation depends on the pinning effect of the precipitates. Therefore, the temperature dependence of the solubility of the alloying precipitates in austenite is important for the austenite grain size at the beginning of the transformation. A number of solubility products for Nb precipitates in austenite can be found

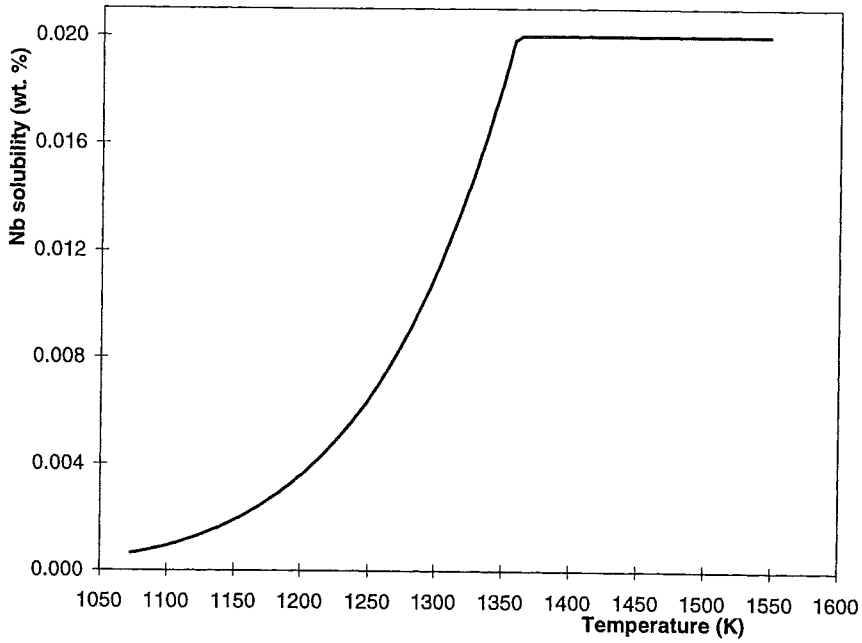

Fig.2.11: The solubility of Nb in austenite calculated with MT-DATA for NbC precipitation in HO4.

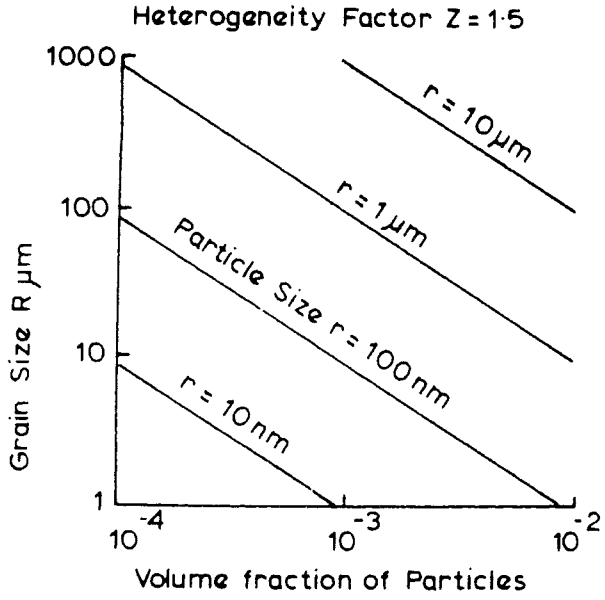

Fig.2.12: The effect of the volume fraction and the size of precipitates on the austenite grain size.

in the literature. For precipitates of composition XY these solubility products are presented based on the general equation:

$$\log[X][Y] = A - B/T \tag{2.3}$$

Solubility products given in literature vary extensively [14] [15]. For NbC precipitates in HO4 the temperature of maximum Nb solubility according to the solubilty products given in literature vary between 1250 and 1450 K. The difference is mainly caused by the methods used for the determination of the solubility products. The Nb solubility for NbC precipitation in austenite has been calculated using MT-DATA (see fig.2.11). This solubility curve is given by :

$$\log[Nb][C] = 3.14 - 7753\ K / T \tag{2.4}$$

with the niobium and carbon concentrations in atomic percentages.
According to this calculated solubility curve, all of the Nb is in solution at temperatures of 1350 K or higher. In reality, however, the precipitates present will not only be just NbC but a mixture of NbC, NbN and NbCN. Therefore, the Nb solubility presented in fig.2.11 should be used as an indication rather than the actual solubility at specific austenitising temperatures. The solubility curves represent the equilibrium conditions. They do not give information concerning the kinetics of the dissolving and precipitation of the precipitates. The kinetics are determined mainly by the diffusion rates of the elements. If the diffusion rate is low, the chance that the precipitating elements meet is lowered. Therefore, at low temperatures the precipitation kinetics become very low. By quenching a sample from the austenitising temperature to room temperature, the microalloying elements that were in solution at the austenitisation temperature remain in solution at room temperature.
Also related to solubility are the coarsening characteristics of the precipitates. Diffusion controlled particle coarsening leads to an increase of the particle size in time at the expense of the smaller precipitates. Due to the smaller pinning effect, a smaller number of larger particles lead to larger austenite grains (see fig.2.12) [16]. Precipitate coarsening will therefore lead to a larger austenite grain size than would be found without precipitate coarsening. It was found that a precipitate with a low solubility will coarsen more slowly than a precipitate with a high solubility as for the latter the small precipitates are less stable [17]. A lower volume fraction of precipitates will also reduce the coarsening rate as the diffusion distances become bigger.

§2.3.2. Precipitation of microalloyed carbonitrides in ferrite

For the microalloying elements that are still in solution at the start of the transformation three situations are possible:

1- Precipitation during the γ/α transformation.

2- Precipitation subsequent to the transformation.

3- No precipitation, the microalloying elements remain in solution due to slow kinetics.

The solid solubilities of the carbides and nitrides of the micro-alloying elements are thought to be approximately an order of magnitude smaller in ferrite than in austenite [17]. Together with the local stress field from the austenite to ferrite interface the driving force for nucleation is therefore increased at the interface, propagating precipitation during the γ/α transformation.

Precipitation subsequent to the γ/α transformation was described by Honeycombe [17] who found that in microalloyed steels transformed isothermally or during continuous cooling, precipitates are formed which are not in association with the γ/α interfaces. Also precipitates were formed within the newly formed ferrite, either at long times or at low temperatures. Microalloyed steels are found to have a much higher dislocation density than plain carbon steels. For a FeCTi steel densities of 10^9 to 10^{11} cm^{-2} were found increasing with decreasing transformation temperatures. The nucleation of these alloy-carbides mostly takes place on dislocations although precipitation on ferrite/ferrite boundaries also occurs.
With decreasing temperature, the diffusion rate of the precipitating elements also decreases, causing the precipitation to become increasingly difficult. The precipitation is slowed down because with decreasing diffusion rates it becomes more difficult for the precipitation components to come together. For low temperatures, almost no precipitation will occur. The microalloying elements will then remain in solution independent of the solubility of these elements at that temperature.

§2.3.3. Effect of precipitation on the grain growth and recrystallisation of austenite

The microalloying precipitates are known to have a pinning effect on the austenite grain boundaries and dislocation arrays.If this pinning is strong enough, the austenite grain growth is inhibited and recrystallisation is delayed. To obtain a sufficient pinning force to inhibit austenite grain growth and delay recrystallisation, the radius of the precipitates must be below a critical radius r_c. This critical radius r_c is given as [17]:

$$r_c = \frac{6R_0 f}{\pi}\left(\frac{3}{2}-\frac{2}{z}\right)^{-1} \qquad (2.5)$$

where: R_0 is the inial austenite grain size
f is the volume fraction of precipitates, and
z is ratio of radii of growing grains to original grains R/R_0.

From this equation, it follows that the critical particle size increases as the volume fraction of particles or the original grain size increases. The stability of austenite grain boundaries at high temperatures is therefore ensured if at that temperature sufficient precipitates are present to pin the austenite grain boundaries. For this to occur, the dispersion must meet three criteria:

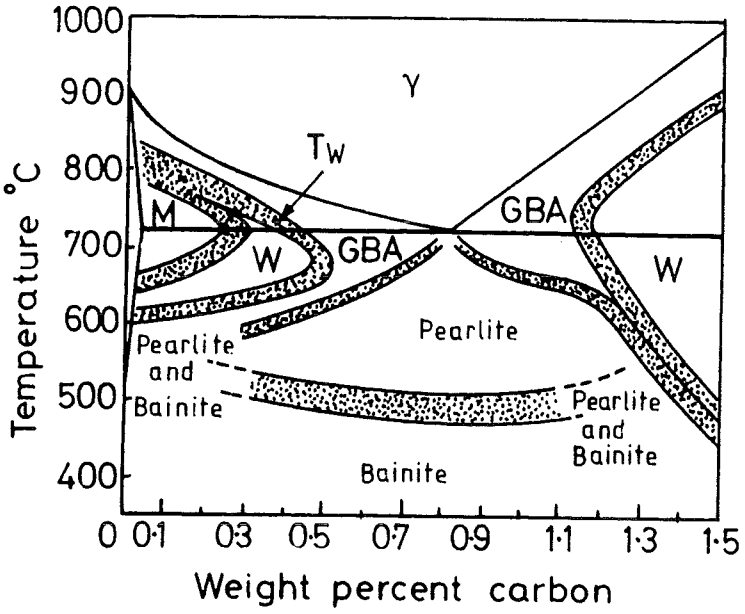

Fig.2.13: An FeC diagram showing the phases that are formed during the transformation at low temperatures.

1) The particle size and spacing must be below critical values.
2) A sufficiently high volume fraction to maintain spacing below critical value.
3) A low rate of coarsening to stabilize the dispersion and keep the radius below the critical r_c.
In practice this means providing sufficient microalloying element and (carbon + nitrogen) to give the correct stoichiometric ratio and to satisfy maximum solubility at the highest temperature involved in the controlled rolling process.
Nb(CN) and Ti(CN) are both very good grain pinning precipitates as they form at relatively high temperatures (compared to rolling temperatures). Vanadium which also combines effectively with C and N is not as efficient a grain refiner as V(CN) forms at lower temperatures and therefore has less effect on the recrystallization of austenite. V(CN) does, however, have the advantage of forming denser dispersions in ferrite compared to the other microalloying elements which leads to an increase in strength [17]
In general terms, fine dispersions delay the onset of recrystallization by pinning both boundaries and dislocation arrays so that the nucleation can only occur after larger deformations, and as a direct result the recrystallized grains are much smaller.

§2.3.4. The effect of precipitation on the γ/α transformation

Precipitation is also thought to influence the transformation mechanism. The formation of ferrite in plain carbon steels proceeds by a diffusional transformation. Usually this transformation is considered to be diffusion controlled. Due to the microalloying precipitates, pinning of the interfaces is believed to occur, lowering the mobility of the interface considerably. The formation of ferrite could therefore become interface controlled instead of diffusion controlled or a combination of these two, described by the mixed mode model. For continuous cooling, delaying the transformation means that the transformation takes place at lower temperatures. As can be seen in fig.2.13 [11], at lower transformation temperatures Widmannstätten ferrite and or bainite can form.

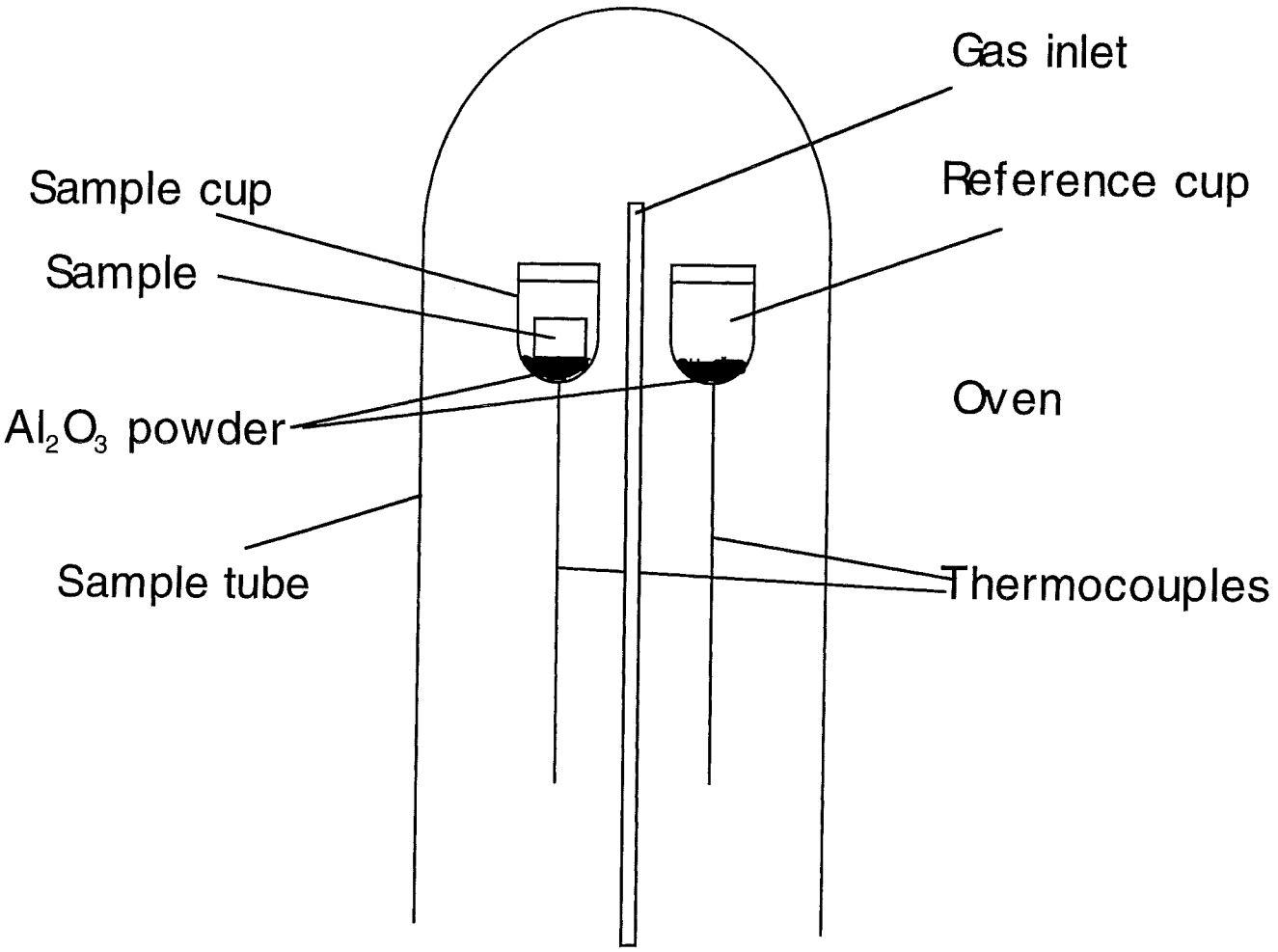

Fig.3.1: A schematic drawing of the sample area of the Perkin Elmer DTA 7.

3 Experimental techniques

§3.1 The Differential Thermal Analysis

In this investigation DTA experiments were performed to determine the effect of niobium on the austenite to ferrite transformation in a niobium microalloyed HSLA steel. DTA stands for Differential Thermal Analysis. With this method the heat effects in a sample during heating or cooling can be measured. As the austenite to ferrite transformation includes a thermal effect (the transformation is exothermic), this transformation can be distinguished using DTA.
Differential Thermal Analysis is based on the occurrence of thermal effects in a sample material during heating or cooling. As this report only concerns DTA experiments during cooling, only cooling will be discussed in this experimental section. In an ideal Differential Thermal Analyser (DTA) a sample cup and an identical reference cup are cooled down under identical conditions and the temperature difference between the cups during cooling is recorded. Without a sample in the sample cup this differential temperature (ΔT) should be zero during cooling as the cups are identical and therefore have the same heat capacity. When a sample is inserted in the sample cup, the heat capacity of the sample cup (including the sample) is no longer identical to that of the reference cup. Cooling will therefore now result in a temperature difference ΔT between the two cups which is determined by the sample's heat capacity. Furthermore, any endothermic or exothermic physical or chemical processes which occur during cooling will result in an increase or decrease of ΔT. The DTA curve, ΔT vs. temperature, therefore consists of a continuous temperature difference due to the difference in specific heat and extra thermal effects at specific temperatures resulting from occurring processes such as phase transformations and the ferromagnetic transition.
In the ideal case, Differential Thermal Analysis is a very simple and powerful technique. However, in practical use, the DTA is, as many instruments, not an ideal instrument.

§3.1.1. The Perkin Elmer DTA 7

For the experiments presented in this report, a Perkin Elmer DTA 7 was used. A schematic drawing of this DTA is given in fig.3.1. The cup holders are mounted individually on the insulating covers of the thermocouples. The atmosphere within the sample tube can be controlled by inserting gas via the gas inlet tube positioned above the cups. At the base of the sample tube there is a gas outlet to maintain a constant pressure. To correct for the instrumental differences between sample cup and reference cup a measurement, the *baseline* measurement, is performed without a sample in the sample cup to determine the effects of the these differences on the signal measured. The *baseline* consists of the ΔT caused by the DTA itself as a function of temperature. By subtracting the baseline from the actual sample

measurement ΔT caused by the sample is derived. From this point on, when discussing DTA, this type of DTA (the Perkin Elmer DTA 7) is discussed.

§3.1.2. Determination of the specific heat using the DTA

In Appendix A, a thermal evaluation of the DTA is presented in which the theorical basis of the DTA is reexamined. The most important equations of appendix A are presented here. It should be noted that there is a difference between the specific heat (c_p) which is a material property and the heat capacity of a sample C_p which is a sample-specific value.
As is shown in Appendix A the DTA curve is the sum of the thermal effects due to the actual heat capacity of the sample $C_{psample}$ and due to the enthalpy change as a result of occurring reactions dH_s/dt :

$$\Delta T_{sample} = -\frac{1}{K}\left(C_{psample}\left(\frac{dT_s}{dt}\right) + \frac{dH_s}{dt}\right), \tag{3.1}$$

where: ΔT_{sample} is the temperature difference between the sample cup and the reference cup,

K is a combination of the heat transfer coefficients involved, and

dT_s/dt is the cooling rate of the sample cup.

As the output of the DTA is a temperature difference and not a specific heat, ΔT has to be converted into c_p before it can be used for quantitative analysis. This can be done using the ratio method (as derived in appendix A), in which the thermal effect of the sample is compared to that of a reference material such as α-corrundum (sapphire). The ratio method using sapphire is given by [18]:

$$\frac{\Delta T_{sample}}{c_{psample} \cdot m_{sample}} = \frac{\Delta T_{sapphire}}{c_{p\ sapphire} \cdot m_{sapphire}}, \tag{3.2}$$

where: c_p calculated this way is the fictional specific heat (per unit of weight), which is the sum of the actual c_p of the material plus the effect of possible occurring reaction:

$$c_p = c_{psample} + \frac{dH_s}{dT}. \tag{3.3}$$

In this report, unless stated otherwise, if c_p is used, the fictional c_p is meant so including the effect of thermal effects.
As the sample is not directly connected to the thermocouple, the Al_2O_3 powder and the Pt cup itself cause a systematic error in the measured temperature. This effect has been examined by Krielaart [19] who derived an equation to correct for this effect. The difference in the measured temperature and the actual sample temperature is a result of the time the thermal energy needs to reach the thermocouples. During this time the DTA continues to cool

and therefore the temperature at which the effect is recorded by the thermocouple is too low. For small amounts of Al_2O_3 powder, this effect can be corrected for using the equation [19]:

$$T_{measured} = T_{sample} + a \cdot \phi \tag{3.4}$$

where a is a time constant, found by Krielaart [19] to be 0.15 min,
ϕ is the cooling rate (which in this work is: -20 K/min),
$T_{measured}$ is the temperature measured by the thermocouples and
T_{sample} is the real temperature of the sample.

§3.1.3. Transformation kinetics

A method to derive the transformation kinetics from the c_p curve of a sample has been presented by Krielaart [proefschrift]. This method, however, can only be used to analyse c_p curves with separate peaks as the complete area of a reaction peak is to be determined.
For the austenite to ferrite transformation, the fractions transformed can be calculated for small temperature steps using:

$$c_p = x^{\gamma} c_p^{\gamma} + x^{\alpha} c_p^{\alpha} + \Delta H^{\gamma/\alpha} \frac{dx^{\alpha}}{dT} , \tag{3.5}$$

where x^{γ} is the mass fraction of austenite,
x^{α} is the mass fraction of ferrite,
c_p^{α} is the specific heat of ferrite,
c_p^{γ} is the specific heat of austenite, and
$\Delta H^{\gamma/\alpha}$ is the enthalpy difference between austenite and ferrite.

When more transformation products are formed, the c_p measured with the DTA can be described by:

$$c_p = x^{\gamma} c_p^{\gamma} + \sum_i x^i c_p^i + \sum_i \Delta H^{\gamma/i} \frac{dx^i}{dT} , \tag{3.6}$$

where i runs over the transformation products present (for example ferrite and pearlite)
x^i is the mass fraction of phase i,
c_p^i is the specific heat of phase i, and
$\Delta H^{\gamma/i}$ is the enthalpy difference between austenite and phase i.

The enthalpy difference for transformation can be determined by way of iteration such that the fraction transformed is in compliance with the expected fraction transformed.
Applying this method to overlapping peaks is not possible as in this case the area of the separate peaks can not be determined as it is unknown which transformation causes the thermal energy in the overlapping part. As this can only be solved by defining the fractions

transformed in the overlapping part, this method can not be used to calculate that very same transformation kinetics.

§3.1.4. Experimental difficulties and new measuring procedure

In order to obtain useful DTA data the DTA experiments need to be performed in a very accurate manner. One of the main problems is a possible baseline change caused by inserting the sample in the sample cup. If the sample cup or the reference cup is moved between the measurement of the baseline and the sample measurement or if the lids are not put back in the same way, the baseline as recorded in the baseline measurement is possibly not correct for the sample measurement. The resulting corrected baseline will therefore also be incorrect.
To get an indication of the validity of the measured baseline a new measuring procedure has been developed. The most important difference with the previous measuring procedure is that the starting value of ΔT, which can be adapted by the operator, should not be changed between the baseline and sample measurement. The temperature programme of the DTA should furthermore not only be used to cool down from the austenitising temperature but also during heating and stabilising at the austenitising temperature. In this way, not only is the temperature programme well defined but also it is possible to record ΔT during stabilising. As ΔT at which the DTA stabilises does not depend on the heat capacity of the sample cup, this value does not depend on the presence of a sample and therefore the stabilised ΔT should be zero for baseline and sample measurement. When applying the new measuring procedure it is therefore possible to compare these values of ΔT and immediately get an indication of the validity of the baseline determined.
The new measuring procedure and an overview of the effect of the different settings of the DTA are presented in appendix B.

§3.2. Nb solubility and precipitates in austenite

To investigate the precipitation behaviour of Nb during the DTA experiments, additional samples have been subjected to the same austenitising treatment applied in the DTA experiments. Instead of slowly cooling down the samples from the austenitisation temperature they are quenched in order to prevent Nb from precipitating. In this way the amount of Nb precipitates at high temperature can be determined in a sample at low temperature. A new method has been developed to determine the amounts of Nb precipitated and Nb in solution in such a sample. Hereto, the sample is dissolved and the solution containing both solute Nb as Nb precipitated is filtered to separate the solute from the precipitated Nb. Next, the Nb content of the solution (solute Nb) and the filters (precipitated Nb) are determined.

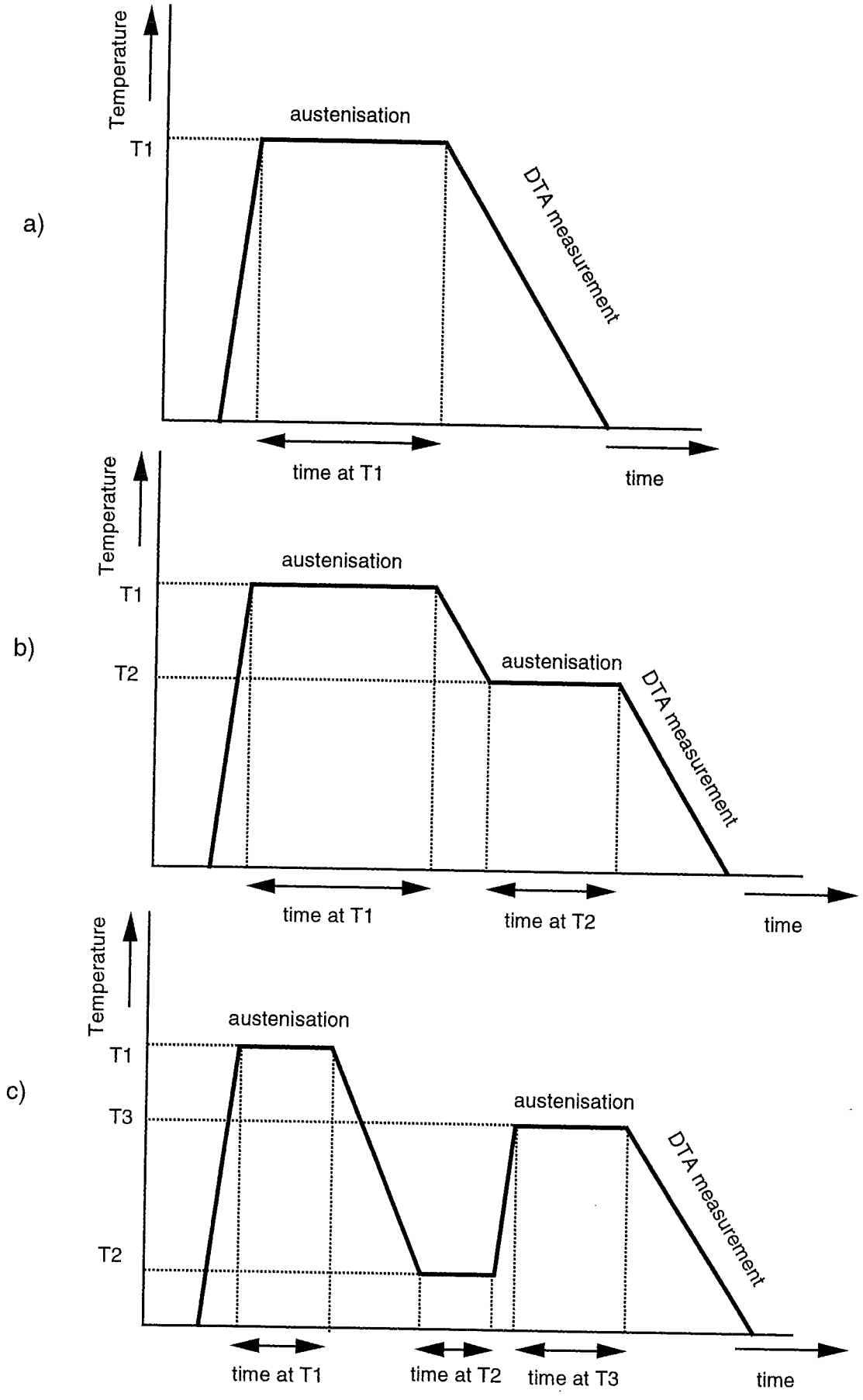

Fig.4.1: The temperature programmes as used in the DTA experiments described in table 4.2 and 4.3.

4. Experimental settings

§4.1. The DTA experiments

The material examined in this investigation is a Nb microalloyed HSLA steel (which, in this report is addressed as HO4). The composition of the steel is given in table 4.1.

Table 4.1: Chemical composition (wt.%) of HO4

C	Mn	Si	Nb	N	S	P	Cr	Mo	Ni	Cu	Al
0.136	1.200	0.017	0.020	0.0036	0.009	0.016	0.025	0.002	0.027	0.013	0.053

The steel is a commercial steel produced by the "Koninklijke Hoogovens NV" where it was hot rolled to a thickness of approximately 6 mm. From this slab cylindrical bars (Ø 3 mm) are machined with the axis of the bar perpendicular to the rolling direction. The DTA samples are prepared from these bars by cutting slices of about 1.7 mm using a Buehler 'Isomet' low speed saw. These samples weigh approximately 90 to 100 mg.

§4.1.1. The instrumental settings of the DTA

The experiments were carried out using platinum cups which were covered with Al_2O_3 lids. Both cups were filled with a small amount of Al_2O_3 powder (5 to 10 mg) to improve the thermal contact between sample and sample cup. The temperatures were measured using S-type platinum-platinum/rhodium thermocouples. All experiments were carried out under a dynamic 25 ml/min Argon-5 gas flow, which was dehydrated and deoxidised before entering the DTA. Before experiments were performed, the temperature scale of the DTA was calibrated using the melting points of aluminium and gold.

§4.1.2. The temperature programme used for the DTA experiments

As already presented in chapter 3, a DTA experiment consists of heating the two cups to the desired temperature, stabilising them at this temperature and then cooling them down applying a constant cooling rate (fig.4.1a). During some experiments the sample was annealed at a second austenitising temperature before cooling down (fig.4.1b). Also some samples were cooled down to temperatures well below the transformation temperatures and were then austenitised for the second time (fig.4.1c). The austenitising temperatures and austentising times applied in the DTA experiments performed are presented in table 4.2 and table 4.3. The important parameters in these experiments are the heating/cooling rates, the stabilising temperatures and the stabilising times. Since the instrumental broadening of the DTA-curve depends on the cooling rate, a fixed cooling rate of 20 K/min was used in all experiments. The heating rate used for the first series of experiments (table 4.2)was 50

K/min. The heating rate fore the experiments (presented in table 4.3) performed following the new measuring procedure as is presented in appendix B was 20 K/min. As the actual measurement is performed during cooling, the heating rate does not affect the shape of the curve.

Table 4.2: The temperature programmes for the DTA experiments performed.

Temp. program	Temp. 1 [K]	Time at T1 [min]	Temp. 2 [K]	Time at T2 [min]	Temp. 3 [K]	Time at T3 [min]
s1	1173	20	-	-	-	-
s2a	1173	20	293	-		
s2b	1173	20	-	-	-	-
s3	1273	10	-	-	-	-
s4	1273	20	-	-	-	-
s5	1273	30	-	-	-	-
s6	1273	60	-	-	-	-
s7	1323	20	-	-	-	-
s8	1373	20	-	-	-	-
s9	1423	20	-	-	-	-
s10	1473	20	-	-	-	-
s11	1523	20	-	-	-	-
s12	1423	10	1173	15	-	-
s13	1423	10	1173	60	-	-
s14a	1423	10	1273	15	293	-
s14b	1423	10	1273	15	-	-
s15	1423	10	1273	25	-	-
s16	1473	20	573	15	1173	20
s17	1473	20	573	15	1273	20
s18	1473	20	573	15	1373	20
s19	1473	20	573	15	1423	20

First analysis of the results of the first series of experiments (presented in table 4.2) showed that during the measurement of the sapphire sample the DTA was not working properly. It was shown that the thermocouples (on which the sample and reference cups are mounted) were not fixed firmly within the DTA. Because of this, the instrumental temperature difference between sample and reference cup (i.e. the baseline) changed significantly. To be able to detect such problems in an earlier stage, a new measuring procedure has been developed (see appendix B). Using this procedure, an indication of the accuracy of the results can be obtained immediately after the experiment. Based upon the results of the first

series of experiments three experiments were performed again now using the new measuring procedure. The temperature programmes for these experiments are presented in table 4.3.

Table 4.3: The temperature programmes for the DTA experiments using the new measuring procedure (in these experiments a heating rate of 20 K/min is used instead of the heating rate of 50 K/min used for the experiments presented in table 4.2)

Temp. program	Temp. 1 [K]	Time at T1 [min]
s20	1273	20
s21	1423	20
s22	1523	20

§4.1.3. Microstructural determination

The austenite grain structure could be made visible using thermal etching. In this method the grain boundaries on a smooth surface can be made visible by annealing at a high temperature. For the DTA it is found that the austenite grain structure was best visible on the part of the sample positioned in the Al_2O_3 powder. Therefore the sample was inserted in the sample cup with the smoothest of the two flat sides of the sample in the Al_2O_3 powder.
The austenite grain size was determined from light microscopy photo's made with amplification factors varying from 30 x to 500 x, using the Lineal Intercept Method. With the Lineal Intercept Method the grain size is determined by counting the number of grains boundaries along 5 lines across the sample. The 95 % confidence limit is calculated with the Student t-value based on the standard deviation of the number of grains counted in these 5 counts.
The phases present in the transformed samples were determined from the DTA samples using light microscopy. The samples were etched for 20 seconds in 2 % Nital.

§4.2. Determination of the fractions solute and precipitated Nb

Experiments were carried out to determine the fractions solute and precipitated Nb at different annealing temperatures. Also the effect of a austenitising at a second lower temperature was examined. For these experiments, samples of the examined HO4 steel are annealed and most samples are gas quenched ($t_{800/500} \approx 2$ seconds) to prevent the Nb from precipitating. One sample was air cooled. The temperature programmes for these experiments are presented in table 4.4. The fractions of both precipitated and solute Nb were determined by dissolving the sample and separating the precipitated from the solute Nb. The samples used for these precipitation experiments are cylindrical with length 10 mm and have a diameter of 5 mm. Annealing was done in the Bähr Dilatometer at Hoogovens.

Table 4.4: The temperature programmes for the precipitation experiments

Temp 1 [K]	Time at Temp 1 [min]	Temp 2 [K]	Time at Temp 2 [min]	quench (y / n)
1273	5	-	-	y
1273	20	-	-	y
1273	60	-	-	y
1473	20	-	-	y
1473	20	1273	20	y
1473	20	1273	60	y
1473	20	-	-	n

For the quantitative analysis of the samples the matrix is brought into solution electrochemically using an EDTA solution. In this process, the precipitates do not dissolve and fall into the electrolyte. This solution is filtered using a filter with a 100 nm pore size. The remaining part of the sample is put into a fresh EDTA solution and is cleaned. ultrasonically to remove as much material from the sample as possible. The solution after the first filtration is called "electrolyte". The amount of sample that is removed this way is measured by determining the mass of the sample before and after the dissolving process. This solution is also filtered using a 100 nm pore size filter. The solution after the second filtration is called "filtrate". The contents of the two filters will be refered to as "melt". The two solutions contain the solute Nb whereas the two filters contain the precipitated Nb.

The particles on the two filters (including the Nb precipitates) are mixed with potasium disulfate salt. This mixture is melted and dissolved in a solution of sulferic and oxalic acid. The Nb concentration in this solution (the precipitated Nb fraction) and in the two other solutions (the fraction Nb in solution) are analysed using a Perkin Elmer Inductive Coupled Plasma - Optical Emission Spectrometer (ICP-OES).

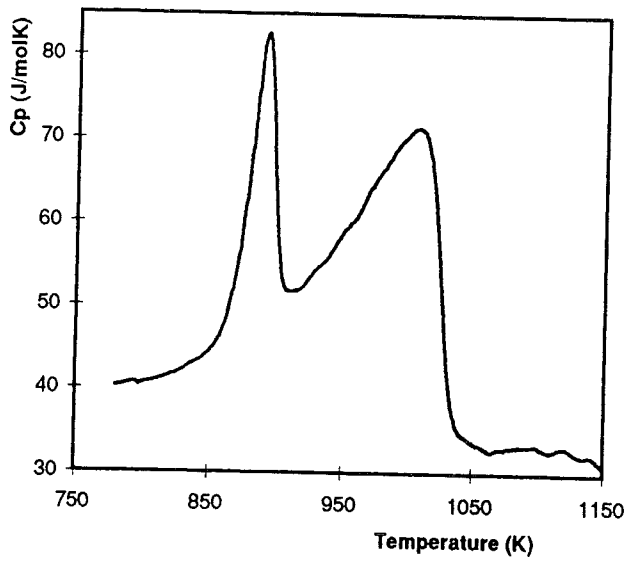

a) S1: T_{aust}: 1173 K Time 20 min

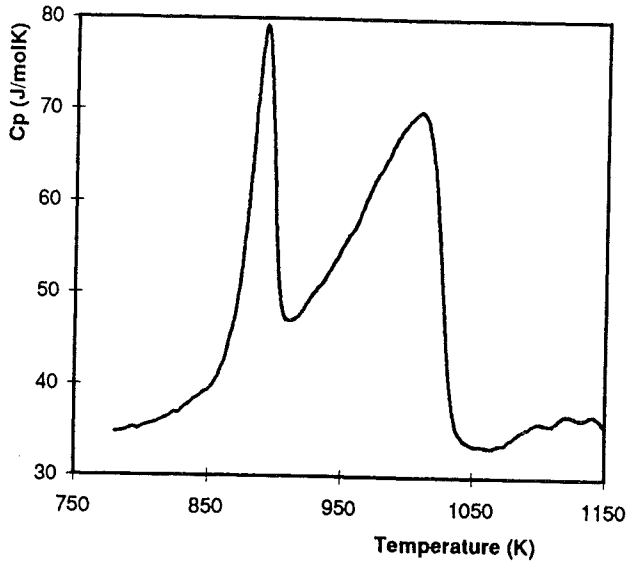

b) S2a: T_{aust}: 1173 K Time 20 min (first run)

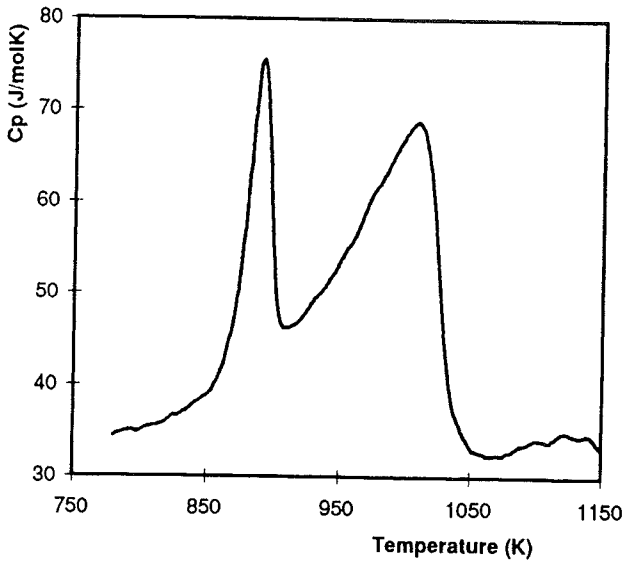

c)S2b: T_{aust}: 1173 K Time 20 min (second run)

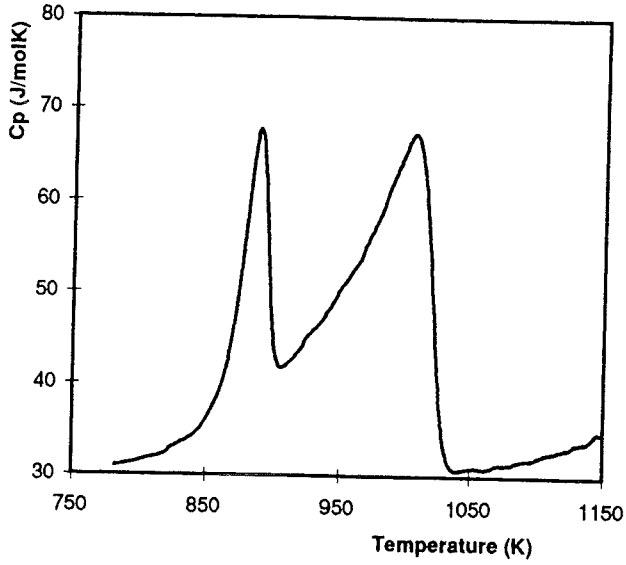

d) S3: T_{aust}: 1273 K Time 10 min

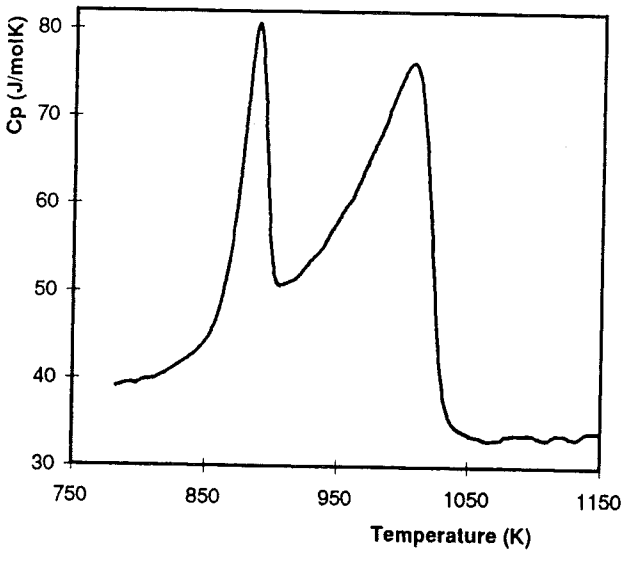

e) S4: T_{aust}: 1273 K Time 20 min

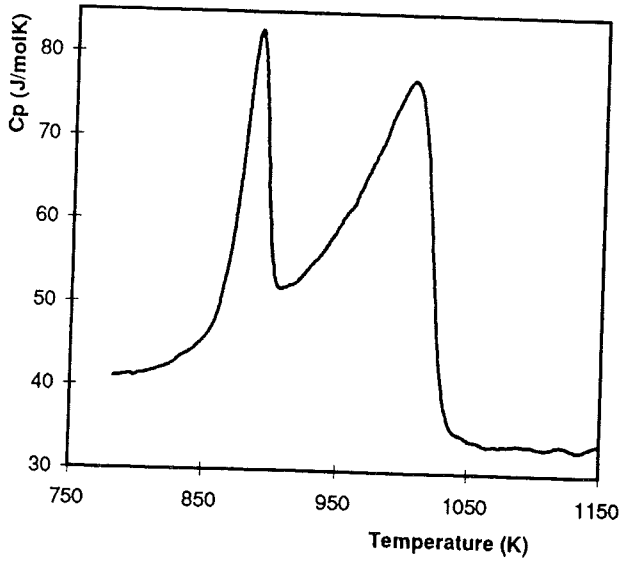

f) S5: T_{aust}: 1273 K Time 30 min

Fig. 5.1 a-f: The c_p vs. temperature measured with the DTA for temperature programmes S1 to S5.

5. Experimental results

§5.1. The DTA experiments

§5.1.1. The c_p vs. temperature

The output from the performed DTA experiments, presented in table 4.2 and 4.3, in the previous chapter, giving ΔT versus T, has been converted to c_p values using the ratio method as described in §3.1.2. For this conversion the data from the same sapphire experiment have been used for all the experiments described. A correction was applied for the effect of thermal lag described in §3.1.2. Also a correction has been applied to the values of ΔT in order to correct for the baseline drift as described in §3.1.4. For this correction a small value was added to ΔT as measured in an experiment. These values varied between -0.2 to 0.2 K for all the experiments in this report, whereas most reaction peaks result in an increase of ΔT of about 1 to 2 K. The required value for the correction was determined by comparing the derived c_p of the fully austenitic state to the value of c_p for austenitic HO4 calculated using Thermocalc. The curves of c_p versus T for the experiments described in table 4.2 and 4.3 in chapter 4.1.2. are presented in fig.5.1 to 5.4. These experiments can be divided in four groups. The first group, presented in fig5.1 and 5.2, are the experiments in which a sample is heated to a single austenitising temperature, annealed for various times and cooled down. These experiments show the effect of annealing two times (fig.5.1b and 5.1c) and the influence of the austenitising time on the c_p curve measured (fig.5.1d to 5.1f and fig.5.2a). Fig.5.2b to 5.2f are the c_p curves for annealing for 20 minutes at increasing austenitising temperatures. Note the upcoming new transformation peaks in the c_p curves first occurring in the samples austenitised at 1373 K (fig.5.2c) and 1473 K (fig5.2e).

In the second group of experiments (fig.5.3a to 5.3e) the samples are annealed for 10 minutes at 1423 K followed by annealing at lower temperatures (1173 K or 1273 K) for varying times. Note that the shape of these curves is different from that for austenitising only once at either temperature. Again, the effect of applying this treatment twice is investigated (fig.3c and d)

For the third group of experiments (fig.5.3f to 5.4c), the samples are annealed at 1473 K and cooled down to 573 K (below the transformation temperatures). After holding the sample at 573 K for 15 minutes, the sample is reheated and annealed at various austenitising temperatures for 20 minutes. Now, the transformation is determined by the second austenitisation temperature. The final three curves (fig.5.4d to 5.4f) are the results of the experiments measured using the new measuring procedure as described in appendix B.

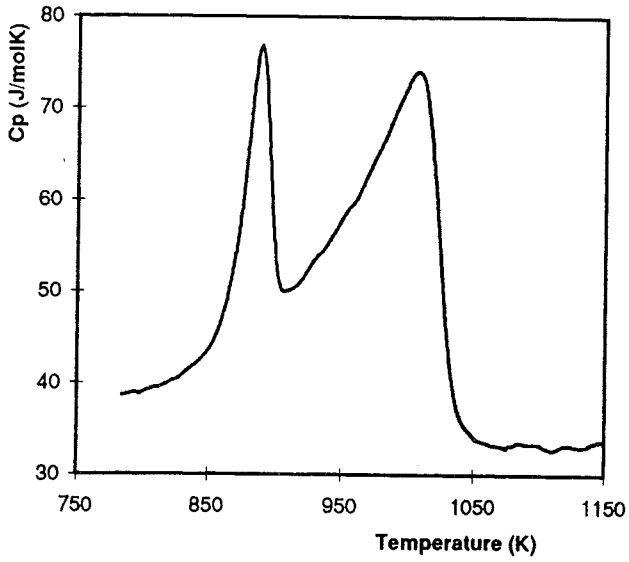

a) S6: T_{aust}: 1273 K Time 60 min

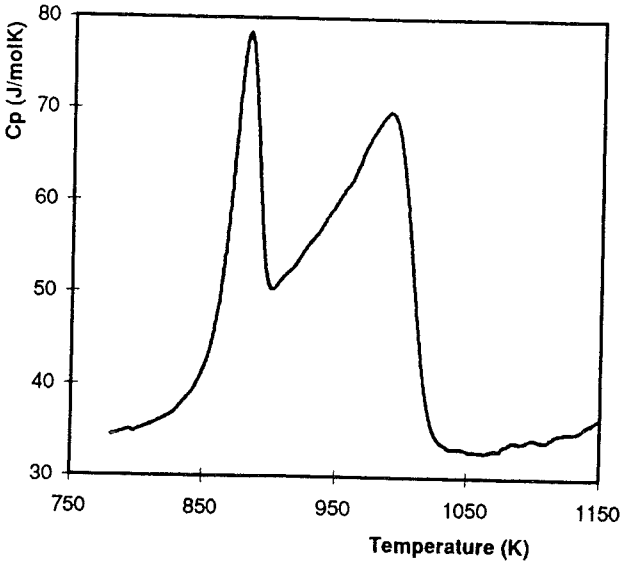

b) S7: T_{aust}: 1323 K Time 20 min

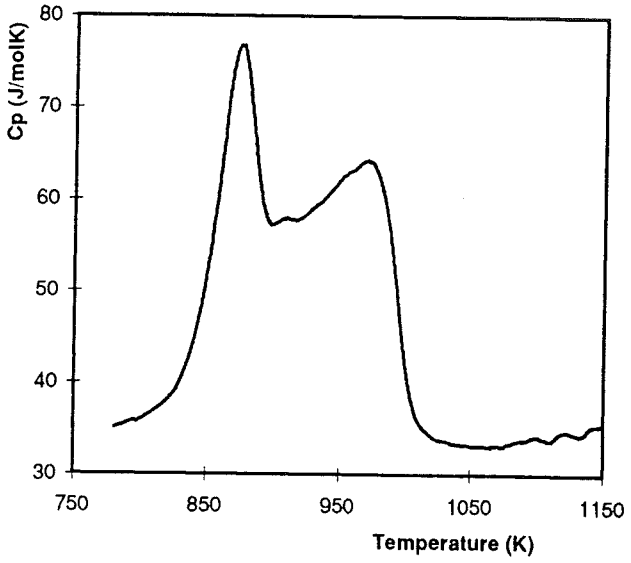

c)S8: T_{aust}: 1373 K Time 20 min

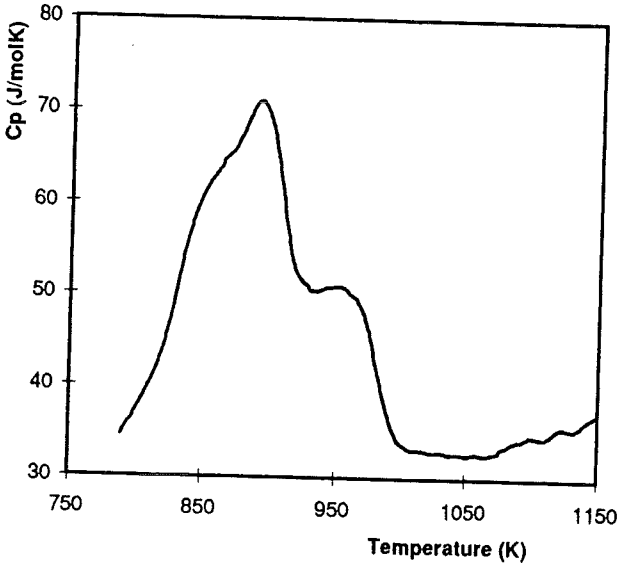

d) S9: T_{aust}: 1423 K Time 20 min

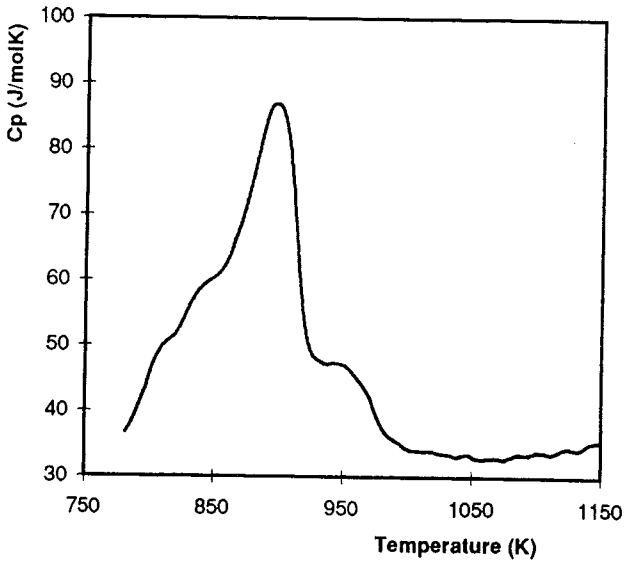

e) S10: T_{aust}: 1473 K Time 20 min

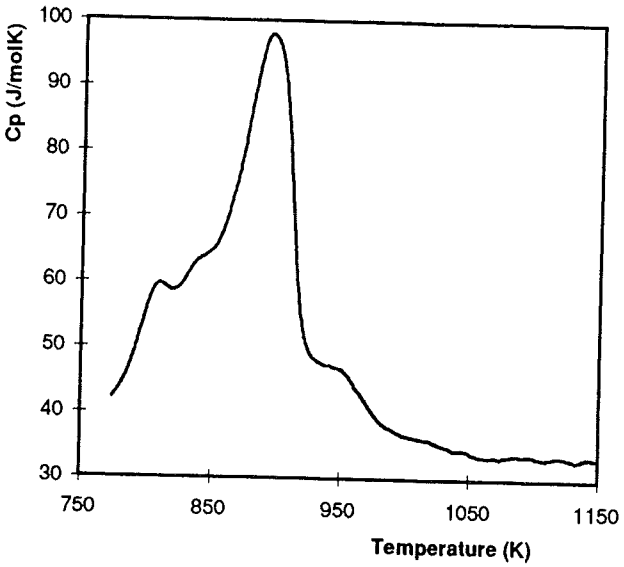

f) S11: T_{aust}: 1523 K Time 20 min

Fig. 5.2 a-f: The c_p vs. temperature measured with the DTA for temperature programmes S6 to S11.

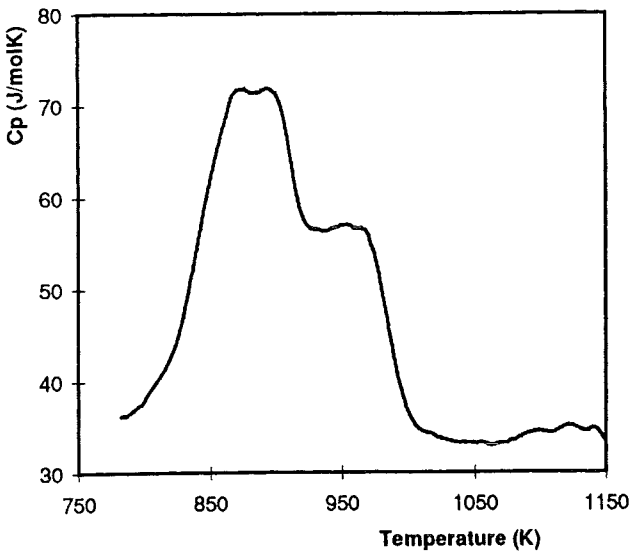

a) S12: T_{aust}: 1423 / 1173 K Time 10 / 15 min

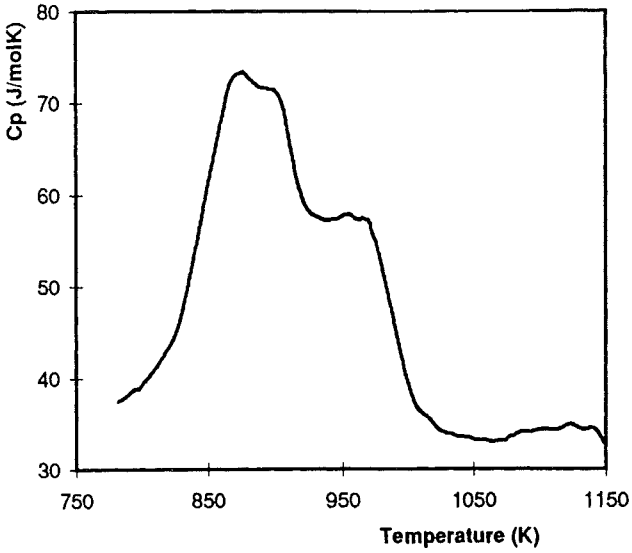

b) S13: T_{aust}: 1423 / 1173 K Time 10 / 60 min

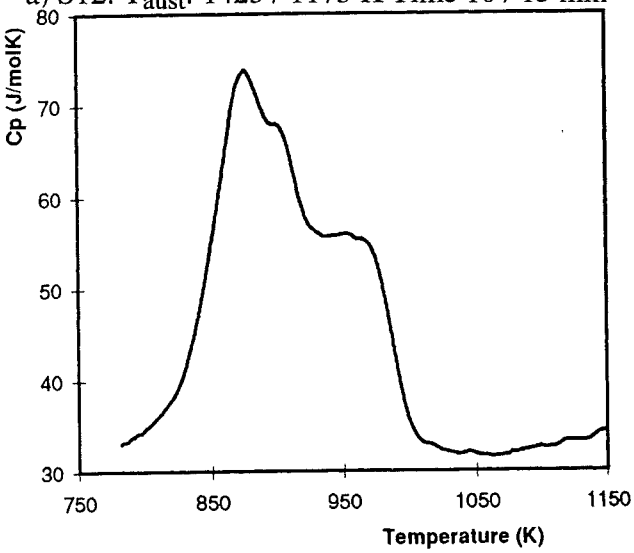

c)S14a: T_{aust}: 1423 / 1273 K Time 10 / 15 min

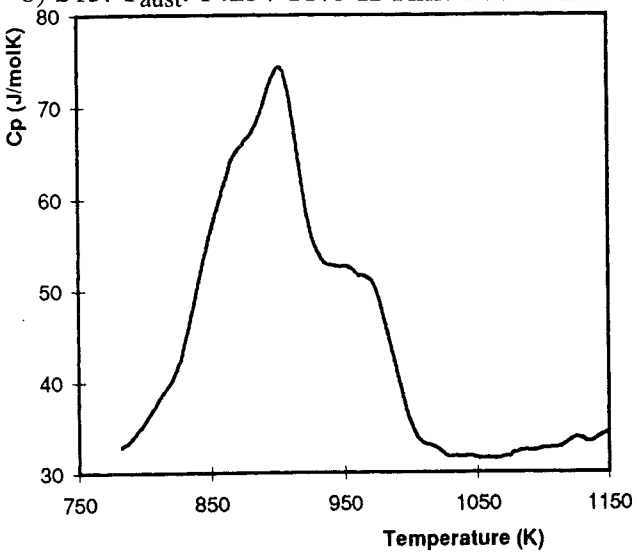

d) S14b: T_{aust}: 1423 / 1273 K Time 10 / 15 min

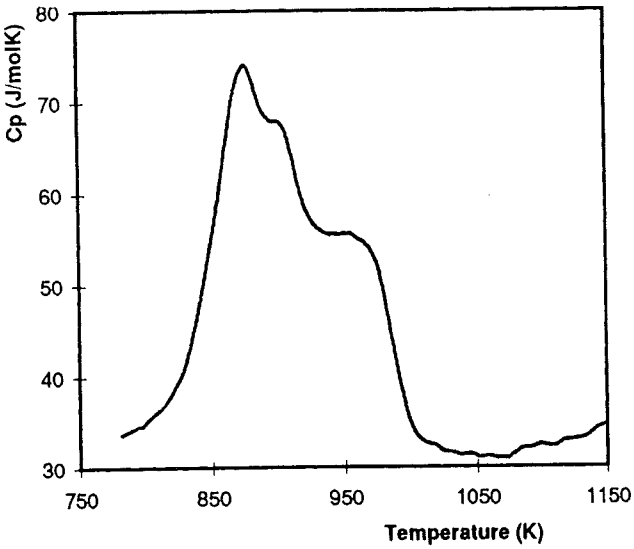

e) S15: T_{aust}: 1423 / 1273 K Time 10 / 25 min

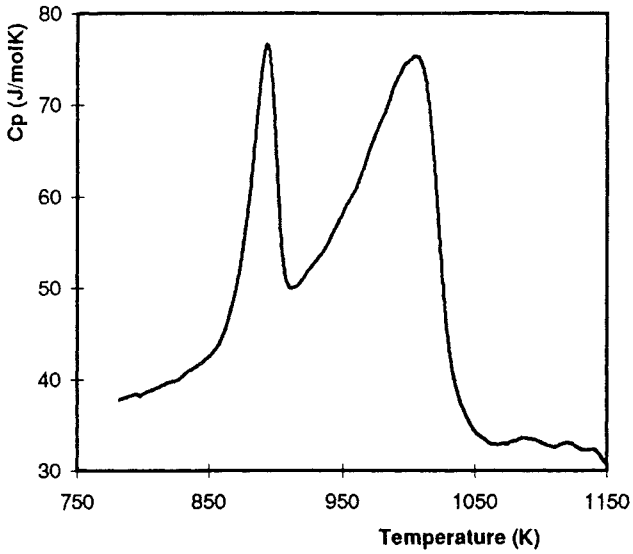

f) S16: T_{aust}: 1473 / 573 / 1173 K
Time 20 / 15 / 20 min

Fig. 5.3 a-f: The c_p vs. temperature measured with the DTA for temperature programmes S12 to S16.

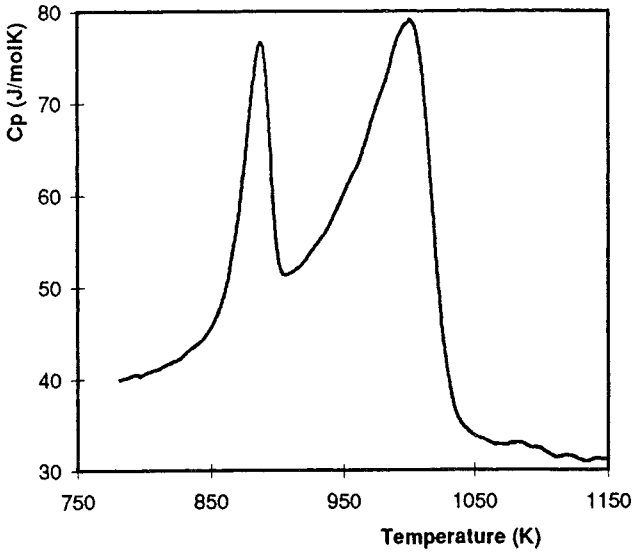

a) S17: T_{aust}: 1473 / 573 / 1273 K Time 20 / 15 / 20 min

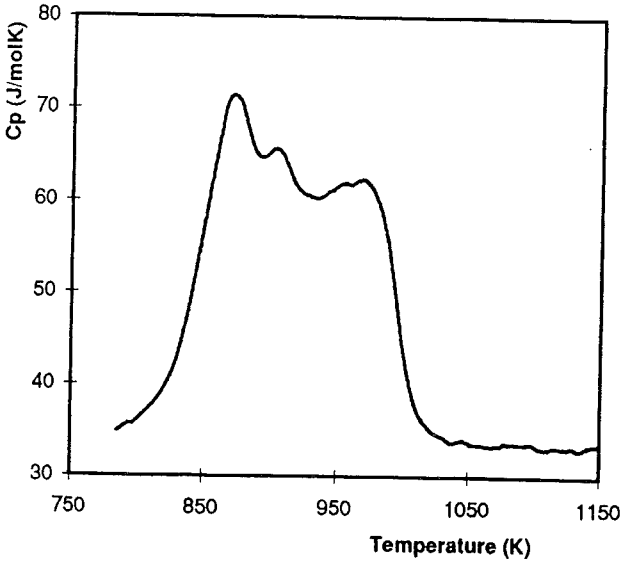

b) S18: T_{aust}: 1473 / 573 / 1373 K Time 20 / 15 / 20 min

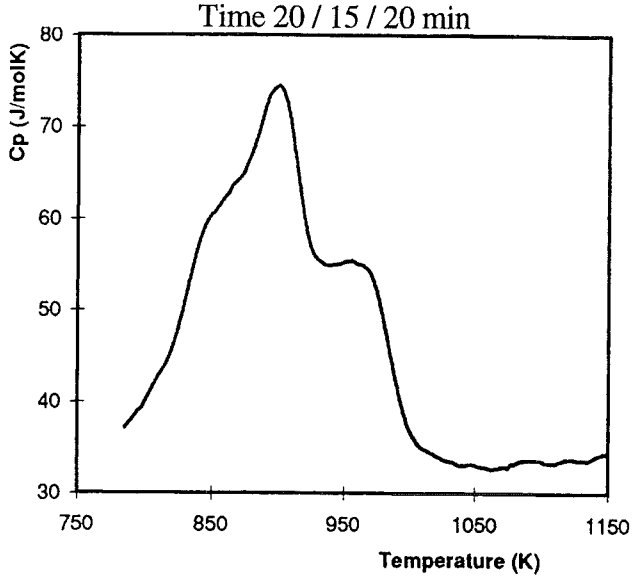

c)S19: T_{aust}: 1473 / 573 / 1423 K Time 20 / 15 / 20 min

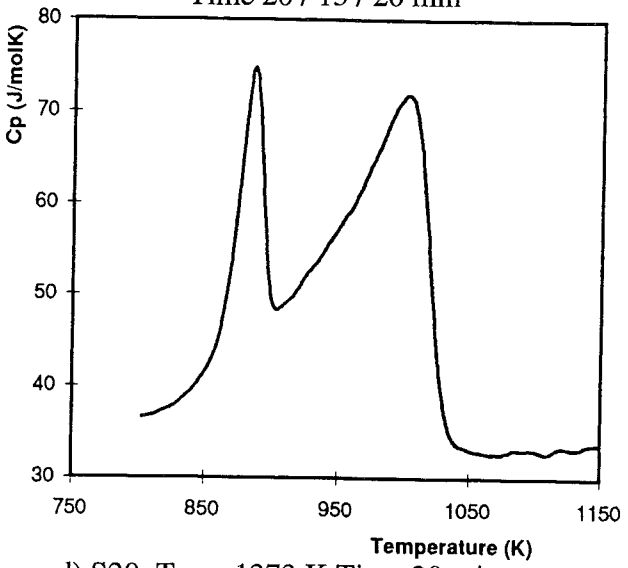

d) S20: T_{aust}: 1273 K Time 20 min

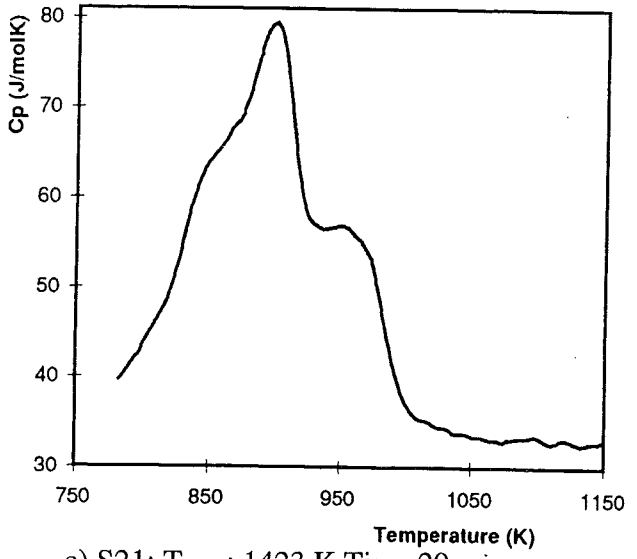

e) S21: T_{aust}: 1423 K Time 20 min

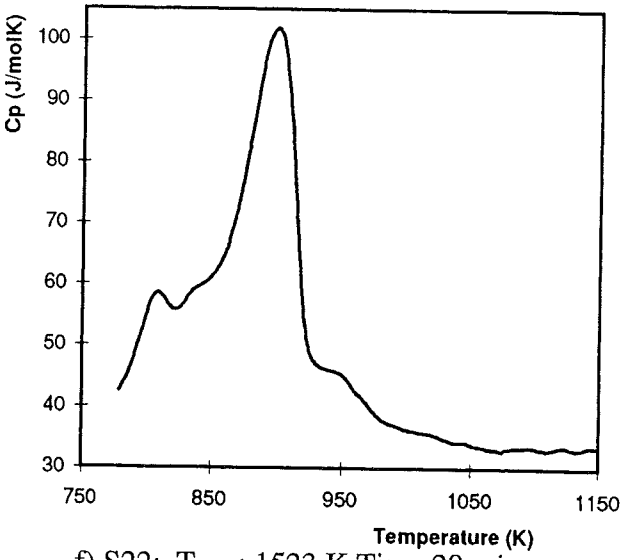

f) S22: T_{aust}: 1523 K Time 20 min

Fig. 5.4 a-f: The c_p vs. temperature measured with the DTA for temperature programmes S17 to S22.

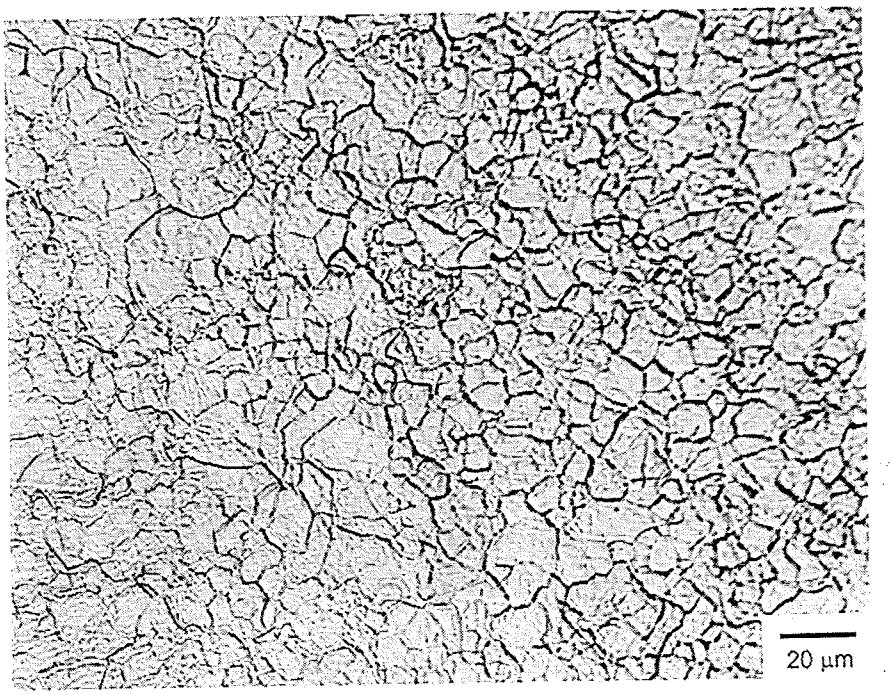

Fig. 5.5: Austenite grain structure (50 x) after annealing at 1273 K.

Fig. 5.6: Austenite grain structure (500 x) after annealing at 1473 K.

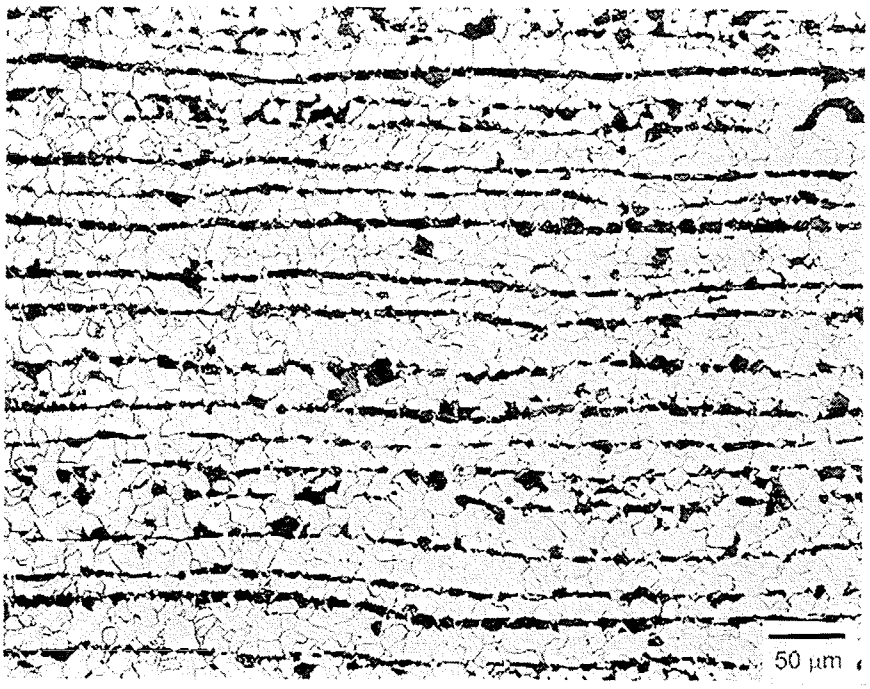

Fig. 5.7: The microstructure (200 x) after annealing at 1273 K and cooling down at 20 K/min, consisting of allotriomorphic ferrite (the white grains) and pearlite (the dark area's).

Fig. 5.8: The microstructure (100 x) after annealing at 1373 K and cooling down at 20 K/min. The microstructure consists of irregular allotriomorphic ferrite, small amounts of Widmannstätten ferrite (needle shaped grains) and pearlite.

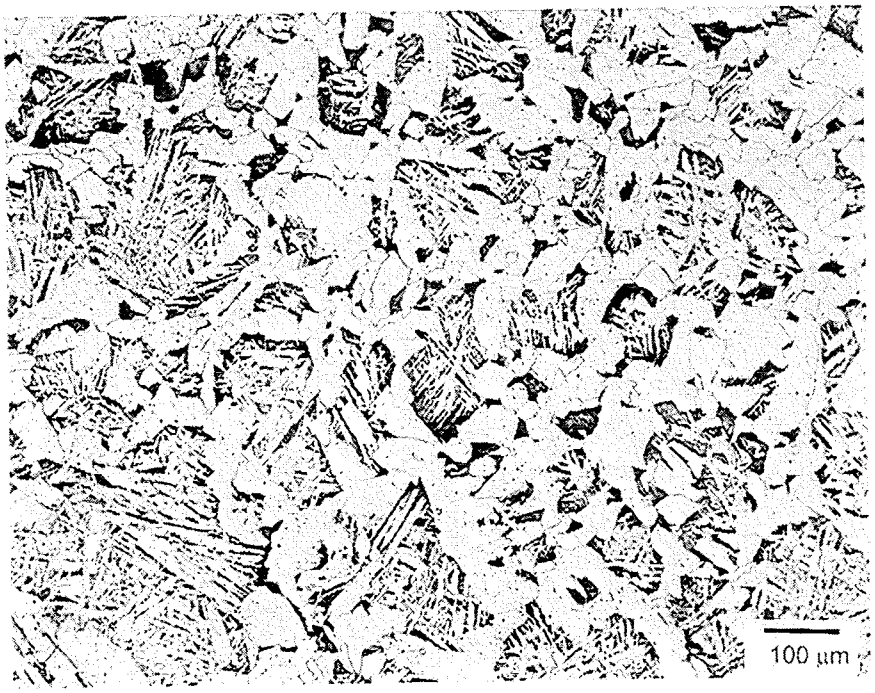

Fig. 5.9: The microstructure (100 x) after annealing at 1423 K and cooling down at 20 K/min. The microstructure consists of allotriomorphic ferrite with pearlite colonies and a mixture of needle-shaped Widmannstätten ferrite with small pearlite colonies in between the Widmannstätten ferrite.

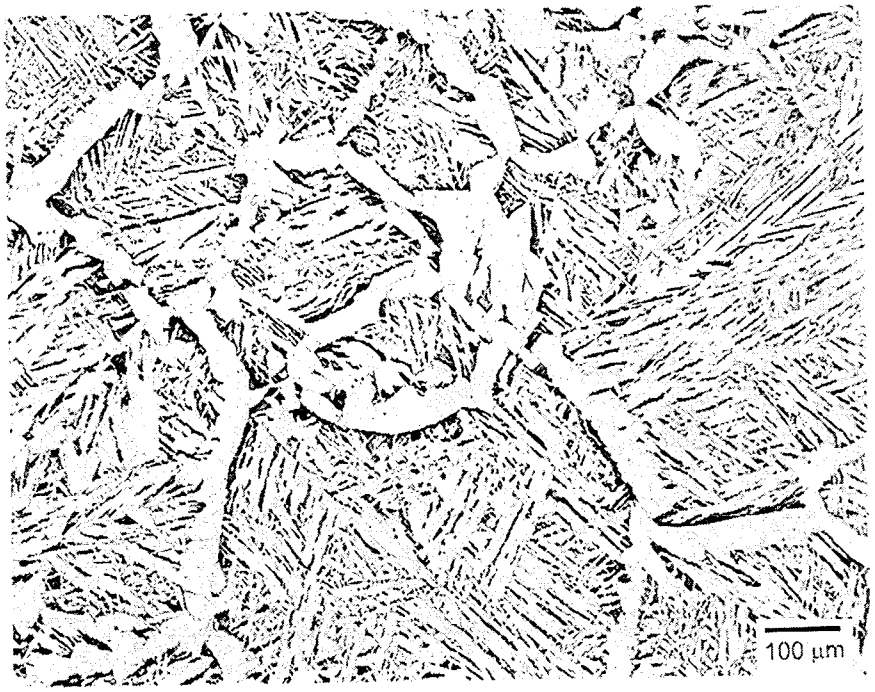

Fig. 5.10: The microstructure (100 x) after annealing at 1473 K and cooling down at 20 K/min consisting of a small layer of allotriomorphic ferrite at the austenite grain boundary, and in the centre of the former austenite grains a mixture of Widmannstätten ferrite, pearlite and a small fraction of bainite.

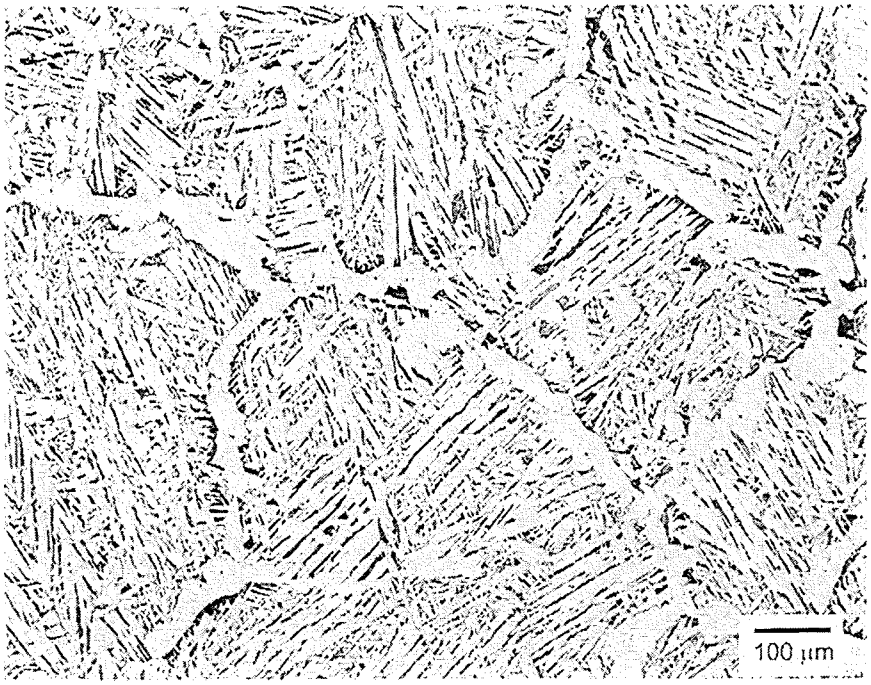

Fig. 5.11: The microstructure (100 x) after annealing at 1523 K and cooling down at 20 K/min consisting of a small layer of allotriomorphic ferrite at the austenite grain boundary, and in the centre of the former austenite grains a mixture of Widmannstätten ferrite, pearlite and bainite.

Fig. 5.12: A close-up of the microstructure (2000 x) after annealing at 1523 K and cooling down at 20 K/min. The dark phase is pearlite and the somewhat lighter, brownish phase is bainite. The white grains are the Widmannstätten needles.

Fig. 5.13: The microstructure (100 x) after annealing at 1423 and 1273 K and cooling down at 20 K/min. The microstructure consists of allotriomorphic ferrite with pearlite colonies and a mixture of needle-shaped Widmannstätten ferrite with small pearlite colonies in between the Widmannstätten ferrite.

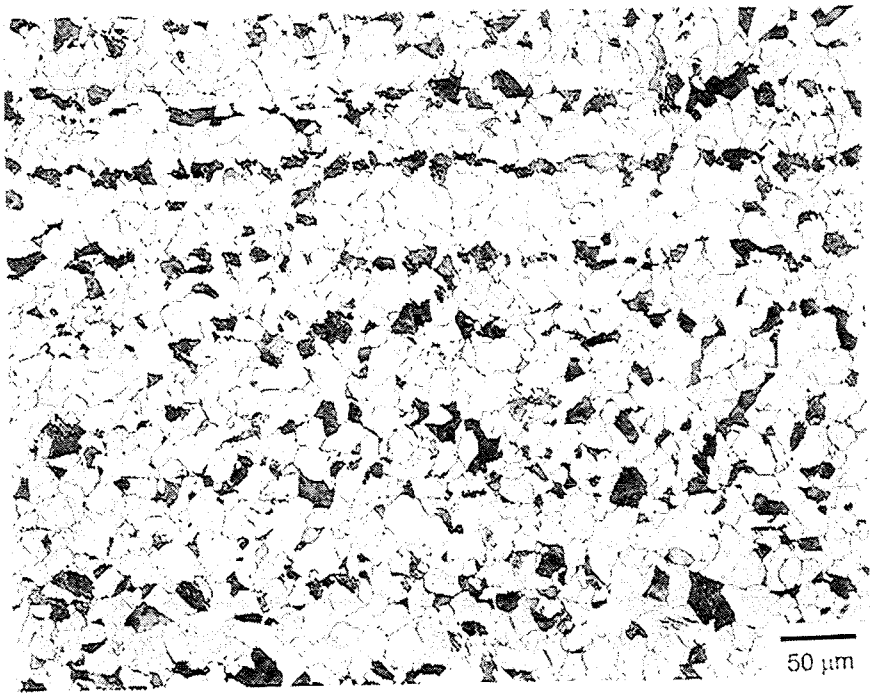

Fig. 5.14: The microstructure (200 x) after annealing at 1473, cooling down to 573 K, annealing at 1273 K and cooling down again (at 20 K/min). The microstructure consisting of allotriomorphic ferrite and pearlite.

Fig. 5.15: The microstructure after annealing at 1473, cooling down to 573 K, annealing at 1423 K and cooling down again (at 20 K/min). The microstructure consists of allotriomorphic ferrite with pearlite colonies and a mixture of needle-shaped Widmannstätten ferrite with small pearlite colonies in between the Widmannstätten ferrite.

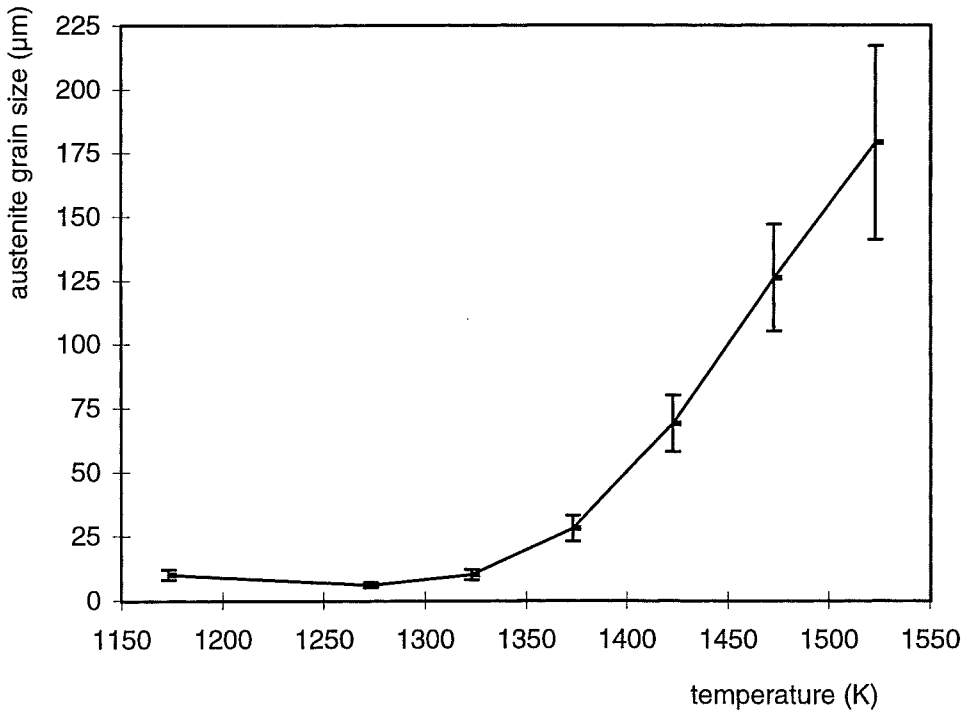

Fig. 5.16: The austenite grain size of HO4 for austenitising 20 min at different austenitising temperatures. The error bars indicate the 95 % confidence limit.

§5.1.2. Light microscopy

Both the austenite and transformed microstructures of the samples used for the DTA experiments have been photographed using light microscopy. A characteristic selection of these photos is presented in the fig.5.5 to 5.15. In fig.5.5 and 5.6 the austenite grain structure is presented for two austenitising temperatures 1273 and 1473 K. The austenite grain growth resulting from the higher austenitisation can be seen very clearly. For the transformed microstructures presented in fig. 5.7 to 5.15, the white, block-shaped grains are allotriomorphic ferrite, the dark area's are pearlite. The white needles, visible in the microstructures for annealing at 1373 K and higher are Widmannstätten ferrite. In fig. 5.12 a close-up is presented of both the bainite (brown area's) and the pearlite (dark area's).

§5.1.3. Austenite grain size

The austenite grain sizes and the 95% confidence limit have been determined from the DTA samples using the Lineal Intercept Technique as described in §4.1.3. The austenite grain sizes measured from the DTA samples as presented in table 5.1 are plotted in fig. 5.16.

Table 5.1: The austenite grain sizes after annealing at different austenitising temperatures

Temp. 1 [K]	Temp. 2 [K]	Austenite grain size [μm]	95% Confidence Limit (i.e. error) [μm]
1173	-	10	2
1273	-	6	1
1323	-	10	2
1373	-	28	5
1423	-	69	11
1473	-	126	21
1523	-	179	38
1423	1273	69	9
1423	1173	73	12

§5.2. Determination of the fractions solute and precipitated Nb

Table 5.2 presents the wt. percentages precipitated and solute Nb for the different austenitising conditions described in table 4.2. For the quenched samples, the amount of solute Nb for the different austenitising conditions is plotted in fig.5.17. The x-axis represents the time during which the sample is austenitised at 1273 K. For three measurements the samples are annealed at 1273 K. Three other measurements are annealed for 20 minutes at 1473 K first and then austenitised at 1273 K for different times. Based on the results of recent analyses, the error in this analysis is estimated to be about 15 %. This error is estimated based on series of duplication determinations. An indication of the

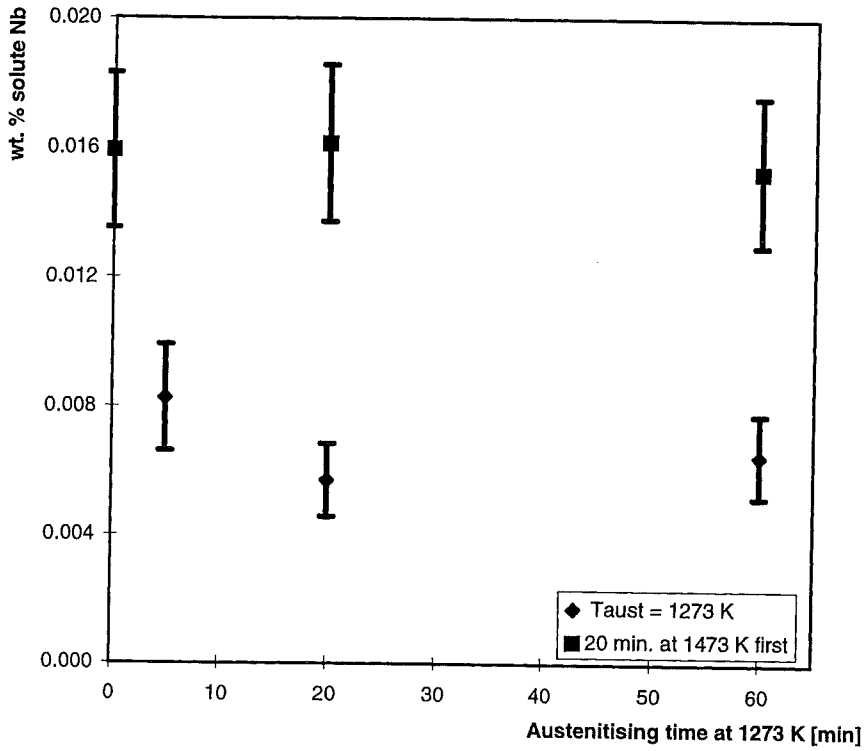

Fig. 5.17: The wt. % Nb in solution for austenitising for different temperatures at 1273. Three samples are austenitised for 20 minutes at 1473 K before holding at 1273 K. Zero minutes at 1273 means that the sample was not held at 1273 K.

systematic error can be derived from the total amount of Nb detected (which for this steel should be 0.020 wt. % Nb).

Table 5.2: The fractions of solute and precipitated Nb in the austenite and the total amount of Nb determined during the analysis after annealing at different austenitising conditions.

			Nb content [wt. % Nb]		
Temp 1 / 2 [K]	Time at T1/T2 [min]	quench	solute Nb a)	precipitated Nb b)	total Nb content
1273 / -	5 / -	y	0.0082	0.0111	0.0193
1273 / -	20 / -	y	0.0057	0.0130	0.0187
1273 / -	60 / -	y	0.0065	0.0121	0.0185
1473 / -	20 / -	y	0.0160	0.0034	0.0194
1473 / 1273	20 / 20	y	0.0162	0.0038	0.0200
1473 / 1273	20 / 60	y	0.0153	0.0039	0.0192
1473 / -	20 / -	n	0.0164	0.0038	0.0202

ad a) The wt. % solute Nb is the sum of the Nb contents of the electrolyte and the filtrate solution.

ad b) The wt. % precipitated Nb is the Nb content in the two filters (i.e. melt).

§5.3. Predicted transformation behaviour of HO4

The progress of the transformation for the HO4 steel was predicted using the transformation model described in §2.2. The transformation behaviour was calculated for a cooling rate of 20 K/min (as used in all DTA experiments) for six of the austenite grain sizes determined from the DTA samples (corresponding to austenitisation at six different temperatures). Using equation 3.6, the predicted phase fractions have been converted into the total c_p (i.e. including the extra enthalpy generated by the transformation). The transformed fractions and the values of c_p for the six austenite grain sizes are presented in fig.5.18 to 5.23. The enthalpy differences between austenite and ferrite and between austenite and pearlite and the specific heat for the different phases required for this calculation are calculated using Thermocalc and presented in fig.5.24.

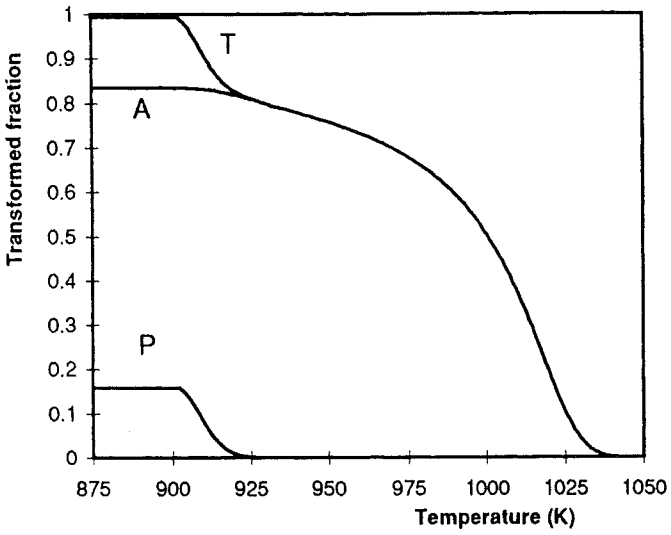

(a)

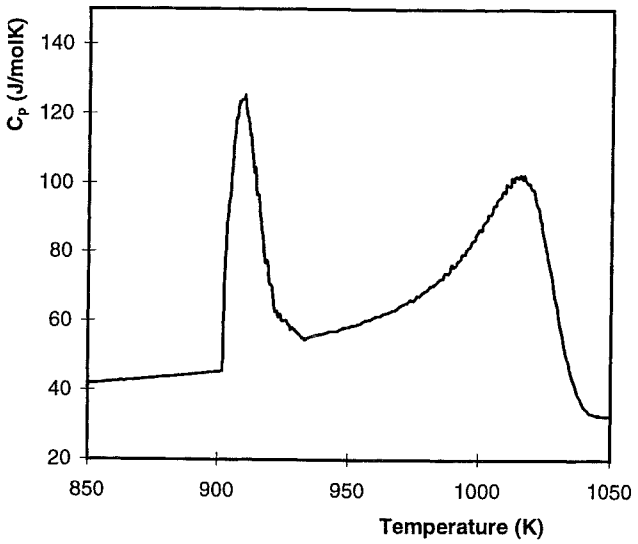

(b)

Fig.5.18: The predicted phase fractions (a) and resulting total c_p (b) for a 6 μm austenite grain size (T_{aust}= 1273 K) where T stands for the total fraction transformed, A stands for the fraction allotriomorphic ferrite and P stands for the fraction pearlite.

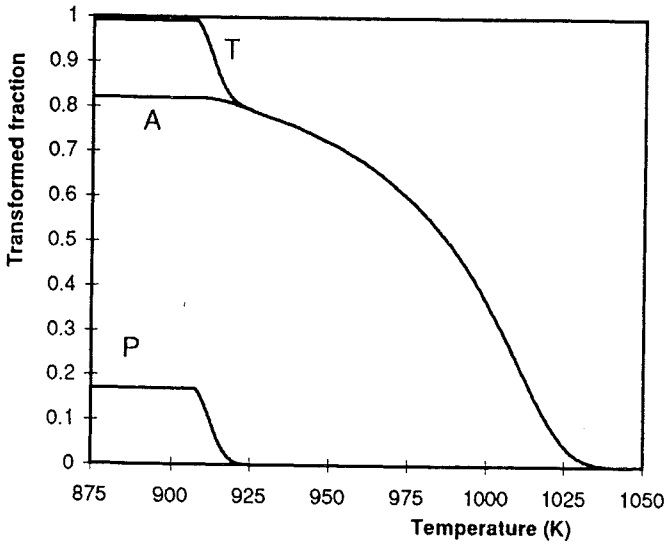

(a)

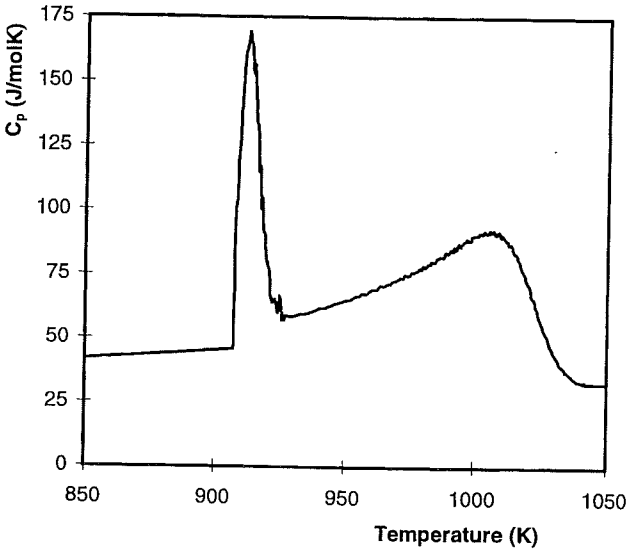

(b)

Fig.19 The predicted phase fractions (a) and resulting total c_p (b) for a 10 μm austenite grain size (T_{aust}= 1323 K) where T stands for the total fraction transformed, A stands for the fraction allotriomorphic ferrite and P stands for the fraction pearlite.

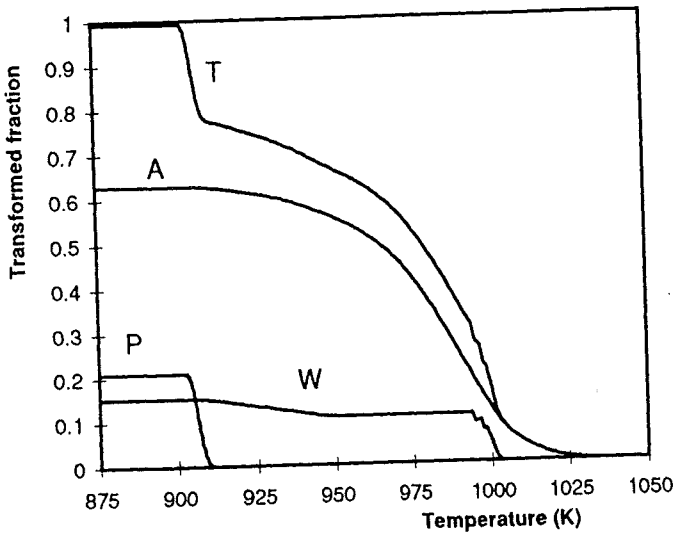

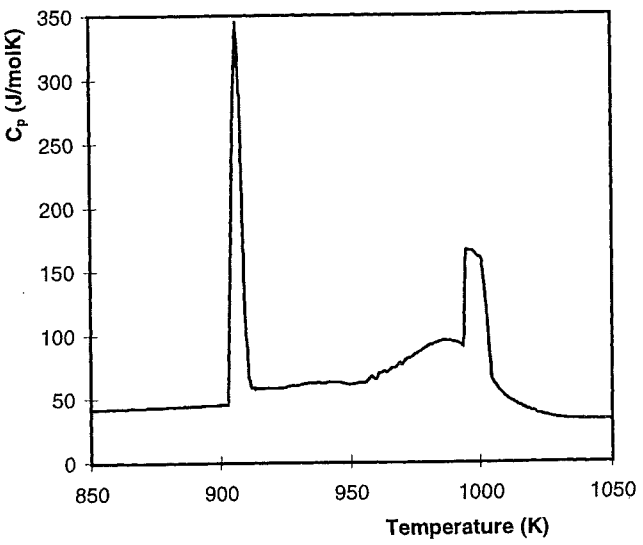

(a) (b)

Fig.5.20 The predicted phase fractions (a) and resulting total c_p (b) for a 28 μm austenite grain size (T_{aust}= 1373 K). T stands for the total fraction transformed, A stands for the fraction allotriomorphic ferrite, W stands for the fractionWidmannstätten ferrite and P stands for the fraction pearlite.

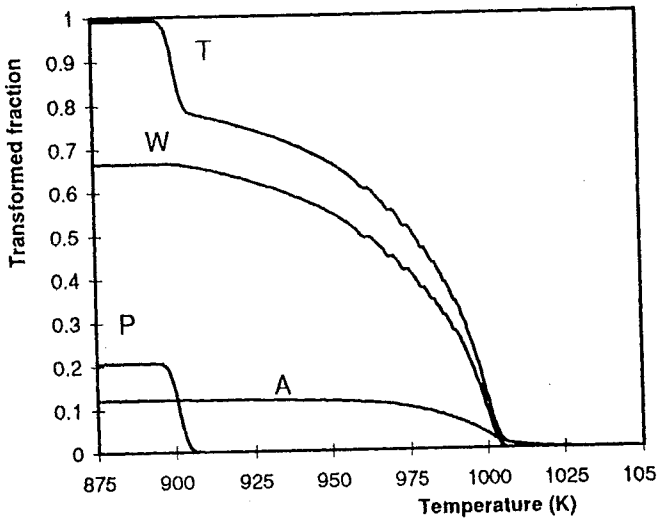

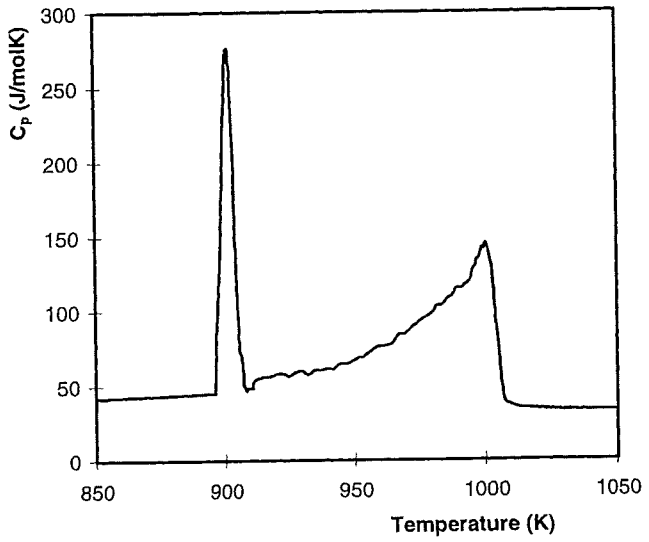

(a) (b)

Fig.5.21 The predicted phase fractions (a) and resulting total c_p (b) for a 69 μm austenite grain size (T_{aust}= 1423 K). T stands for the total fraction transformed, A stands for the fraction allotriomorphic ferrite, W stands for the fraction Widmannstätten ferrite and P stands for the fraction pearlite.

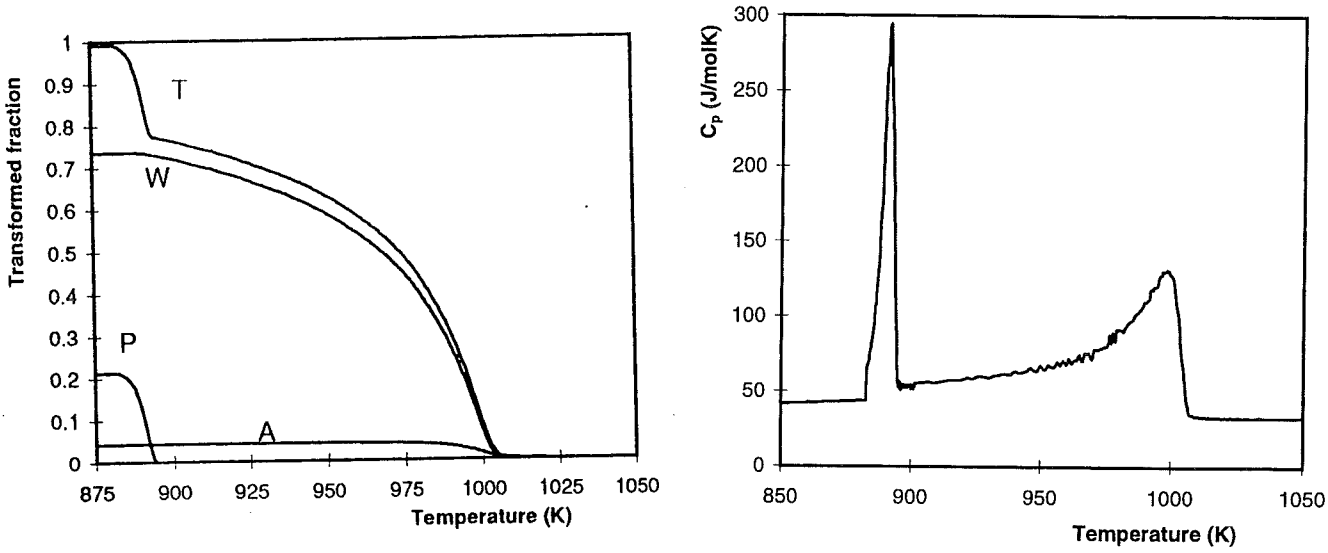

(a) (b)

Fig.5.22 The predicted phase fractions (a) and resulting total c_p (b) for a 126 μm austenite grain size (T_{aust}= 1473 K). T stands for the total fraction transformed, A stands for the fraction allotriomorphic ferrite, W stands for the fraction Widmannstätten ferrite and P stands for the fraction pearlite.

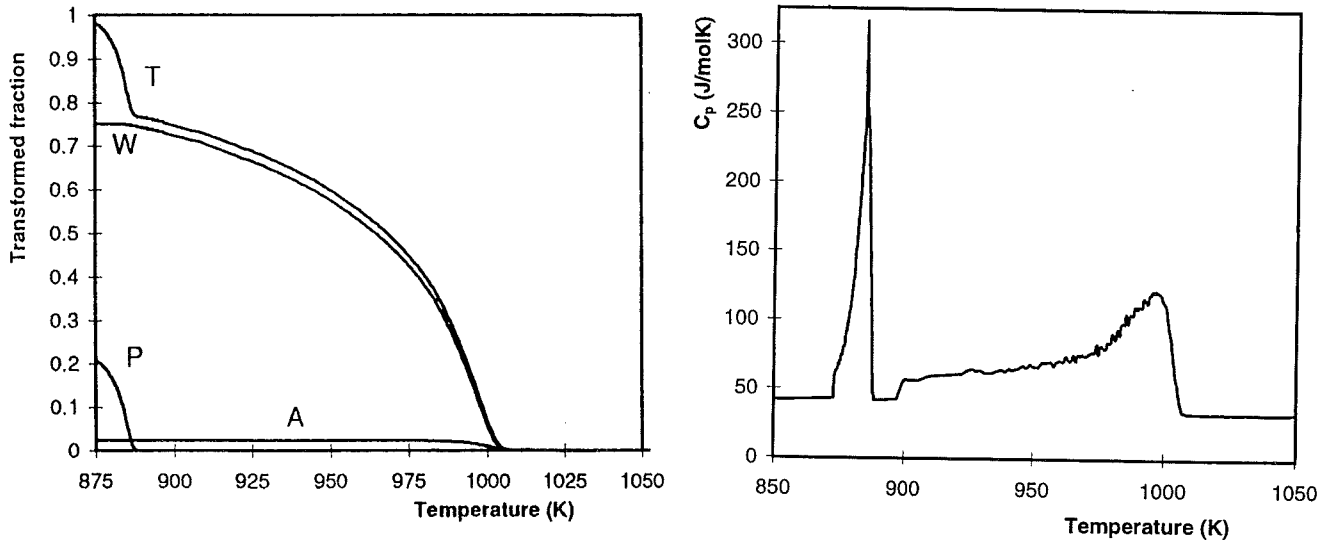

(a) (b)

Fig.5.23 The predicted phase fractions (a) and resulting total c_p (b) for a 179 μm austenite grain size (T_{aust}= 1523 K). T stands for the total fraction transformed, A stands for the fraction allotriomorphic ferrite, W stands for the fraction Widmannstätten ferrite and P stands for the fraction pearlite.

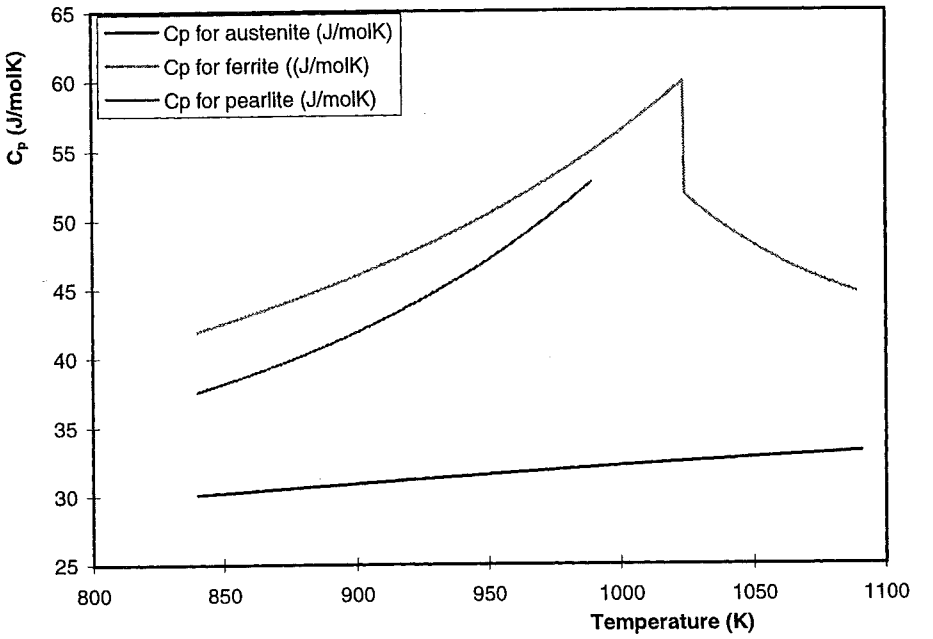

(a)

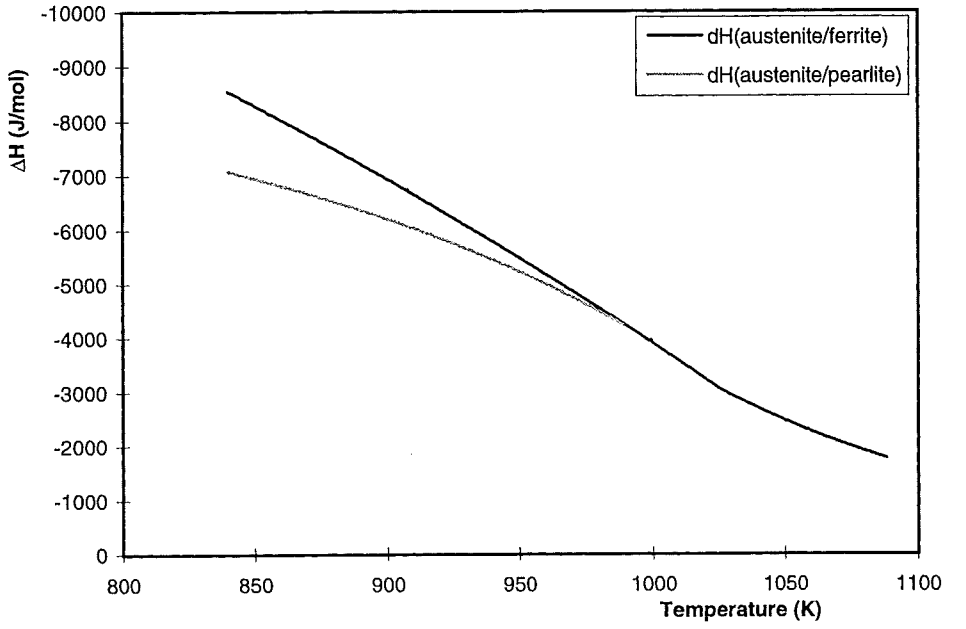

(b)

Fig. 5.24: Values for c_p (a) of austenite, ferrite and pearlite and the enthalpy differences $\Delta H^{\gamma/\alpha}$ and $\Delta H^{\gamma/P}$ (b) calculated by Thermocalc.

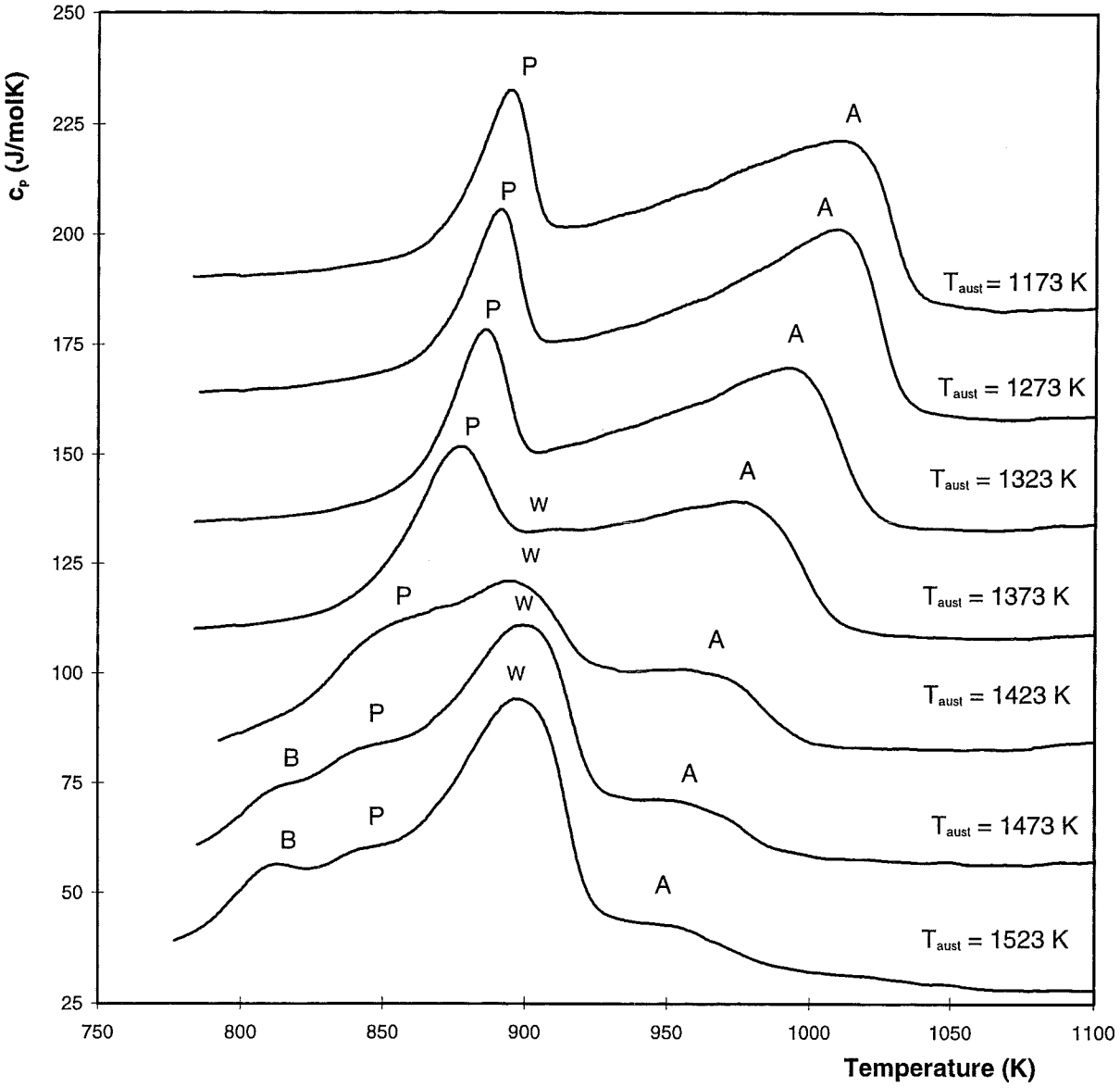

Fig. 6.1: The c_p curves for annealing at different austenitising temperatures as measured with the DTA. The value of c_p is raised 25 J/molK for each curve above the curve for austenitisation temperature 1523 K. Four peaks can be distinghuished which are marked A, W, P and B for, respectively, allotriomorphic ferrite, Widmanstätten ferrite, pearlite, and bainite.

6 Discussion

§6.1 The DTA experiments

§6.1.1. The c_p curves

When looking at the c_p curves for the different austenitising temparatures, it can be seen that an increasing austenitising temperature leads to a significantly different transformation behaviour. Three different transformation patterns can be distinguished. When austenitising at a low temperature (T_{aust} up to 1323 K), two transformation peaks (the A peak and the P peak) are found. For austenitising at 1373 K, a third transformation peak (the W peak) becomes visible between the A and the P peak. When austenitising at 1423 K, the W peak increases at the expense of the other two transformation peaks. After annealing at even higher austenitising temperatures (T_{aust} =1473 K and 1523 K), a fourth transformation peak (the B peak) becomes visible at transformation temperatures lower than those of the already existing transformation peaks. Also from fig. 6.1 it can be seen very clearly that with increasing austenitising temperature, the transformations shift to lower temperatures.

§6.1.1. The development of the microstructure with increasing austenitising temperature

The phases that are formed during transformation causing the transformation peaks mentioned above can be identified by studying the microstructure of the DTA samples (fig.5.7 to 5.15). The microstructure of the sample austenitised at 1273 K (fig.5.7) shows an allotriomorphic ferrite/pearlite microstructure which means that the first transformation peak is the formation of allotriomorphic ferrite followed by the formation of pearlite. The microstructure of the samples austenitised at temperatures of 1373 K or higher show an increase with temperature of the amount of Widmannstätten ferrite. The extra transformation peak found for these samples can therefore be identified to be caused by the formation of Widmannstätten ferrite. As the total amount of ferrite that is formed does not change much as a result of the carbon contents of the steel, the increasing formation of Widmannstätten ferrite leads to a corresponding decrease in the amount of allotriomorphic ferrite that is formed as can be seen in fig.6.1. This can be seen very clearly from the microstructure of the sample austenitised at 1523 K (fig.5.11) where the grain boundaries are covered with allotriomorphic ferrite and the centre of the austenite grain consists of Widmannstätten ferrite and pearlite.

The fourth transformation peak (the B peak) which only becomes visible after austenitising at 1473 K and 1523 K is identified to be upper bainite. This upper bainite, which can be seen in fig.5.12 can be distinguished from pearlite by its light brown appearance and the lack of alternating (relatively coarse) ferrite/pearlite plate structure.

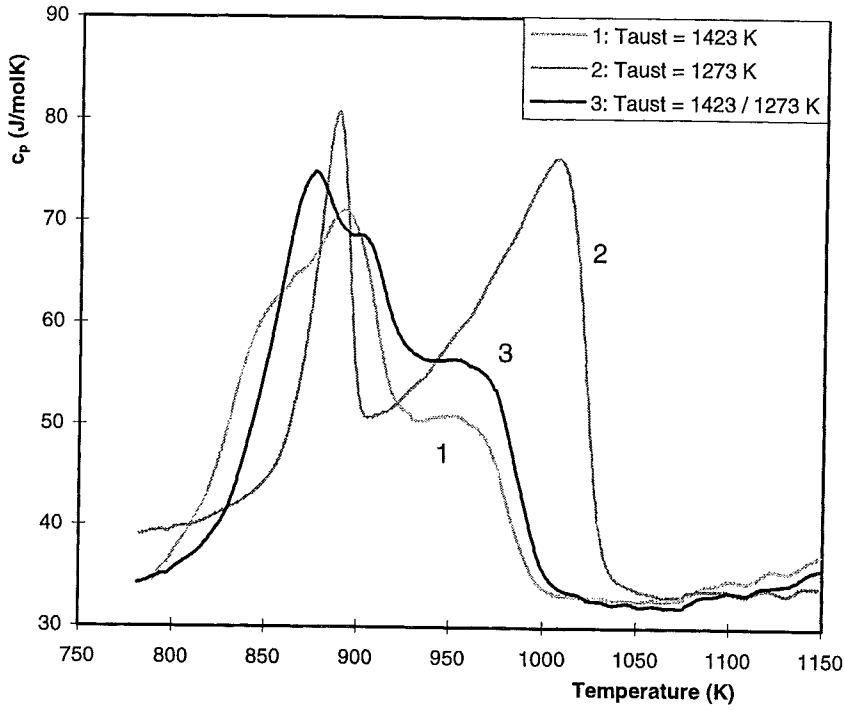

Fig. 6.2: The DTA curves for austenitising at 1423 and 1273 K next to the DTA curve for austenitising first at 1423 K followed by austenitising at 1273 K.

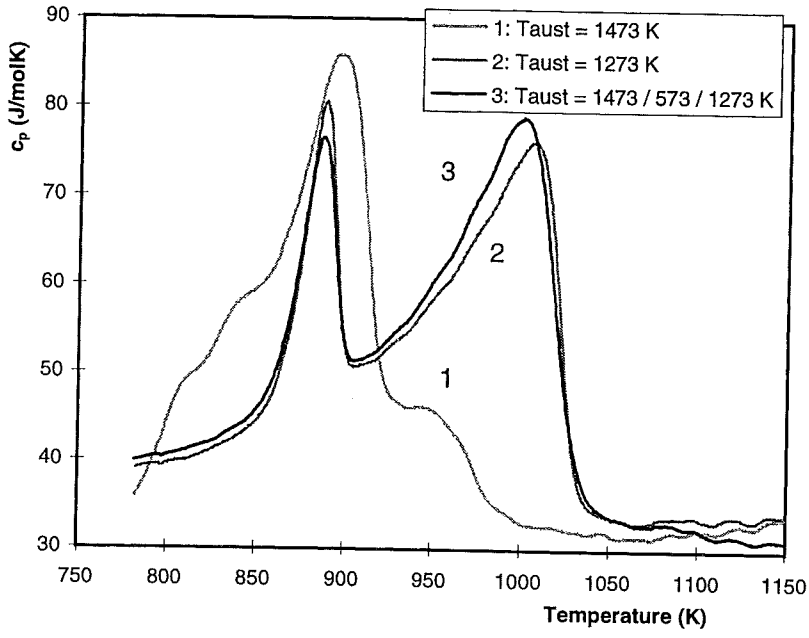

Fig. 6.3: The DTA curves for austenitising at 1473 and 1273 K next to the DTA curve for austenitising at 1473 K cooling down to 573 K followed by austenitising at 1273 K.

Although the formation of this bainite reduces the amount of pearlite that is formed, this only partly accounts for the decrease of the height of the pearlite peak that can be observed in fig.6.1. The main reason for this decrease of the pearlite peak height is the formation of Widmannstätten ferrite. The growth mechanism of Widmannstätten ferrite results in local carbon enrichment of the remaining austenite due to which the temperature range of pearlite formation is enlarged and the peak height is reduced. Finally, decarburisation will also cause a small reduction of the fraction of pearlite formed. Although this effect will be small compared to the reduction caused by annealing a sample twice (as in exp S2 and S14), annealing at higher austenitising temperatures will increase decarburisation and reduce the fraction of pearlite formed.

If ferrite is formed at temperatures above the Curie temperature, the exothermic transition of paramagnetic ferrite to ferromagnetic ferrite also causes a peak in the DTA curve. Using Thermocalc, the Curie temperature has been determined to be 1024 K. Only for samples annealed at low temperatures a small fraction of ferrite will have formed at this temperature and the thermal effect will therefore be very small. Also, the thermal effect caused by the formation of ferrite itself will dominate the extra thermal energy caused by this transition. The magnetic transition does therefore not result in a visible peak in the c_p curve.

As can be seen in fig.6.1, an increase in the austenitising temperature results in a significant decrease of the transformation start temperature. Whereas the transformation after austenitising at 1173 K starts at about 1040 K, the starting temperature of the transformation after austenitising at 1523 K is lowered to approximately 990 K. Such a retardation is also observed for the formation of pearlite for which the peak temperature is lowered from approximately 890 K (T_{aust} = 1173 K) to about 840 K (T_{aust} = 1523 K).

If the sample is austenitised at a second, lower austenitising temperature, the transformation behaviour changes (see fig.6.2). It can be seen that holding the sample at 1273 K after austenitising it at 1423 K first (curve 3), results in a increase of the transformation start temperature of approximately 10 K. Also the fraction allotriomorphic ferrite formed increases at the expense of the fraction Widmannstätten ferrite. As discussed earlier in this paragraph, less Widmannstätten leads to a smaller temperature range of pearlite formation, resulting in a higher and more narrow pearlite peak as can be seen in curve 3.

However, if the sample has been cooled down to 573 K between the two austenitising steps as can be seen in fig.6.3 the transformation behaviour is fully dominated by the second austenitising temperature. The small decrease of the pearlite peak in favour of the ferrite peak is caused by decarburisation as during heating for the second time carbon diffusion supplies the decarburised outer layer with carbon from the centre of the sample. During the second austenitisation, however, this outer layer is decarburised again.

§6.2. The effects of the austenitising temperature on the sample before transformation

By varying the austenitising temperature, the fraction of Nb precipitates changes as the solubility of Nb increases with temperature. At higher austenitising temperatures, more of the Nb is brought into solution thus reducing the volume fraction of Nb precipitates. As the volume fraction of Nb precipitates decreases, the spacing between these precipitates increases. As a result, the pinning effect that is inhibiting the austenite grain growth, is reduced. For austenisation temperatures at which most or all of the Nb is in solution, extensive austenite grain growth can occur.
Both the precipitation behaviour of Nb and the austenite grain sizes have been examined and will now be discussed.

§6.2.1. Nb precipitates

The experiments to determine the amounts of NbCN precipitates and solute Nb at two different austenitising temperatures show that the Nb solubility increases with austenitising temperature as already shown in fig.2.11.
Based on these results however no significant influence of the austenitising time can be found. The error of approximately 15 % in the determination of the solubility is mainly caused by two problems in the analysis. One problem is the dissolution procedure of the sample. The samples do not dissolve completely. The remaining sample is like a sponge indicating that the dissolving was not homogeneous. This is believed to be the reason that almost all analyses find the total amount of Nb to be less than expected, as, although precipitates at the outer layer of the remaining sponge are not removed if the surrounding matrix is partly dissolved. This would lead to the underestimation of the total Nb content determined. As only precipitates and no solute Nb will remain in the spongelike sample in this way, in this work it is assumed that the difference between the analysis and the Nb content in the steel are Nb precipitates. The fractions of precipitated Nb presented in table 5.2 and fig.5.17 should therefore be corrected for this. The total fraction of precipitated Nb therefore consists of the contents of precipitated Nb as determined in the analysis plus the difference between the determined Nb content and the Nb content of the steel. In the discussion therefore, these corrected values for the precipitated fraction Nb are used.
Another problem causing an underestimation of the precipitated fraction is the size of the precipitates. As especially the newly formed precipitates are expected to be very small (as small as a few nm) the pore size of the used filters is relatively large (0.1 μm pore size). Some of the smaller precipitates will therefore be counted to be solute Nb instead of precipitated Nb. This is also indicated by the experiments in which the sample is annealed at 1473 K. As can be seen in fig.5.11, the amount of solute Nb in these samples is independent of the subsequent treatment. Even for the sample that was air cooled, the Nb solubility is still found to be equal to that at 1473 K. It should therefore be concluded that the current method

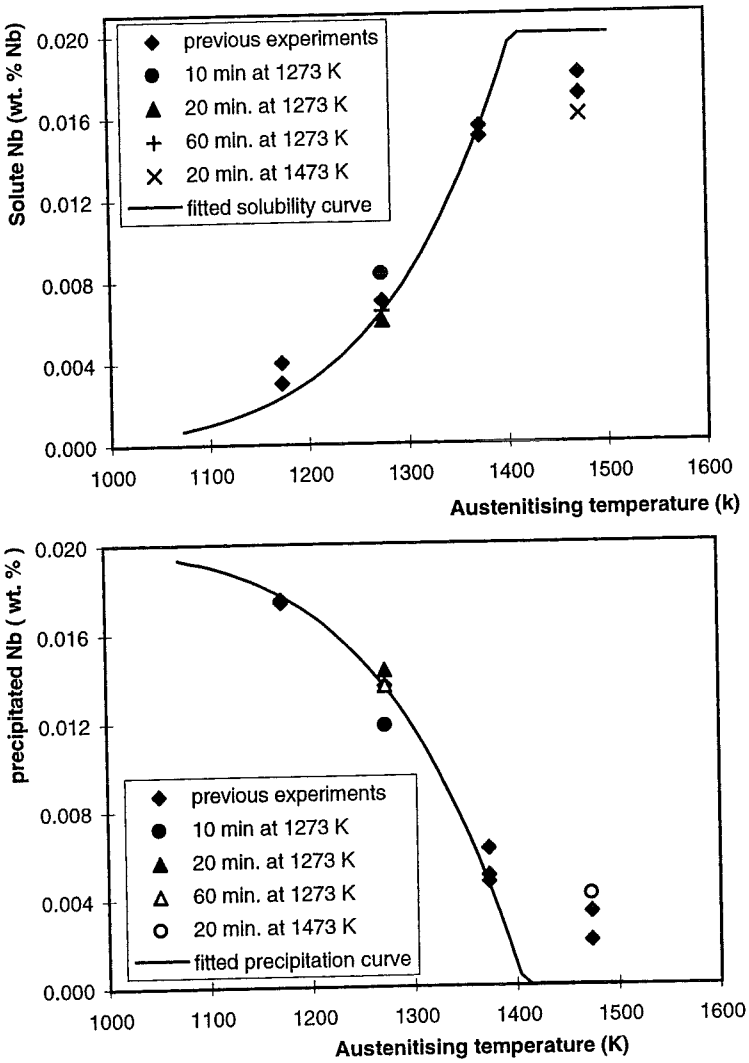

Fig. 6.4: The wt. percentages of solute Nb (a) and precipitated Nb (b) as presented in table 5.2 together with the results of recent experiments to determine the solubility of Nb in HO4 (unpublished data).

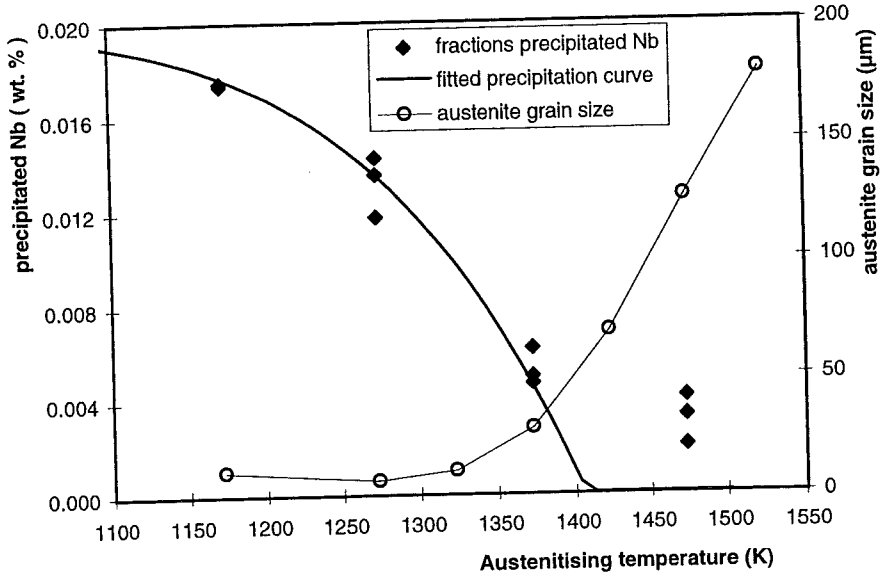

Fig. 6.5: The determined fraction of precipitated Nb plotted together with the determined austenite grain size for annealing at different austenitising temperatures.

of analysis can only be used to determine the solubility of Nb at the highest austenitising temperature. A finding that shows that the newly formed precipitates are much smaller than precipitates that were not dissolved during austenitisation.
Knowing this, the somewhat smaller solubility found for the samples annealed for 20 and 60 min at 1273 K, compared to the solubility of the sample annealed for 5 min at 1273 K, might be caused by Ostwald ripening. Because of this the larger precipitates coarsen at the expense of the smallest, less stable precipitates. This reduces the amount of precipitates passing through the filter and therefore reduces the solubility determined. To determine whether this effect is significant, the amount of Nb precipitates in both electrolyte and filtrate should be determined for several annealing times. A possible way to determine if any precipitates are still in the two solutions is to do an extra filtration using a filter with a smaller pore size (ceramic filters or membranes).
For high austenitising temperatures another problem is found to affect the analysis. Recent experiments [20] show that although all the Nb is expected to be in solution, the analysis always shows a fraction of Nb precipitates of about 0.0035 wt. % Nb. For the determination of a solubility curve these results should be used with caution.
Based on the experiments presented in this report and previous experiments to determine the solubility of Nb in HO4 [20], the solubility curve for Nb in HO4 is reconstructed (fig.6.4a). Based on equation 2.2, a solubility curve has been fitted to indicate the progress of solubility for other austenitisation temperatures. The fitted solubility curve is given by:

$$\log [Nb][C] = 2.2 - 6700\ K/T \qquad (6.1)$$

As it is assumed that the total amount of Nb should be 0.02 wt.% Nb, the corrected fraction of precipitated Nb is the difference of the amount of Nb in solution and the total amount of Nb present in HO4. In fig.6.4b this corrected amount of precipitated Nb is plotted. The fitted solubility curve presented in this figure is defined by the amount of Nb that is not in solution:

$$[Nb]_{precipitated} = [Nb]_{total} - [Nb]_{in\ solution} \qquad (6.2)$$

§6.2.2. The austenite grain size

At temperatures above 1373 K, the austenite grain size of the DTA samples shows a strong increase with austenitising temperature (fig.5.16). This increase of the austenite grain size is a result of the decreasing amount of NbCN precipitates at these high austenitising temperatures. With increasing austenitising temperature, the solubility of Nb in austenite increases. When the solubility approaches the Nb content present in the steel, the volume fraction of Nb precipitates inhibiting the growth of the austenite approaches zero, leading to extensive austenite grain growth. In fig.6.5, the austenite grain size as determined from the DTA samples is presented together with the fractions Nb precipitated (with the correction for the Nb loss during the analysis discussed above). The austenite grain size can be seen to grow excessively for a decreasing fraction precipitated Nb.

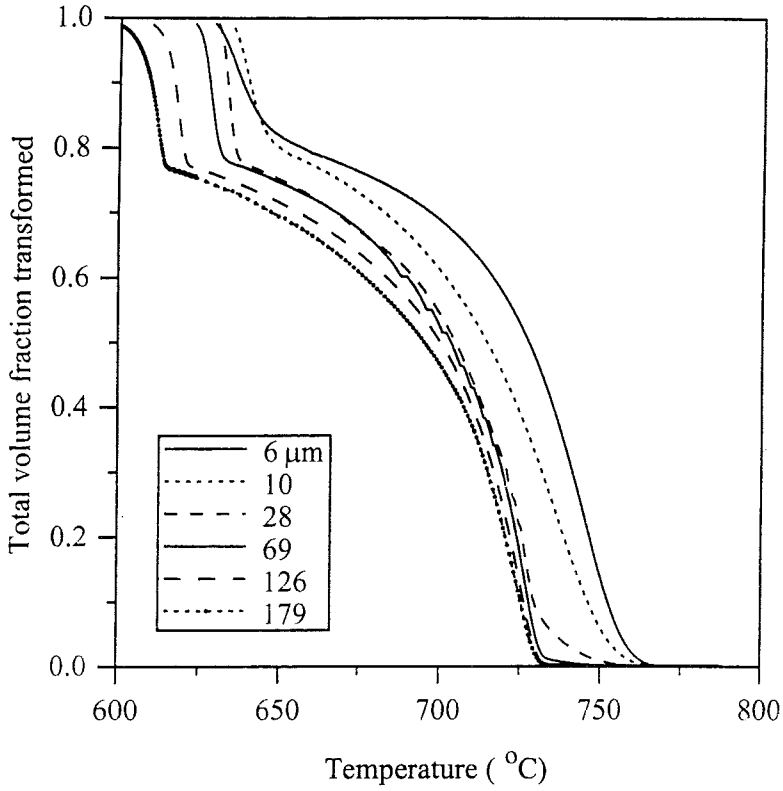

Fig. 6.6: The total fraction transformed predicted by the Cambridge transformation model for the 6 different austenite grain sizes determined for the different austenitising temperatures used in the DTA experiments.

§6.3. Modelling the transformation behaviour for varying austenite grain sizes

The effects of the austenite grain size on the transformation behaviour of HO4 were examined by predicting the transformation behaviour for different austenite grain sizes using the transformation model (§2.2). The total transformed fraction for the different austenitising temperatures (i.e. austenite grain sizes) predicted by the model (fig.6.6) show that an increase of the austenite grain size causes a delay in the start temperature of the ferrite formation and therefore of the pearlite formation. This delay is caused by a reduction of the number of nucleation sites for increasing austenite grain sizes. Also, as can be seen in the figures showing the separate fractions (fig.5.18 to 5.19), the formation of Widmannstätten ferrite as found in the DTA samples, is also predicted for austenitising at 1373 K or higher temperatures.

The growth mechanism of the Widmannstätten ferrite as used in the model is however not in compliance with the results found in the experiments. In the model it is allowed that the Widmannstätten ferrite forms at the same time as allotriomorphic ferrite. Based on the results found in this investigation however, this assumption should be considered to be false. From the microstructures of the DTA samples austenitised at high temperatures (fig.5.10 and 5.11) it can be seen that the austenite grain boundaries are completely covered with allotriomorphic ferrite and that the Widmannstätten ferrite nucleates on the boundary between the allotriomorphic ferrite and the remaining austenite, growing into the centre of the austenite grain. As the allotriomorphic ferrite nucleates on the austenite grain boundaries first, covering all austenite grain boundaries, the microstructures found indicate that the formation of Widmannstätten ferrite occurs subsequent to the formation of allotriomorphic ferrite. Also, the separate transformation peaks for the allotriomorphic and theWidmannstätten ferrite for the samples austenitised at high temperatures (fig.6.1) show that the Widmannstätten ferrite forms subsequent to the allotriomorphic ferrite.

To be able to compare the measured transformation behaviour to the predicted transformation behaviour the predicted fractions transformed are converted into c_p curves (see fig.5.18 to 5.23).

The Widmannstätten growth mechanism assumed in the model has a significant effect on the c_p curves calculated from the predicted phase fractions. If both phases are formed at the same time, the thermal effects as a result of the formation of the two phases are summated. The calculated c_p curves in such cases therefore do not show a separate peak for the formation of the Widmannstätten ferrite. The calculated c_p curves being based upon theoretical calculations, differ from the experimental c_p curves in a few ways.

First, by comparing the experimental with the predicted c_p curves it can be seen that the peak area for the predicted c_p curves is significantly larger than for the experimental c_p curve. Up to now the reason for this difference is not clear. In the near future, this effect is planned to be investigated.

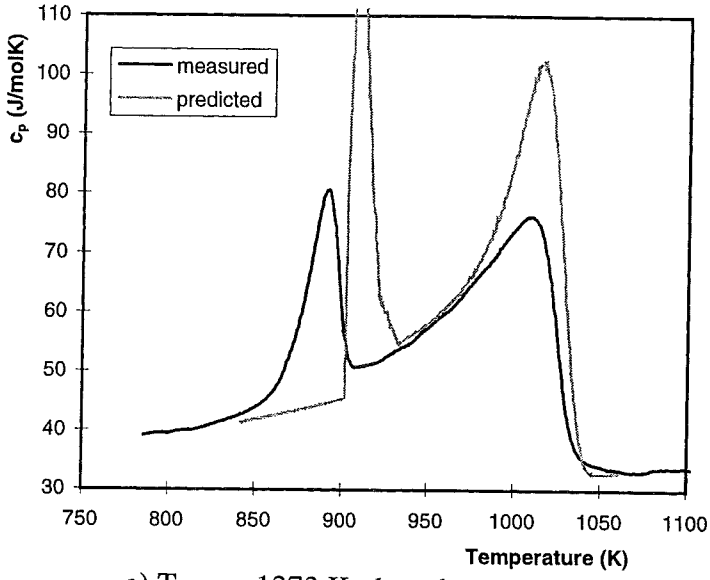

a) T_{aust} = 1273 K; $d\gamma$ = 6 µm

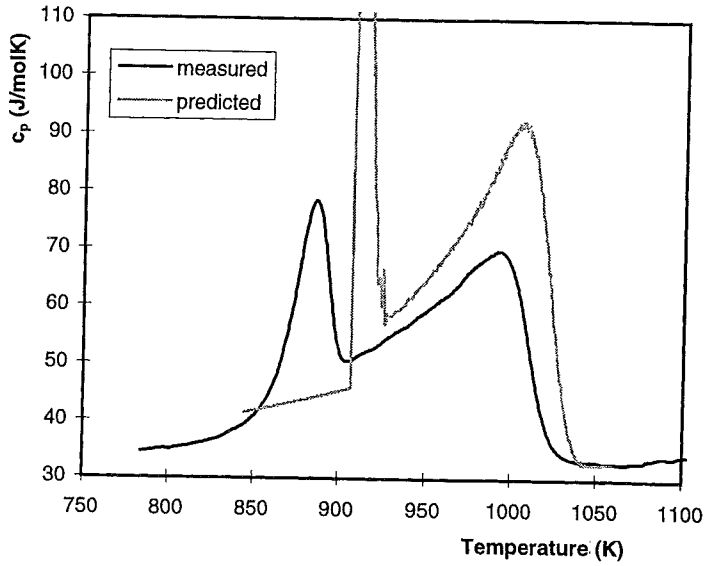

a) T_{aust} = 1323 K; $d\gamma$ = 10 µm

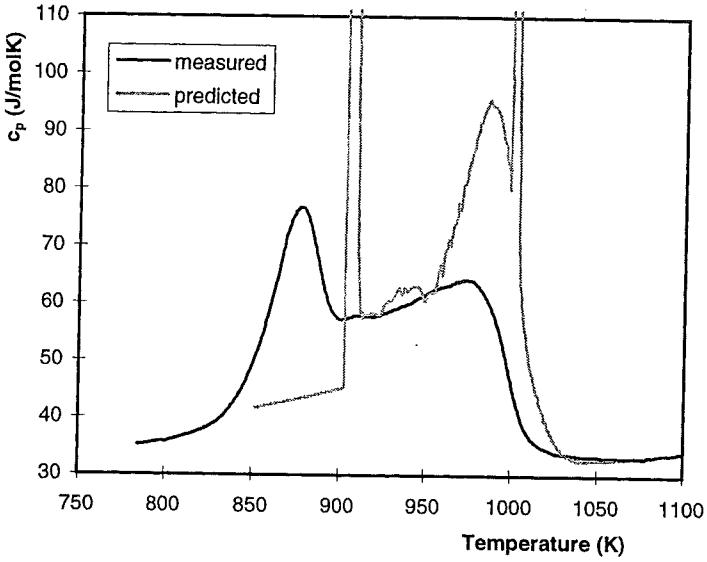

c) T_{aust} = 1373 K; $d\gamma$ = 28 µm

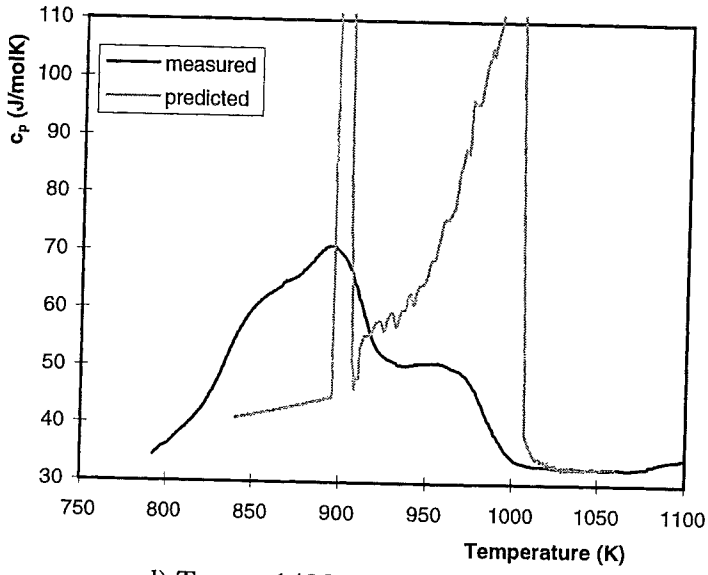

d) T_{aust} = 1423 K; $d\gamma$ = 69 µm

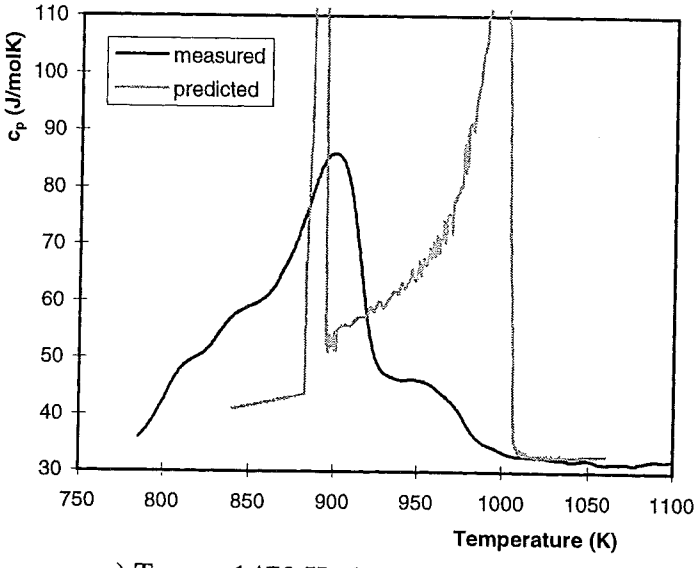

e) T_{aust} = 1473 K; $d\gamma$ = 126 µm

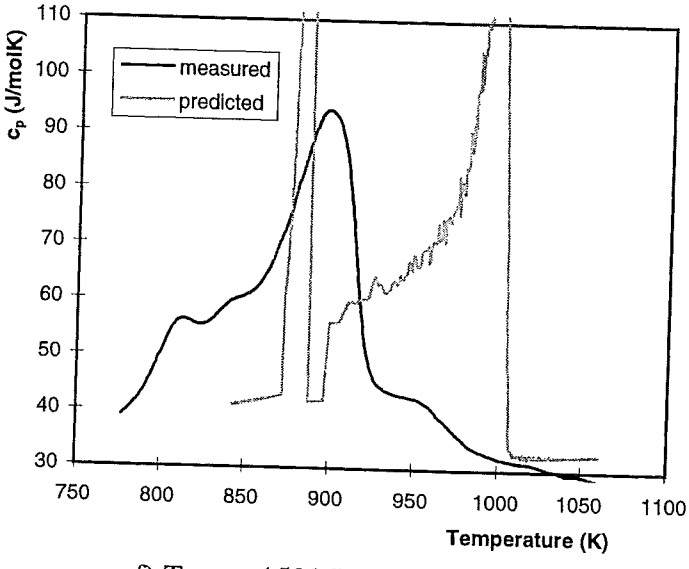

f) T_{aust} = 1523 K; $d\gamma$ = 179 µm

Fig. 6.7: The c_p curves measured with the DTA next to the predicted c_p curves for six different austenitising temperatures (and corresponding austenite grain sizes found in the DTA samples).

A second difference between the calculated and the measured c_p curves are the heat transfer kinetics. In an actual DTA sample, the presence of the Al_2O_3 powder and the sample cup between sample and thermocouple causes a temperature lag. As this effect is absent for the predicted fractions, the predicted c_p increases immediately at the start of the transformation, and shows an immediate decrease of c_p at the end of the transformation as no more reaction energy is developed.

A combination of this effect and the assumption that Widmannstätten and allotriomorphic ferrite can grow at the same time, can be seen in fig.5.20. The fast formation of both Widmannstätten as allotriomorphic ferrite causes a sharp extra peak added to that caused by the allotriomorphic ferrite. As the Widmannstätten formation stops very abruptly, the c_p decreases immediately. In an actual DTA experiment, the strong fluctuations would not be measured and the peak would broaden to lower temperatures as a result of the thermal lag. For the comparison with the experimental results the strong fluctuations caused by the thermal lag are removed since such effects can not be measured with the DTA.

Finally, as discussed in chapter two, the Al_2O_3 powder and the sample cup itself cause a temperature lag between the moment that the sample temperature is increased and the moment this increase is measured by the thermocouples. A correction for this effect (as described by equition 3.4) was already included in the calculation of the c_p from the ΔT's measured.

Noting these differences, when comparing the c_p curves calculated from the predicted phase fractions transformed with the experimental c_p curves presented in fig.6.7a to f, it can be seen that the delays of the start temperature predicted by the model do not correspond with the delays determined experimentally.

Although for a 6 μm austenite grain size the start of the ferrite formation measured is similar to the start temperature predicted, for HO4 there is a strong retardation in the start of the formation of pearlite indicating a lower ferrite growth rate. The delay of the transformation with increasing austenite grain size predicted by the model is the result of the decrease of the number of nucleation sites for larger grain sizes. The delay of the transformation start found in the experiments is, however, much larger.

The experiments show a strong retardation of the formation of both Widmannstätten ferrite and pearlite compared to the predictions. Although the assumption used in the model that Widmannstätten ferrite and allotriomorphic ferrite can grow simultaneously within one grain is shown not to be correct, for situations with low fractions of Widmannstätten ferrite (Fig.6.7a and b) or if almost all of the ferrite is Widmannstätten ferrite (fig.6.7e and f) the effect of this assumption will be small. As the predictions are made based on the actual austenite grain size determined from the measured DTA samples it should therefore be concluded that the presence of Nb in the steel delays the start of the transformation and slows down the ferrite growth rate.

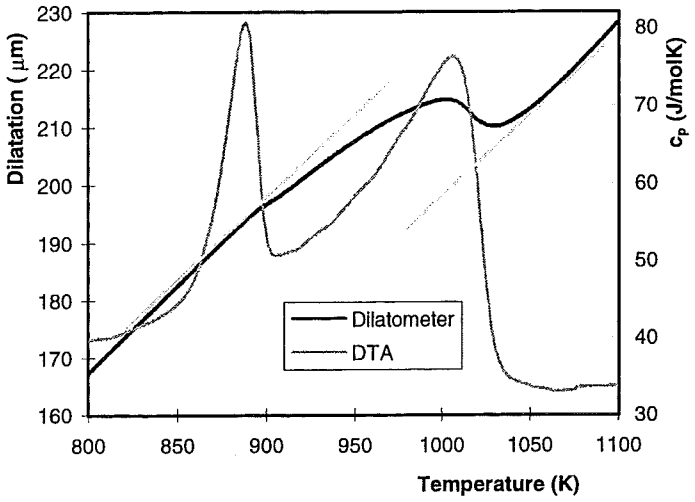

Taust = 1273 K

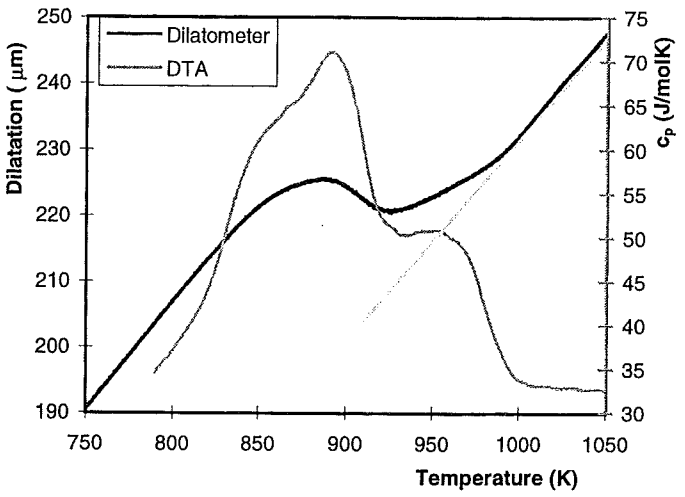

Taust = 1423 K

Fig. 6.8: The transformation behaviour determined using DTA (c_p) and Dilatometry (Dilatation) for austenitising at 1273 K and at 1423 K.

Table 6.1: A review of the data found in this investigation giving the austenite grain sizes, start temperatures and peaktemperatures as found with the DTA, the transformation model and with dilatometry.

Austenitising temperature (K):		**1173**	**1273**	**1323**	**1373**	**1423**	**1473**	**1523**
DTA								
Grain size (µm)	austenite	10	6	10	28	69	126	179
Start temperature (K)	allotriomorphic ferrite	1042	1043	1030	1021	1006	988	983
	Widmannstätten ferrite	-	-	-	925	935	935	935
	pearlite	910	910	903	899	875	865	860
Peak temperatures (K)	allotriomorphic ferrite	1009	1009	990	972	960	955	950
	Widmannstätten ferrite	-	-	-	911	895	899	898
	pearlite	894	892	886	875	863	845	842
	bainite	-	-	-	-	-	813	813
Transformation model								
Start temperature	allotriomorphic ferrite	1044	1045	1044	1040	1036	1033	1030
	Widmannstätten ferrite	-	-	-	1003	1005	1005	1005
	pearlite	925	930	925	912	908	897	888
peak temperature	allotriomorphic ferrite	1007	1017	1007	986	-	-	-
	Widmannstätten ferrite	-			999	1000	998	997
	pearlite	912	910	912	906	901	892	885
Dilatometry								
Start temperature (K)	allotriomorphic ferrite	-	1043	-	-	998	-	-

§6.4. Dilatometry

Using a Bähr dilatometer, the dilatation of a HO4 (Ø 3 mm) cilinder was recently determined for austenitising 20 min. at 1273 K and at 1423 K (using the same cooling rate as used in the DTA experiments). These experiments which are presented together with the DTA curves of the identical tests in fig.6.8a and b show that the transformation start temperature found with the DTA is reproduced using the dilatometer. Also for the sample annealed at 1423 K, the transition of allotriomorphic ferrite to Widmannstätten ferrite can be distinguished with the dilatometer. The formation of pearlite, however, is determined best with DTA. For these reasons, the combination of DTA and dilatometry as described by Kop [21] could give the data needed to separate the reaction peaks determined in the DTA experiments, making it possible to get a complete picture of the transformation kinetics.

§6.5. Review

The results found in this investigation are presented together in table 6.1. Fig.6.9 presents the transformation start temperatures for allotriomorphic ferrite and pearlite given in this table. In fig.6.10 the final phase fractions estimated from the DTA samples and those predicted with the transformation model are presented.

From table 6.1 it can be seen that for low austenitising temperatures (1173 K and 1273 K) the experimental transformation behaviour is predicted very well with the Cambridge model. For higher austenitising temperatures, however, there is a significant difference between the experimental transformation start temperatures and those predicted with the Cambridge model. The increase in austenite grain sizes results in a lowering of the transformation start temperature because of the reduction of nucleation sites with larger austenite grains. This does, however, not account for the retardation of the transformation start temperatures found in the experiments. Since the two important factors influencing the transformation behaviour are the austenite grain size and the addition of Nb, this extra retardation is supposed to be the result of the Nb. The retardation can however be caused by either the NbCN precipitates or the solute Nb. Either way, the Nb must be at the austenite grain boundary if it is to delay the nucleation.

As can be seen in fig. 6.11 [11], the concentration of solute Nb at the austenite grain boundary is much higher than within the austenite grains. Although fig.6.11 is not specified for the system of HO4, the atomic solubility in HO4 will be no more as approximately 10^{-4}. The Nb concentration at the austenite grain boundary is than found to be in the order of 10^4 times that of the austenite matrix. The solute Nb will therefore preferably be at the austenite grain boundary. Because of the lower solubility of Nb in ferrite than in austenite, nucleation of ferrite at the austenite grain boundary would require either the precipitation of Nb or the diffusion of Nb from the nucleation site, both causing an increased activation energy for the ferrite nucleation. A higher austenitising temperature will lead to an increase of the solute Nb content at the austenite grain boundary. When during cooling the precipitation kinetics are so

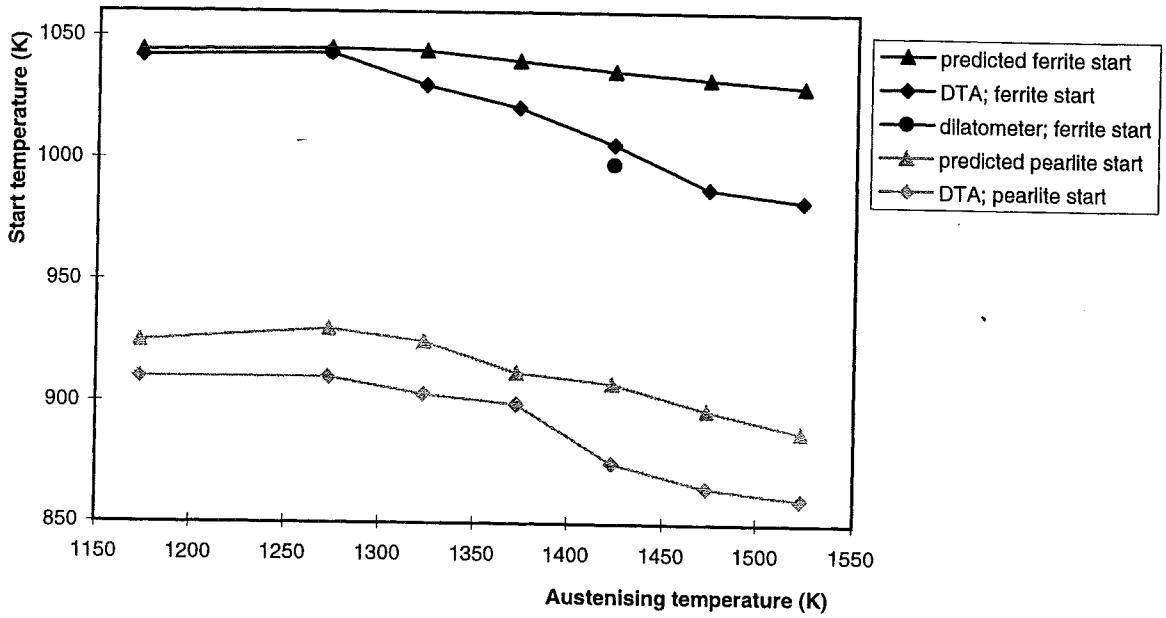

Fig.6.9: The start temperatures for allotriomorphic ferrite and pearlite as presented in table 6.1.

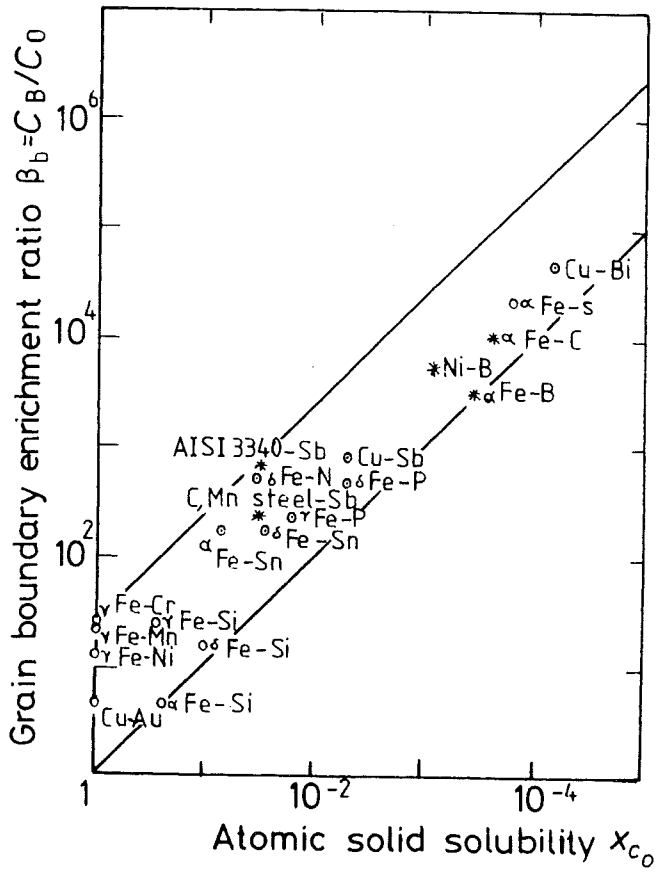

Fig.6.11 The increasing grain boundary enrichment with decreasing solid solubility.

that the equilibrium Nb solubility is not be reached, the amount of solute Nb at the moment of transformation increases with increasing austenitising temperature. This would lead to a decrease of the transformation start temperature with increasing austenitising temperature as is found in the experiments.

If the precipitated Nb would be responsible for the delay of the ferrite nucleation, at low austenitising temperatures there would have to be few precipitated Nb at the austenite grain boundaries. However, for these low austenitising temperatures, the very small austenite grain size (about 5 to 10 μm) shows the presence of the Nb precipitates at the austenite grain boundary.

In fig.6.2 it is also indicated that the solute Nb rather than the precipitated Nb causes the delay of the nucleation. During the austenitisation at 1273 K (after first austenitising at 1423 K), more Nb will precipitate than when not holding at that temperature. If the delay of nucleation would be caused by Nb precipitated, this would lead to a further delay. The delay of nucleation is however less than that found when cooling directly from 1423 K as would be expected if solute Nb causes the delay of the ferrite nucleation. It is therefore concluded that the delay of nucleation is caused by the content of solute Nb at the austenite grain boundary.

The increased fraction of allotriomorphic ferrite resulting from the second austenitisation at 1273 K (fig.6.2) also indicates a faster growth rate of the allotriomorphic ferrite. This complies with the assumption that precipitation of Nb during the transformation slows down the transformation. As the amount of solute Nb is lowered, less precipitation will occur at the transformation front resulting in a faster growth rate of the allotriomorphic ferrite.

When cooling down to 573 K before austenitising at 1273 K (fig.6.3) most of the Nb is precipitated during the transformation. When heating to the second austenitising temperature of 1273 K the amount of solute Nb will be that of 1273 K without any effect of the prior austenitisation at 1473 K. In fig.6.3 it can be seen that the transformation behaviour is indeed fully determined by the second austenitising temperature.

The formation of Widmannstätten ferrite was observed in both the experimental and the predicted results. For larger austenite grain sizes (i.e. higher austenitising temperature) the time required for complete transformation increases. The critical undercooling resulting in the formation of Widmannstätten ferrite is therefore reached in an earlier stage of the ferrite formation. The fraction of Widmannstätten ferrite will therefore increase with increasing austenitising tempeatures. Due to the retardation of the ferrite nucleation caused by the solute Nb, the critical undercooling is reached even earlier, causing even more Widmannstätten ferrite to be formed. The formation of bainite for annealing at higher austenitising temperatures is caused by the large undercoolings at which the pearlite is formed. The Cambridge model does not include the formation of bainite. The absence of bainite in the predicted transformation behaviour therefore does not indicate on an effect of Nb.

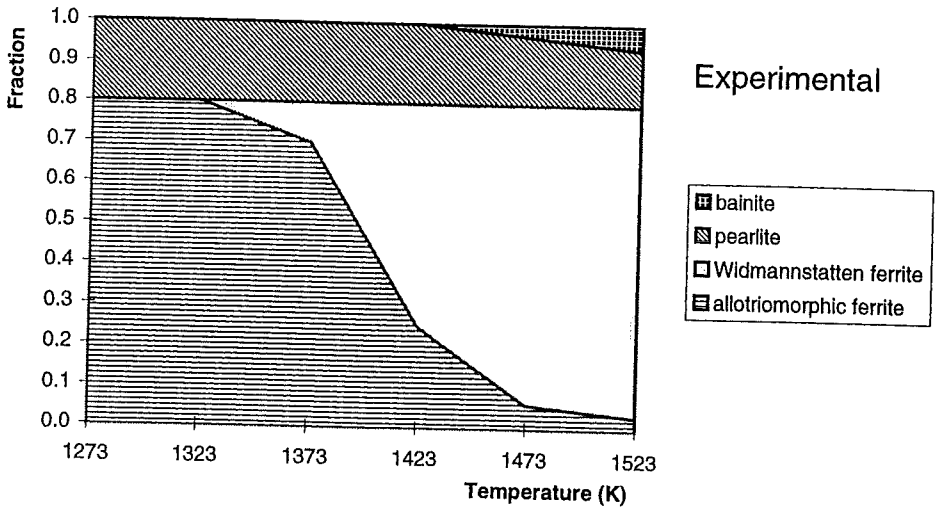

(a)

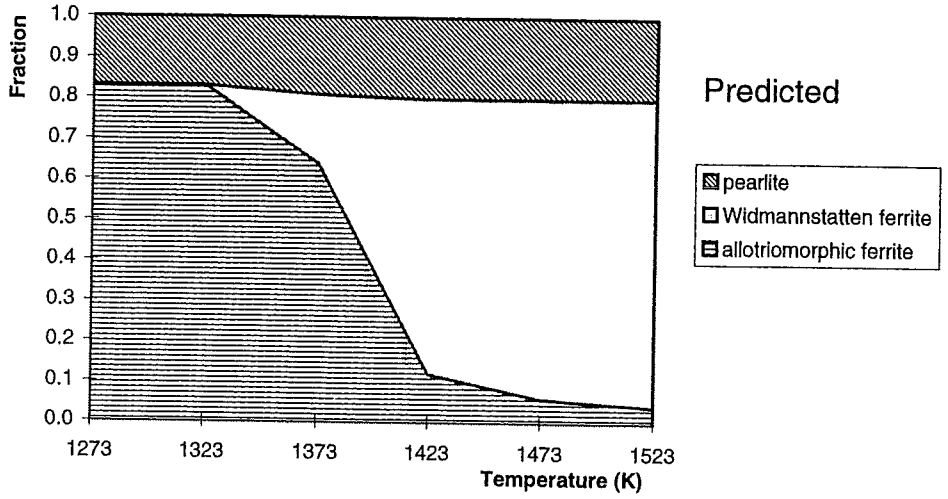

(b)

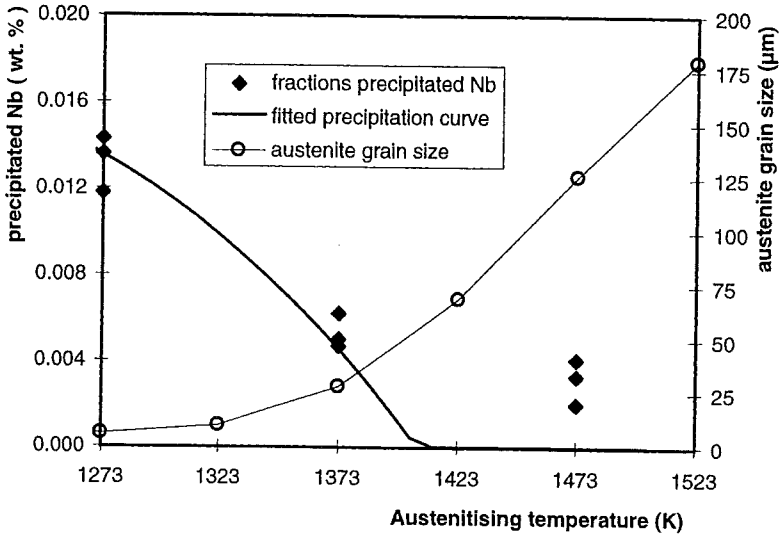

(c)

Fig.6.10: The fractions of the phases formed for varying austenitising temperature estimated from the DTA samples (a) and predicted by the transformation model (b). Also the amount of precipitated Nb with the austenite grain size (as presented in fig.6.5) are plotted for the austenitising temperatures applied (c).

This investigation is only the first part to determine the effect of Nb on the transformation behaviour in the production of HSLA steels. Not discussed in this report, but an important factor in the production of High Strength Low Alloy steels is deformation of the austenite. In the hot-rolling mill, the combination of the Nb precipitates with deformation of the austenite results in the small austenite grain sizes leading to the strength characteristic for HSLA steels. In the future, the extra effect of deformation is to be investigated using a Bähr deformation dilatometer. By applying deformation the excessive austenite grain growth as found in this investigation can be prevented giving a more uniform austenite grain structure.

7 Conclusions

The effect of the austenitising temperature on the transformation behaviour of a Nb microalloyed HSLA steel was examined by varying the austenitising conditions. The experimental results were compared to a transformation model predicting the transformation behaviour for the austenite grain sizes found in the experiments but without including Nb. Based on the results found in this investigation, the following conclusions can be drawn.

- Nb precipitates delay austenite recrystallisation and inhibit austenite grain growth.
  Increasing fractions of Nb precipitates therefore result in a smaller, retained austenite grain size. As for increasing austenitisation temperatures, the volume fraction of precipitated Nb decreases, the austenite grain size increases.

- The retardation of the start temperature of the formation of allotriomorphic ferrite is caused by the solute Nb at the austenite grain boundaries causing a delay of the ferrite nucleation.
  The solute Nb at the austenite grain boundary causes an increase of the activation energy for the nucleation of allotriomorphic ferrite. Because of this increased activation energy the driving force required for the formation of allotriomorpic ferrite increases. The start of the transformation will therefore shift to lower temperatures.

- The transformation behaviour is determined by both the highest austenitising temperature as well as the last austenitising temperature.
  Without recrystallisation caused by deformation, the austenite grain structure at the start of the transformation is determined at the highest austenitising temperature. This austenite grain structure remains unchanged until the start of the transformation. The Nb, brought into solution at the highest austenitising temperature, will preferably be at the austenite grain boundary. The delay of the ferrite nucleation resulting from the solute Nb is determined by the last austenitising temperature as, at this temperature, the amount of solute Nb at the start of the transformation, is determined. The ferrite growth rate is also determined by the amount of solute Nb at the start of transformation and is therefore determined by the last austenitising temperature.

- The time at the highest austenitising temperature has no significant influence the progress of the transformation. For the times at the austenitising temperature used in this investigation (10 to 60 minutes) no effects on the transformation behaviour are found.

- When performing DTA measurements it is best to use the new measuring procedure as presented in Appendix B. By using this measuring procedure it is possible to determine the extend of stabilisation of ΔT at the start of the cooling stage. Also, an indication of the accuracy of the measurement is attained during the experiment rather than at the end of a serie of experiments.

8 Recommendations for future investigations

- Comparing the results to the results of identical DTA experiments examining a steel with the same composition except without Nb.

- A method should be developed to detect the precipitates smaller than 100 nm. Using ceramic filters or membranes could possibly be a solution.

- The progress of transformation of the separate phases could be investigated by combining the result of DTA and dilatometer experiments.

- Deformation experiments are to be done to determine the effect of strain induced precipitation and due to which recrystalisation minimises the effect of the prior austenite grain size on the transformation.

Acknowledgements

First of all, I would like to thank Sybrand van der Zwaag whose commitment and hard work enabled the existence of this stimulating group in which I finished my study. Also I would like to thank Theo Kop, Jilt Sietsma and Sybrand van der Zwaag for their discussions and guidance during the progress of this work. I thank Pieter Colijn for his assistance in the determination of the various microstructures. I thank Sally Parker at the Cambridge University for the predictions of the transformation behaviour and for the discussions concerning these results. Also, I thank Jeroen Colijn and Tom Hoogendoorn of Hoogovens NV for the possibility and performing the dilatometric experiments and for the valuable discussions concerning measuring techniques and precipitation. Finally, I thank everyone in the section PT2 and at the Laboratory of Material Science for the very nice time I had studying in Delft.

References

[1] J.W. Gibbs; On the equilibrium of heterogeneous substances, collected works; vol.1, Longmans, Green and Co., 1928, New York

[2] Nucleation; A.C. Zettlemoyer; Marcel Dekker, 1969, New York

[3] K.C. Russel; Nucleation in solids; Phase Transformations; American Society for Metals 1970

[4] J.W. Cahn; The kinetics of grain boundary nucleated reactions; Acta Metall., Vol. 4, 1956, pp.449-459

[5] M. Umemoto; Mathematical modeling of phase transformation from work-hardened austenite; Proc. int. symp. on mathematical modeling of hot rolling of steel; ed. by S. Yue, CIM, Montreal, 1990 p.404

[6] R.C. Reed; Modelling of the growth kinetics of allotriomorphic ferrite; mk67 lecture notes

[7] J.R. Bradley, J.M. Rigsbee, H.I. Aaronson; Growth kinetics of grain boundary ferrite allotriomorphs in Fe-C alloys; Met. Trans. A, vol. 8A feb.1977 p.323

[8] G.P. Krielaart; Primary ferrite formation from supersaturated austenite; Ph.D. thesis Delft University of Technology 1995

[9] A. de Sy, J Vidts; Teoretisch en Toegepaste Metaalkunde; Rijksuniversiteit Gent 1966

[10] H.I. Aaronson, C.Laird, K.K. Kinsman; Phase Transformations; American Society for Metals, Ohio 1970

[11] D.A. Porter, K.E. Easterling; Phase Transformations in Metals and Alloys; Van Nostrand Reinhold, London 1989 (first ed. 1981)

[12] S.V. Parker; first semester report; Appendix 2 of Improvement of Hot rolled Products by Physical and Mathematical Modelling; ECSC Project; Technical Report no.1, 1994; A.A. Howe; BST; Rotherham

[13] S.V. Parker;third semester report; Appendix 5 of Improvement of Hot rolled Products by Physical and Mathematical Modelling; ECSC Project; Technical Report no.3, 1995; A.A. Howe; BST; Rotherham.

[14] E.J Palmiere, C.I. Garcia, A.J. DeArdo; Compositional and microstructural changes which attend reheating and grain coarsening in steels containing niobium; Metallurgical and Materials Transactions A, vol 25A, Feb. 1994 pp. 277-285

[15] Th.M. Hoogendoorn, M.J. Spanraft; Quantifying the effect of microalloying elements on structures during processing; Microalloying 75, Oct. 1-3 1975, Washington, Union Carbide Corporation New York 1977

[16] F.B. Pickering; The spectrum of microalloyed High Strength Low Alloy steels; HSLA steels, technology and applications; ed. by M. Korchynsky; ASM, Metalspark 1984

[17] R.W.K. Honeycombe; Fundamental aspects of precipitation in microalloyed steels; HSLA steels Metallurgy and Applications; Bejing, 4-8 November 1985; ed. by J. M. Gray; ASM International, 1986 pp.243-250

[18] R.F. Speyer, Thermal Analysis of Materials, Marcel Dekker Inc. N.Y. (1994)

[19] G.P. Krielaart; Internal report; Kalibratie van de Perkin-Elmer DTA-7; Delft sept. 1993

[20] Unpublished data, department of Materials Science, Delft University of Technology

[21] T.A. Kop, J. Sietsma, S. van der Zwaag; The Transformation Kinetics of Construction Steels; to be published in Proceedings Euromat '97, April 1997

Appendices

Appendix A:

A thermal evalutation of the Perkin Elmer DTA 7.

Appendix B:

Performing Differential Thermal Analysis measurements on the Perkin Elmer DTA 7.

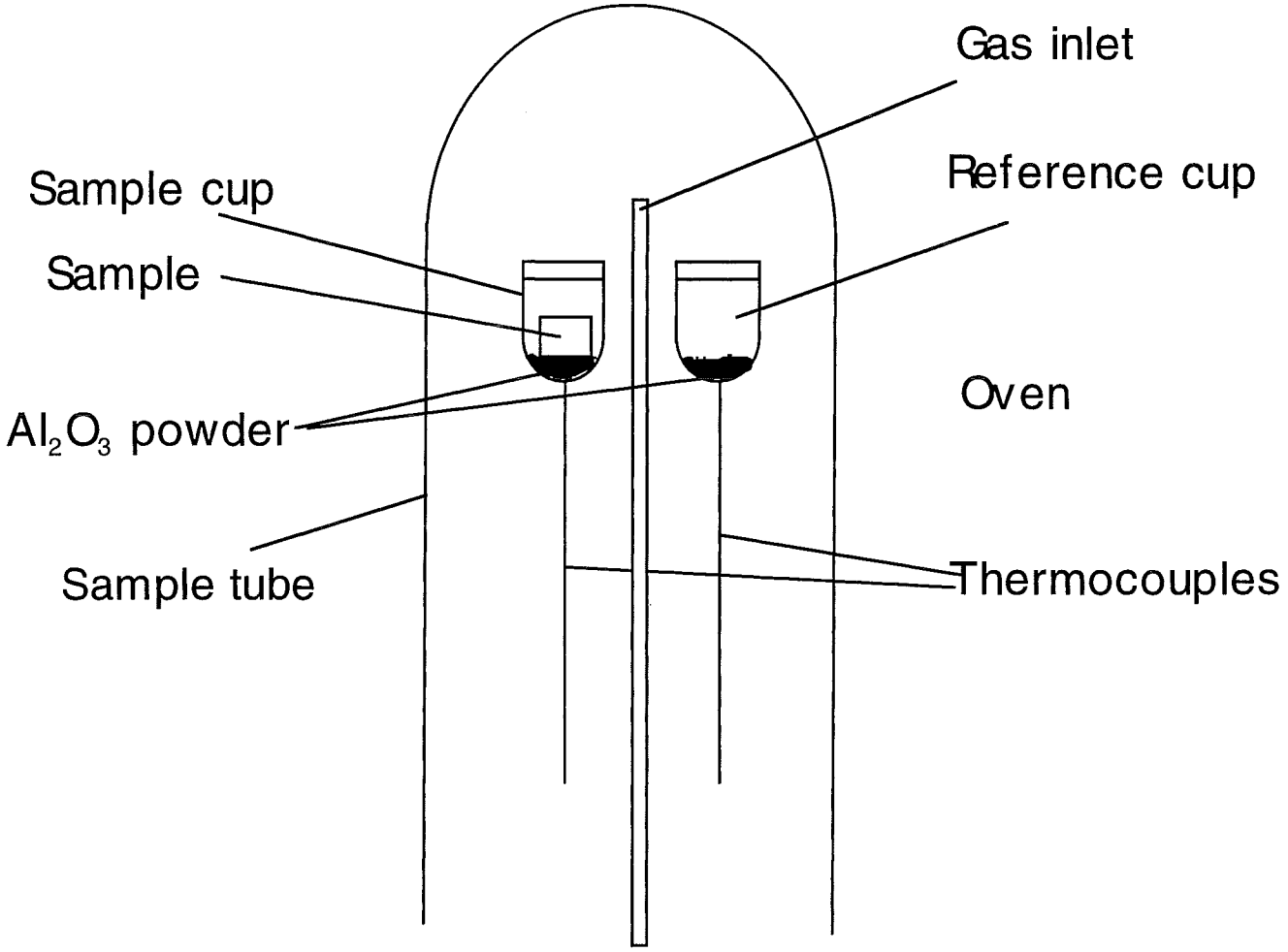

Fig.A.1: A schematic drawing of the sample area of the Perkin Elmer DTA 7.

Appendix A:

A thermal evaluation of the Perkin Elmer DTA 7

The DTA as discussed is schematically shown in fig.A1. For this evaluation
s stands for sample cup (including Al_2O_3 powder and lid but without the sample),
r stands for reference cup
f stands for the furnace (its temperature is assumed equal to that of the sample tube)
T is the temperature of the specified part (T_s is the temperature of the sample cup,
K is the heat transfer coefficient
C_r is the heat capacity of the reference cup
C_s is the heat capacity of the sample cup
C_{sample} is the heat capacity of the sample
c_p is the specific heat
ΔH is the change in entalpy of the specified part
ΔT is the temperature difference between sample cup and reference cup
Φ_x is the total heat flow to x
Φ_{xy} is the heat flow from x to y

The heat of the furnace is passed on to the sample tube. As the position of the cups with respect to the sample tube is identical, in the ideal case the furnace temperature is equal for both cups.

Assumption 1: At any height of the sample tube its temperature is uniform all arround (this means that the temperature of the sample tube T_f is identical for sample cup and reference cup). The temperature of the sample tube is assumed to be the temperature of the furnace.

Assumption 2: The cups have one uniform temperature T_s or T_r so there is no temperature gradient in the cups.

Assumption 3: The heat transfer coefficient of an object depends on the outer surface of that object. Although the cups may have a slightly different mass and different contents, the outer surface is not affected. It is therefore assumed that the heat transfer coefficient for the sample cup/furnace is equal to that for reference cup/furnace and is called K' (i.e. $K_{sf} = K_{rf} = K'$).

Now the heat flow to the sample cup is given by the heat flow from both the furnace and from the reference cup. The heat flow to the sample cup Φ_s is therefore given by:

$$\Phi_s = \Phi_{fs} + \Phi_{rs} = K_{sf}(T_f - T_s) + K_{sr}(T_r - T_s) \qquad \text{(A1)}$$

The heat flow to the sample cup is used to heat up this sample cup or to supply energy dH for a reaction (positive for an endothermic and negative for an exothermic reaction). The energy in- or decrease of the sample cup is given by:

$$\Phi_S = C_S \frac{dT_S}{dt} + \frac{dH_S}{dt} \tag{A2}$$

Similar equations can be derived for the reference cup:

$$\Phi_r = \Phi_{fr} + \Phi_{sr} = K_{rf}(T_f - T_r) + K_{sr}(T_s - T_r) \tag{A3}$$

$$\Phi_r = C_r \frac{dT_r}{dt} + \frac{dH_r}{dt} \tag{A4}$$

A difference should be made between baseline measurement (without a sample) and sample measurements (with a sample). First the baseline measurement will be discussed.
Before a sample is measured, a baseline measurement should be performed to determine the ΔT caused by the instrument. For the sample cup the heat flow $(\Phi_S)_b$ is given by:

$$(\Phi_S)_b = K_{sf}(T_f - T_S) + K_{sr}(T_r - T_S) = C_S \frac{dT_S}{dt} + \frac{dH_S}{dt} \tag{A5}$$

For the reference cup, $(\Phi_r)_b$ is given by:

$$(\Phi_r)_b = K_{rf}(T_f - T_r) + K_{sr}(T_s - T_r) = C_r \frac{dT_r}{dt} + \frac{dH_r}{dt} \tag{A6}$$

As the cups are both inert, for both cups applies: dH/dt = 0.
$(\Phi_S)_b$-$(\Phi_r)_b$ therefore now becomes:

$$(\Phi_S)_b - (\Phi_r)_b = K_{sf}(T_f - T_S) - K_{rf}(T_f - T_r) - 2K_{sr}(T_S - T_r) = C_S \frac{dT_S}{dt} - C_r \frac{dT_r}{dt} \tag{A7}$$

Following assumption 3, $K_{sf} = K_{rf} = K'$ so equation (A7) can be written as:

$$-(2K_{sr} + K')(T_s - T_r) = C_S \frac{dT_S}{dt} - C_r \frac{dT_r}{dt} \tag{A8}$$

With the definition $K = 2K_{sr} + K'$ and the equality $T_s = T_r + (T_s - T_r)$ equation (A8) can be written as:

$$-K(T_s - T_r) = C_S \frac{dT_r}{dt} - C_r \frac{dT_r}{dt} + C_S \frac{d(T_s - T_r)}{dt} \tag{A9}$$

By replacing $T_s - T_r$ by ΔT, $\Delta T_{baseline}$ is now given by:

$$\Delta T_{baseline} = -\frac{1}{K}\left((C_S - C_r)\frac{dT_r}{dt} + C_S \frac{d\Delta T}{dt}\right) \tag{A10}$$

Now, similar equations are derived for the sample measurement.
For a sample measurement the specific heat of the total sample cup changes as a sample with heat capacity C_{sample} is added. Also, there might be extra changes in the enthalpy change dH/dt due to reactions occuring in the sample.

As it is assumed that the heat transfer coefficients depend solely on the outer area of the cups, K is not influenced by the sample. For the sample measurement, equation (A8) is now given by:

$$-(2K_{sr} + K')(T_s - T_r) = \left(C_s + C_{sample}\right)\frac{dT_s}{dt} - C_r\frac{dT_r}{dt} + \frac{dH_{sample}}{dt} \qquad (A11)$$

with: $2K_{sr} + K' = K$;

$T_s = T_r + (T_s - T_r)$ and

$T_s - T_r = \Delta T$

this yields:

$$-K(T_s - T_r) = C_{sample}\frac{dT_s}{dt} + (C_s - C_r)\frac{dT_r}{dt} + C_s\frac{d(\Delta T)}{dt} + \frac{dH_{sample}}{dt} \qquad (A12)$$

Subtracting the baseline from the sample measurement now gives the ΔT caused by the sample itself:

$$\Delta T_{sample} = \Delta T_{measurement} - \Delta T_{baseline}$$

thus:

$$\Delta T_{sample} = -\frac{1}{K}\left(C_{sample}\frac{dT_s}{dt} + \frac{dH_{sample}}{dt} + C_s\left(\frac{d\left(\Delta T_{sample}\right)}{dt} - \frac{d(\Delta T_{baseline})}{dt}\right)\right) \qquad (A13)$$

As long as C_s is not much larger than C_{sample} and the cooling rate is not very small:

$$C_s\left(\frac{d\left(\Delta T_{sample}\right)}{dt} - \frac{d(\Delta T_{baseline})}{dt}\right) \ll C_{sample}\frac{dT_s}{dt} + \frac{dH_s}{dt} \qquad (A14)$$

Equation (A13) can now be approximated by:

$$\Delta T_{sample} = -\frac{1}{K}\left(C_{sample}\frac{dT_s}{dt} + \frac{dH_{sample}}{dt}\right) \qquad (A15)$$

From equation (A15) it can be seen that the DTA curve is the sum of the heat capacity effect and the heat effect caused by occuring reactions. The area of the "reaction peak" in the DTA curve is proportional to the heat evolution (or absorption) during the reaction.

During the cooling down from the austenite range of a pure Fe sample ΔT will be positive as dT_s/dt is negative for cooling. The $\gamma \Rightarrow \alpha$ transformation and ferro/para magnetic transition which are both exothermic, result in a negative dH/dt (as dH/dt is defined as the heat flow to the sample) and this therefore results in positive peaks in the DTA curve.

C_{sample} can also be written as the total enthalpy change of the sample dH/dT_s. Equation (A15) can therefore be written as:

$$\Delta T_{sample} = -\frac{1}{K}\left(\frac{dH}{dT_s}\cdot\frac{dT_s}{dt} + \frac{dH_{sample}}{dt}\right) = -\frac{1}{K}\left(\frac{dH}{dt} + \frac{dH_{sample}}{dt}\right) \qquad (A16)$$

Combining this with the cooling rate ϕ equation (A16) becomes:

$$\Delta T_{sample} = -\frac{\phi}{K}\left(\frac{dH}{dT_S} + \frac{dH_{sample}}{dT_S}\right) \tag{A17}$$

By defining C_p as the sum of the heat capacity of the sample (dH/dT_S) and the heat effect due to occuring reactions (dH_S/dT_S) equation (A17) can be written as:

$$\Delta T_{sample} = -\frac{\phi}{K} \cdot C_p' \tag{A18}$$

As this evaluation does not apply specifically to steel samples, equation (A18) also applies to a sapphire sample (α-corundum). For the same cooling rate, the factor $K\phi$ is identical for both the sample and the sapphire. As the c_p as a function of temperature is known for sapphire and sapphire has no thermal reactions in the temperature range concerned, c_p of the sample can be calculated using a ratio method [A1]:

$$\frac{\Delta T_{sample}}{c_{p\ sample} \cdot m_{sample}} = \frac{\Delta T_{sapphire}}{c_{psapphire} \cdot m_{sapphire}} \tag{A19}$$

where $c_{p\ sample}$ is the specific heat of the sample (including thermal effects),
$c_{p\ sapphier}$ is the specific heat of sapphier, and
m is the sample mass

So using sapphire as a reference material, the measured ΔT of a sample can be converted into c_p which is the sum of the actual specific heat of the sample material and the reaction heat during cooling resulting from thermal effects.

References

[A1] Thermal Analysis of Materials, R.F. Speyer, Marcel Dekker, Inc. N.Y. (1994)

Appendix B

Performing Differential Thermal Analysis measurements on the Perkin Elmer DTA 7

Using the DTA, heat effects in a sample during heating or cooling can be examined. Since phase transformations in steel involve heat effects, they can be examined both qualitatively and quantitatively by means of DTA. In order to be able to analyse the DTA data quantitatively, the experiments must be carried out correctly. In this report important experimental factors are discussed ([1] to [4]) and an optimised measuring procedure is presented.

Experimental set-up:

- When to calibrate

As long as there are no changes to the instrument operating conditions, the temperature and energy calibration of the DTA should remain unchanged. A new calibration will normally be required whenever:

- the temperature range of the experiment changes to temperatures outside the range of the furnace calibration;
- the slope control is adjusted after the calibration
- the gas type or gas flow rate is changed calibration should be checked for highest accuracy by performing a temperature check (see below)
- parts of the DTA are replaced (like thermocouples or cups) or repositioned
- the DTA has been turned off for long periods of time the calibration needs to be checked with a temperature check.

A temperature check can be performed to see if a new calibration is required. In this check the melting points of aluminium and gold are measured and compared to the literature (considering the heating/cooling rate). As the temperature calibration changes with the scan rate it is best to calibrate using the scan rate that will be used in the experiments. If several scan rates are to be used, it is best to calibrate at the slowest scanning rate that will be used during the experiments.

A change in the amount of Al_2O_3powder in the sample cup might result in a change in the baseline. This does not require a new calibration. If the amount of powder lost is significant a similar amount of new powder can be added. After adding new Al_2O_3 powder, an extra run should be done (1 hour at 1000°C) to enable the new powder to settle in the cup.

If a new calibration is performed the new settings must be entered in the back of the laboratory journal.

- Which cups to use

The choice of what cups to use depends mainly on the heat effect that is to be examined [3]. To examine exothermic reactions, a cup made out of a material with a high thermal conductivity gives a better peak resolution than one made of a material with a low thermal conductivity. Since the formation of ferrite and pearlite from austenite is exothermic, it is advisable to use cups with a high thermal conductivity. The use of the platinum cups is therefore preferred to the use of the Al_2O_3 cups.
Only Al_2O_3 lids are available from Perkin Elmer. Although some tests are done using self designed platinum lids. So far this however, has not been succesfull and therefore the Al_2O_3 are still to be used.

- Furnace atmosphere

Generally, two types of gaseous atmospheres can be used [3]. A static and a dynamic atmosphere. The static atmosphere is usually in an enclosed system but is difficult to reproduce due to furnace convection currents and also due to gas leaks in the furnace. The dynamic atmosphere in which a gas flows through the furnace is easier to control and reproduce. The gasflow rate used during experiments should therefore be the same as used during calibration. Also, the temperature gradient due to this dynamic gas flow require strictly that the position of the cups is not changed between baseline and sample (or sapphire) measurements. Inserting the sample must therefore be done without moving the sample cup holder.
Normally, experiments are done in a dynamic Argon atmosphere which is dehydrated and deoxidised. The gas flow is controlled using a gas flow controller which is usually set at a gas flow of 50% (which approximately equals 26 ml/min). The gas flow used during the measurements should be the same to the flow rate used during calibration.

- Sample size

The size of the sample influences the shape of the curve peaks. A large sample size results in broad peaks, low resolution and temperature accuracy. Also a low heating rate is required to prevent large temperature gradients in the sample.
However, the smaller the sample size, the smaller the reaction peaks will be. Therefore, the sample size is chosen so that the reaction peaks are approximately 1 to 1.5 °C. For steel alloys this normally means a sample weight of about 90 to 100 mg.
As the inside diameter of the sample cup is about 4 mm diameter with a spherical bottom, the sample size must not exceed 3.5 mm. Normally the samples are cut from cylinders with a

diameter of 3 mm. Such samples have a constant and relatively large contact area with the Al_2O_3 powder in the cup.
As some elements can react very strongly with platinum, the samples should not be in contact with the platinum cups during the measurement. This is especially important for aluminium and gold during the temperature checks!!!

- The temperature programme

By already using the temperature programme during heating, the heating rate and especially the times at the annealing temperature(s) can be well defined. By starting data recording well before the start of the actual experiment (the cooling from the austenitising temperature), an insight can be obtained concerning the stability of ΔT and the shift of the start of the corrected baseline from $\Delta T=0$. Also this information can be used to make a decision concerning the accuracy of the baseline.
The temperature programme can be divided in three parts: heating, holding and cooling. These three parts will be discussed separately.

- Heating rate

When doing transformation experiments during cooling, the heating rate should be chosen depending on the specific experimental wishes. Before starting an experiment, ΔT should be stabilised at the austenitising temperature. If using a higher heating rate, the time needed for ΔT to stabilise increases. A lower heating rate means that it takes longer time for the sample to reach the desired austenitising temperature but also that less time is needed to stabilise at the high austenitising temperature.
For carbon containing alloys, longer times at the austenitising temperature means more decarburisation. The extra time at low temperatures however has little influence. A low heating rate should therefore be considered.
As FeX alloys don't have the problem of decarburisation, larger austenitising temperatures are not a problem. Also if determining the Prior Austenite Grain Size using "thermal etching", longer times at low temperatures leads to heavier etching of the ferrite and pearlite. This will make the determination of the PAGS more difficult. Higher heating rates are therefore preferred.
In general, lower heating rates (10-20 °C/min) for FeC alloys and higher heating rates (50 °C/min) for FeX alloys are recommended.

- Holding time

As could be seen above, the times required at the stabilising temperature depend on the heating/cooling rate used to reach this stabilising temperature. A lower heating/cooling rate requires a shorter stabilising time and a higher rate a longer stabilising time.

Holding times needed for ΔT to stabilise should best be examined for the specific system by measuring while stabilising.
For temperatures higher than 1000 °C, long holding times (>1 hour) should be avoided because of oxidation of the cups and sample.

- Cooling rate

The cooling rate has a profound influence on the position and shape of the peaks. Increasing the cooling rate results in a decreased resolution as a larger undercooling is derived. This also results in a shift of the starting temperatures to lower temperatures.
As the reference cup cools down faster with increasing cooling rates ΔT will increase and therefore the sensitivity of the DTA will increase with increasing cooling rates.

- Measurements needed

To get a correct measurement it is important that baseline and sample/sapphire measurement are as similar as possible. In this way the baseline measured will differ from the instrumental baseline during the sample/sapphire measurement as little as possible.
In order to be able to calculate C_p of the sample, a similar sapphire measurement is required. It is best to perform this sapphire measurement under the same conditions as the sample measurement. Therefore, a sapphire measurement should be done following each sample measurement (as can be seen in the measuring procedure below).

-The DTA journal

All experiments should be entered in the journal present in the lab. This entry should include: date; operator; filename; sample reference (or baseline); sample weight; and temperature programme. Also changes in the instrumental set-up of the DTA (calibrations, new Al_2O_3 powder etc.), any restarts of the UNIX system and changes in the DTA settings should be entered in the journal.
New calibrations must also be entered in the back of the journal so the last calibration can easily be found.

-Inserting or removing samples

Open the oven cover (this requires some skill). Remove the sample tube knurled nut while making sure the sample tube does not move by holding the top of the sample tube. Lift the sample tube from the sample leading it along the purge tube behind the thermocouples. In this way the cups are least likely to be touched by the sample tube. Position the sample table to give support. Remove sample lid and insert or remove sample. It is very important to do all of this as careful as possible. Removing ferro magnetic samples can be done using magnetic tweezers. Put the lid back on the sample cup and put the sample tube back in place. Again by leading it along the purge tube. Place the sample tube knurled nut over the sample

tube and fasten it by hand. Lower the over cover. Wait 15 minutes before starting the experiment to enable the Argon to drive out the oxygen and enable the DTA to stabilise.

Measuring procedure

1- measure baseline using the chosen temperature programme (the same for all measurements) (enter all experiments in the DTA journal!)
2- measure the weight of the sample
3- open the DTA and insert sample into sample cup and close the DTA
4- wait at least 15 minutes after closing the DTA to enable the Ar to drive out the oxygen.
5- perform the sample measurement (again using the chosen temperature programme)
6- open the DTA and remove the sample using the magnetic tweezers (bring one hand of the tweezers above the sample and lift it out of the cup). In this way the position of the cup is least expected to be changed.
7- remove any remaining Al_2O_3 powder from the sample and measure the weight of the sample again.
8- close the DTA and wait for 15 minutes to enable the Ar to drive out the oxygen
9- measure the baseline again using the chosen temperature programme.
10- measure the weight of the sapphire (α- Al_2O_3)
11- open the DTA and insert the sapphire into sample cup
12- wait at least 15 minutes after closing the DTA
13- measure sapphire using the same temperature programme
14- open the DTA and remove the sapphire from the sample cup. Since the sapphire is not ferromagnetic, the sapphire can not be lifted out. Care must be taken to take out the sapphire as carefully as possible. If necessary the sample cup can now be taken out to remove the sapphire so the sample thermocouple and sample cup holder are not damaged. Al_2O_3powder loss from the sample cup should be prevented as much as possible, however as the measurement series should be completed, this does not influence the results.
15- close the DTA and wait for 15 minutes
16- measure the baseline again using the same temperature programme

From theoretical evaluation it is concluded that ΔT reached for baseline and sample measurement at the end of the holding period should be the equal. Therefore, comparing these values is believed to give an indication on how reliable the baseline is. Further measurements must give experimental proof for the correctness of this test method. If the baseline taken before the actual experiment, stabilises at the same ΔT as the baseline taken after the measurement, the baselines should be "identical".

References

[1] DTA-7 Instruction Manual, Perkin-Elmer Corp., Norwalk (1993)

[2] Kalibratie van de Perkin-Elmer DTA-7, Gerben Krielaart, internal report, 1993

[3] Thermal Methods of Analysis, W.W. Wendlandt, Second ed.,John Wiley & Sons (1974)

[4] Thermal Analysis of Materials, R.F. Speyer, Marcel Dekker, Inc. N.Y. (1994)